DESIGN OF A RAPIDLY DEPLOYABLE SURGICAL RETRACTOR

by

Andrew Charles Neil

B.S., Mechanical Engineering, University of Pittsburgh, 2016

Submitted to the Graduate Faculty of

Swanson School of Engineering in partial fulfillment

of the requirements for the degree of

Master of Science

University of Pittsburgh

2017

UNIVERSITY OF PITTSBURGH

SWANSON SCHOOL OF ENGINEERING

This thesis was presented

by

Andrew Charles Neil

It was defended on

November 17, 2017

and approved by

Mark C. Miller, Ph.D., Associate Professor, Department of Mechanical Engineering and Materials Science

William W. Clark, Ph.D., Professor, Department of Mechanical Engineering and Materials Science

Thesis Advisor: Jeffrey S. Vipperman, Ph.D., Vice Chair, Department of Mechanical Engineering and Materials Science

DESIGN OF A RAPIDLY DEPLOYABLE SURGICAL RETRACTOR

Andrew Charles Neil, M.S.

University of Pittsburgh, 2017

As surgical techniques continue to evolve during the modern era of medicine, efforts have been made to maximize the potential for positive surgical outcomes. In a trauma situation, every moment of time is critical to the welfare of an injured patient. When an injured patient is brought into an operating room, room preparation and device setup time must be kept to a minimum in order to maximize the chance of a positive patient outcome. This work focuses on the development of a rapidly deployable surgical retractor that requires a fraction of the setup time required by current surgical retraction systems that have been in use for at least the past 30 years. This work represents the evolution of a new and improved surgical retractor, which was demonstrated through the development of two prototypes. Both prototypes were similar in that they each contained a motor box, an articulating arm composed of links, and a retractor blade at the end. The motor box had an electric motor and force feedback control system for Generation I (Gen-I) and a pressure-regulated, pneumatic actuator for Generation-II (Gen-II). The arm is composed of links that stack to form ball and socket joints. A central cable can be tightened by the motor box to lock the arm into virtually any configuration. The arm development was a considerable focus of this work and spanned across both Gen-I and Gen-II development. Considerations were made regarding both the strength (geometry and materials) of the arm when placed under bending load, as well as the ability for the joints to lock into place without slipping when the cable is tensioned. The distal end of the arm contains the retractor blade. For Gen-I, a Richardson style retractor was

3D printed and integrated into the end of the arm [33]. In comparison, a blade adaptor was developed for Gen-II that permits interchangeable Bookwalter retractor kit blades to be used [33].

Keywords: articulating column, retractor system, retractor arm, abdominal surgery, surgical retraction.

TABLE OF CONTENTS

LIST OF TABLES

LIST OF FIGURES

PREFACE

The research performed in this thesis was fueled by a lifelong interest in improving human life through the combination of engineering and medicine. Having grown up in a family of medical professionals, the author has always sought ways to contribute his knowledge to the medical field to improve the quality of human life through designing technology to aid medical professionals. The author would like to thank his advisor, Dr. Jeffrey S. Vipperman, for his guidance throughout a long academic career. Also, the author would like to thank Jeffrey Speakman of the Swanson Center for Product Innovation for his long hours of assistance with manufacturing of parts for the project and for his suggestions and expertise. The author would also like to thank Jakub Toman of the Chmielus lab for his assistance with material property testing. The author extends special thanks to his colleague, Alexander Howard, for his help with tabulating design specification data and for drawing system schematics. Finally, the author would like to thank his family for their lifelong support.

TERMINOLOGY

Throughout this paper, the terms “articulating column”, “arm”, “retractor arm”, and “column” may be used interchangeably to refer to the retractor arm itself. The column contains many ball and socket joints. The device as a whole, including the “arm” and supporting hardware box, will be referred to as the “retractor system”. The retractor tool at the end of the arm will be referred to as a “retractor blade” or simply “retractor”. When the term “link” is used, it refers to one component of the “arm” and one link contains a ball on one end and a socket on the other. Many “links” comprise a full length “arm”.

1.0 INTRODUCTION AND HISTORY OF SURGERY

Surgical procedures have been performed on human beings for the past 40,000 years, during the time when the first known tools were being developed from stone [37]. The first documented cases of human surgery occurred in France and involved trephining, which is the drilling of a small hole into the skull [14]. The practice occurred during pre-Classical times, dating as far back as 6,500 BCE [14]. The primitive surgery was considered a possible remedy for people thought to be possessed by spirits [14]. During ancient surgeries, men would hold or strap patients down, and the surgeon would use unsterilized tools to make incisions [9]. Neither the surgical environment nor the tools were sterile. Also, the concept of anesthesia had not been developed. Early surgeons would either perform the surgery with no sedative or offer the patient alcoholic beverages to drink or ice to locally decrease pain levels [9]. It was not uncommon for a patient to choose to let a condition run its course to death or even commit suicide to avoid a painful surgery [9]. Even if a surgery was performed successfully, there was a very large risk for potentially deadly post-operative infection [9].

The first significant advancements in surgery were made in the 16th century [9]. During this time, it was discovered that cleaning wounds with topical antiseptics was more effective at reducing infection risk than the traditional method of wound cauterization. Also, the use of sedatives became more common during this time. Improved tools were developed, including tissue retractors, which were developed to hold human tissue up and away from internal organs so that

proper exposure could be achieved. Despite improvements in surgical tools and wound treatment, as well as the development of anesthesia, the risk of post-operative infection was still high [9].

During the 20th century, considerable advancements were made in surgical tool development and sterilization [25]. During this time, three major methods for sterilization of medical equipment were developed. Currently, autoclaves are used regularly, and metal tools and instruments are sterilized by this method. Also, ethylene oxide is used for sterilization purposes. Finally, steam can be used to sterilize instruments. At the same time, antiseptics were developed and used to clean incisions and wounds. Surgical methods continued to develop and improve rapidly during the 20th century. Also, significant advancements were made in the surgical environment. Operating rooms are usually held under positive pressure and a sterile field is generated around the patient. To accomplish this, sterile drapes are used to divide sterile items and regions from unsterile items. Maintaining a sterile field greatly minimizes chances for post-operative infection. As surgeons attempted to perform new and more invasive surgeries, they realized that current instruments proved inadequate. This was particularly true for abdominal surgeries where it is difficult to achieve proper exposure of individual organs [25]. In fact, new surgical tools are constantly being developed to aide surgeons with virtually any procedure [25].

There are several steps to the modern, general, open surgical process [3]. Surgeries begin by preparing the patient and the surgical field, including the sterilization and preparation of medical instruments. After placing a patient under general anesthesia, verification of patient identity and procedure to be performed occurs. Next, an incision is made to expose the internal organs or structures of interest. A surgeon must be able to see the internal area where the surgery is performed, which is achieved by holding tissue and organs out of the way (i.e. retraction). The view of the operative area is called “the exposure,” or “surgical exposure,” the equality of which

represents one of the most important facets of surgery [15]. Regardless of whether the surgery is exploratory, for repair or resection, transplantation/implantation, or correcting physical structures, the surgeon must be able to hold the tissue out of the way using a retractor, while also having both hands free to perform the surgical procedure. Additionally, the vital signs of the patient must be monitored continuously, and sufficient clamping must be used to prevent excessive hemorrhaging.

1.1 RETRACTOR SYSTEMS

As surgeons began to perform more difficult, invasive surgeries, they began to realize that they lacked sufficient tools to perform surgery. With the adoption of sterile, "Listerian" surgical methods, the need for surgeons to retract tissue in the abdomen and pelvis blossomed [5].

Surgical retraction can be achieved in many ways. The earliest retractors, which appeared in the later 1800s, were hand retractors, some of which are still in use today [5]. As the name suggests, these retractors have a hand grip on one end and a retractor on the other. Typically, a medical student or resident will hold a retractor to keep the incision open, allowing both hands of the attending surgeon or senior resident to be free to perform surgery. The retractor blades come in various shapes and sizes. Some blades are more compliant than others and some contain lighting for deep surgical procedures.

A breakthrough in surgery was made when self-retaining surgical retractor systems were developed by Doyen in 1885 [5]. "Self-retaining retractors," as the name suggests, do not require a person to hold the incision open. They are either mounted to the surgical table, or wedged between the two sides of the incision and held in place by tissue restoring force. Self-retaining retractors continued to evolve, including ones by W.W. Keen (1894), MacCormac (1903),

followed by the Balfour retractor (1912), which is still in use today [5]. All of these retractors are wedged inside of the wound, confining retraction to the plane of the retractor itself. The first self-retaining retractor system that had acceptance in this country was the Balfour retractor, developed in 1912 [11]. This device is explained in detail in a subsection to follow. The next self-retaining retractor system was known as the Smith retractor. This device contained a circular ring from which retractors were mounted, which set the Smith retractor apart from its predecessors. The ring was mounted over the patient by attaching to the hospital bed on either side. Retractor blades were mounted to this ring, providing outward as well as upward retraction of tissue [28], [5]. Most retractors in use today are adaptations of the Smith retractor. Since the 1960s, self-retaining retractor systems have continued to evolve [5]. In fact, there are four main self-retaining systems available today that specialize in application to open abdominal surgeries [32]. These are highlighted below.

1.1.1 The Thompson Retractor

The first major surgical retractor system to gain popularity is known as the Thompson Retractor, developed and patented by Richard C. Thompson, M.D. in 1965 [34] as the first table-mounted surgical retractor system. Thompson developed the idea for his retractor after watching tonsillectomies being performed on children using a mouth gag [12]. He was concerned that there was no way to hold the gag without the weight of the tool resting on a child's chest. Dr. Thompson also noticed that other tools in operating rooms operated on the principle of a universal joint, allowing them to be easily adjusted in almost any position [12]. These ideas are what ultimately lead Dr. Thompson to develop his retractor. The Thompson Retractor is currently manufactured

by Thompson Surgical Instruments, and it is commonly used in most open abdominal procedures; particularly for open appendectomies, hernia repairs, and abdominal reconstructions [24]. The Thompson Retractor is also commonly used in transplant surgeries due to its ability to be adjusted for large incisions [24]. The Thompson retractor contains 60 parts that must be accounted for before, during, and after a surgical procedure [2]. It is highly effective, but initial setup of the system can be time consuming and complex. Also, components of the system can often interfere with a surgeon's reach, especially for shorter surgeons. It is worth noting the complexity of the system as pictured in Figure 1. All components of the retractor system must be assembled an adjusted properly before a surgical procedure can begin, requiring valuable, life critical setup time.

Figure 1. Thompson Retractor System (*Source: [24])*

1.1.2 The Bookwalter Retractor

The next breakthrough in surgical retraction came when John Bookwalter, M.D. developed the idea for a single post surgical retractor. After falling asleep while holding a hand retractor as a surgical resident, he realized that a system could be developed to hold a retractor more securely and steadily [15]. Dr. Bookwalter resented that medical students were often only used to hold handheld surgical retractors, because this meant that they could not gain experience with practicing surgeries as a student. This inspired him to develop and patent a retractor system that mounted to the side rails of an operating table by a single post that held a notched ring over the patient [8]. Dr. Bookwalter was awarded a patent for his device in 1981. The Bookwalter Retractor is also primarily used for open abdominal procedures [7]. Note in Figure 2 that the Bookwalter Retractor uses a single, substantial main support post while the Thompson Retractor uses two supporting posts. The device is currently manufactured by Symmetry Surgical, Inc, and BR Surgical [6], [33]. Although his original design featured two posts, after experimentation, he realized that it performed just as well with only one supporting post. Retractors could be securely placed along the notched ring, freeing the hands of the surgeon and residents to assist with the surgery itself. Although it contains fewer pieces than the Thompson retractor system, the Bookwalter retractor system still contains 30 parts [2] and requires minutes to setup, even for experienced surgeons. Also, as the exposure needs change, periodic readjustment of the system is necessary during most procedures. One major downfall of the Bookwalter system is due to the nature of having to work through the notched ring that holds the retractors. Shorter surgeons will sometimes stand on a step stool to achieve a better view through the ring [27]. Also, the ring can inhibit residents from being able to assist surgeons, since working space is limited.

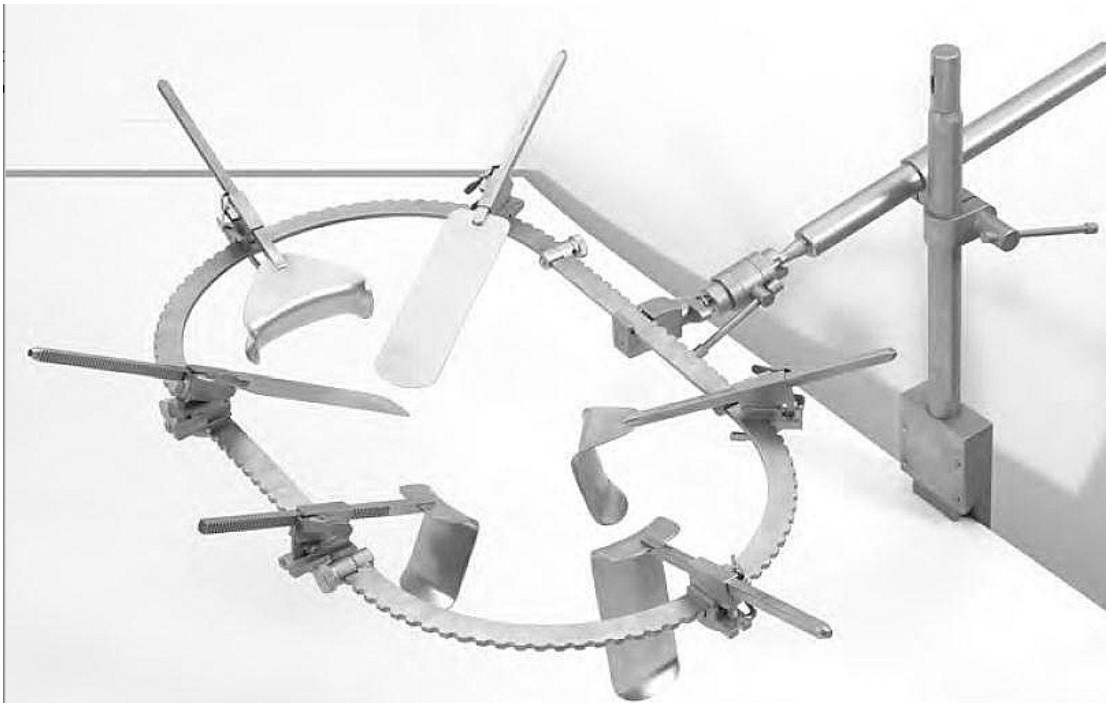

Figure 2. Bookwalter Retractor System Setup with the Largest Available Ring (*Source: [6])*

1.1.3 The Omni-Tract Retractor

Another commonly used retractor system is the Omni-Tract retractor system. Patented by Samuel Pelta in 1990, this system contains a post that secures to an operating table rail in as similar manner to the Bookwalter system [21]. The Omni-Tract retractor system is largely used for vascular surgeries [2]. In lieu of a ring, two bent support rods form a wishbone appearance and are used to mount surgical retractors (Figure 3) [19]. The system also contains another rod mounted on hinges, which can be used to close the wishbone if more retraction is needed [30]. This system is currently manufactured by Integra. Like the Bookwalter and Thompson retractor systems, the

Omni-Tract system can be used on a wide range of patient sizes and it can be used for any open abdominal surgery. The Omni-Tract retractor system contains fewer parts than the Bookwalter and Thompson kits. In fact, the Omni-Tract retractor contains only 10 parts; however, this system offers less flexibility than the Bookwalter and Thompson systems [19].

Figure 3. Omni-Tract Retractor System (*Source: [19]*)

1.1.4 The Balfour Retractor

A final retractor system that is commonly used for open abdominal surgeries is known as the Balfour retractor system. It was developed in the early 1900s by Donald Church Balfour while practicing surgery at the Mayo Clinic [11]. It is currently manufactured by Miltex. It features two

fenestrated loops at its ends which are used to spread tissue to hold an incision open. These loops are pushed apart, and a ratcheting mechanism holds them in place. Between the two loops is a retractor that retracts tissue in a third direction in order to obtain adequate surgical exposure (Figure 4). This retractor system contains only three main components; far fewer components than the Omni-Tract, Bookwalter, and Thompson systems [4]. It is quite commonly used during Cesarean sections; where the abdominal cavity must be held wide open in order to deliver a child [16]. Unlike the other systems, the Balfour retractor system is also used frequently in veterinary medicine [39].

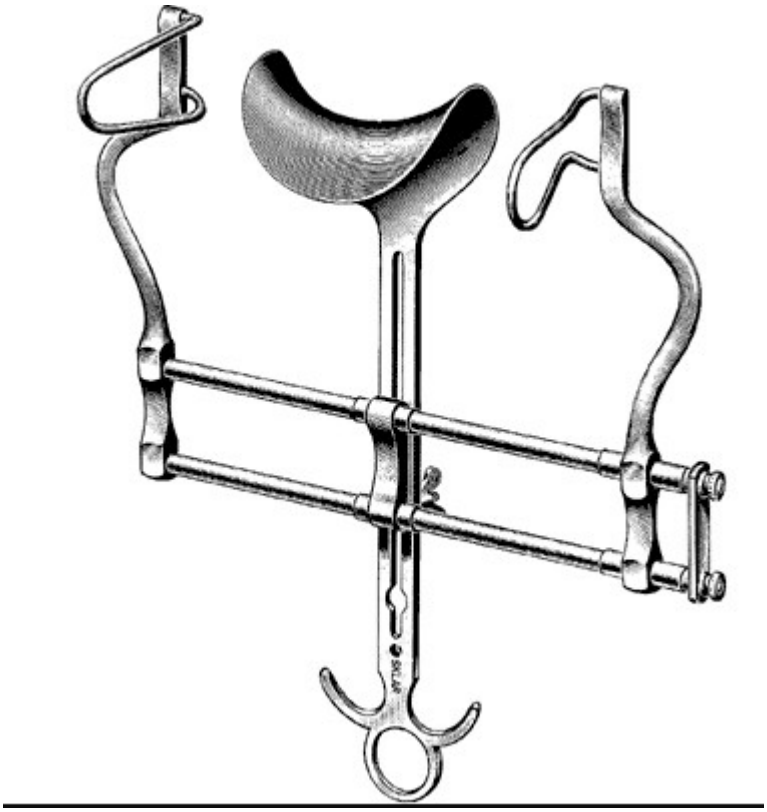

Figure 4. Balfour Retractor System (*Source: [4])*

After numerous interviews with practicing surgeons, it was determined that Thompson and Bookwalter retractor systems are currently the two most commonly used retractor systems for open abdominal procedures [13]. The Omni-Tract system is also used, but less frequently. The Balfour retractor system is often limited to OBGYN related procedures [16]. Selection of one kit over another is often dependent on preference of the surgeon. Surgeons will often be introduced to and gain experience with a particular retractor system during residency and use it throughout their entire career. Although the Thompson and Bookwalter kits are highly effective, they have a few shortcomings. Both kits contain many pieces; therefore, initial setup of the devices is time consuming and difficult. This is a particularly significant issue during trauma situations, because every minute is critical for patients suffering from significant internal injuries. Also, these kits often require readjustment during a procedure as exposure needs change or if components of the retractor kit are moved accidentally. Finally, while performing a procedure with one of these kits, all pieces of the kit must be counted numerous times during the procedure. This is to verify that one of the many metal pieces of the retractor kit does not inadvertently remain inside the patient after closing the incision. If the part counts do not match for any reason, an x-ray must be performed on the patient to determine whether a component was left inside the patient. While the Bookwalter and Thompson kits are highly effective, setup time is lengthy, taking away precious time that is critical to the survival of an injured patient. In fact, many surgeons still opt for handheld retractors, especially if adequate medical personnel are present to assist with the procedure. After conducting approximately 50 interviews with practicing surgeons, it was determined that while most of them use either the Bookwalter or Thompson kits, surgeons wish that these retractor kits were easier and less time consuming to setup and use [13]. Most surgeons admitted to having

difficulty using these devices at times during certain procedures, and wished that there was an easier and faster alternative to these traditional retractor kits.

The Sounds, Systems, and Structures laboratory was approached by surgeons with a need for the development of a retractor system that is faster to setup and easier to use than existing retractor systems that were developed in the 1960s and 1970s. While completing his residency requirements as a medical student, Peter Allen, M.D. developed the concept of a rapidly deployable surgical retractor that may be able to replace the Bookwalter and Thompson systems. The system would always be “at the ready”, requiring mere seconds to assemble compared to the several minutes required by other systems. This new method of supplying surgical retraction can meet the needs of surgeons, as it can perform similar tasks to handheld, Thompson and Bookwalter kits, all while being easier to use and reducing setup time. In order to meet the needs of surgeons, design specifications were developed.

The remainder of this paper is organized as follows. In Chapter 2.0, the retractor system design requirements are discussed, including both functional and mechanical requirements. After that, the actuation mechanism is discussed in Chapter 4.0. This includes the selection of a pneumatic cylinder, the pneumatic and electrical designs and packaging. Chapters 4-6 focus on the design of the articulable column, including the strength (Chapter 3.0), geometry and friction in the links (Chapter 5.0), and the design of an adapter that allows Bookwalter blades to be used with this new device (Section 6.1). Finally, conclusions are drawn in Chapter 7.0.

2.0 RETRACTOR SYSTEM DESIGN REQUIREMENTS

After performing customer discovery interviews with other surgeons, design requirements for the new surgical retractor system were dictated by consumer need and potential effectiveness of the device when used for open abdominal surgeries [2], [3], [27]. Retraction force required varies between type of procedure and can also be surgeon-dependent [2]. Sternal retraction is noted for its high force values, ranging between 60-80 lbf [36], while most abdominal procedures require between 10-20 lbf [36]. Retractor force was measured with three surgeons using a luggage scale. When a normal or average sustained amount of force was requested, the measurements ranged from 14-18 lbf, while when the maximum expected (short duration) force was requested, it ranged about 32-35 lbf. Thus, a value of 20 lbf was chosen for the design specification of this device. An overall system factor of safety was specified for safe operation of this device based on the yield stress of individual components. This section outlines these design requirements in detail and specifies their meaning. In other discussions with surgeons, the maximum permission deflection (or relaxation after positioning the arm) is 0.4 inches.

2.1 FUNCTIONAL DESCRIPTION OF RETRACTOR

This new, rapidly deployable retractor system consists of a motor box that mounts to the side of an operating table, an attached articulating column, and a retractor blade at the end, as schematically depicted in Figure 5. The box, or boxes (if multiple retractors are desired), would

typically be mounted to an operating room (OR) bed rail as part of the normal OR preparation. The box(es) could also permanently reside on tables, particularly if used for emergency surgeries.

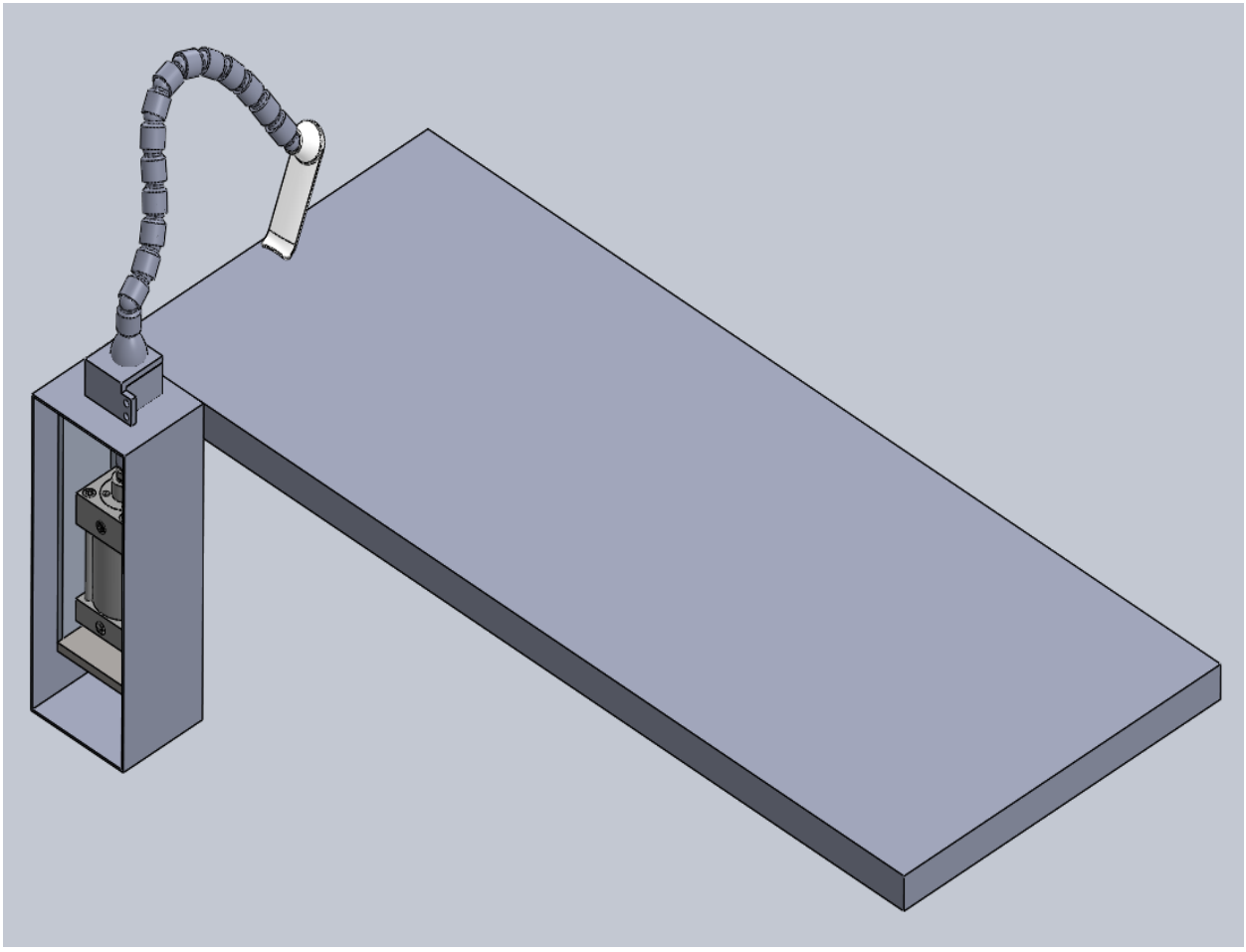

Figure 5. CAD Rendering of Retractor System attached to an OR table

2.1.1 Overview of Device Function

As can be seen in Figure 5, the two main components of the retractor system are the base "motor box" and the articulating column. Composed of ball and socket joints, the column contains an integral cable routed through its center. When a tensile preload is applied to the cable, an equal magnitude compressive load is generated within the ball and socket joints of the column. This load generates sufficient friction within the joints to allow the column to become rigid and retract human tissue to achieve proper surgical exposure. When the load is released, the column can be easily and quickly moved to improve surgical exposure as a surgery progresses. The columns can be either disposable or reusable, and are autoclavable if chosen to be reused [17]. The base can be reused for many surgeries. Columns quickly mount to the base quickly and easily via a sliding lock mechanism. A keyway connected to the linear actuator receives the integral cable when the column is installed, ensuring a one-step installation process.

2.2 FUNCTIONAL REQUIREMENTS

The design requirements for the new surgical retractor system include a maximum required retraction force (treated as a radial force for worst case mechanical scenario), a maximum arm deflection, a minimum arm length and a minimum overall system factor of safety (FOS) based on the yield stress of individual system components.

Table 1. System Design Requirements

Arm Length	Retraction Force	Maximum Allowable End Deflection	System FOS
36 in	20 lbs.	0.4 in	3
91.44 cm	89 N	1 cm	3

2.2.1 Arm Length

The length of the modular arm must be at least 36 inches long. This length starts at the pneumatic actuator base attachment and ends where the abdominal retractor is attached to the retractor arm (at the end of the arm).

2.2.2 Retraction Force

To be discussed in section 4.1.1, tension is applied to the cable to achieve arm rigidity and ultimately retraction force. It was determined that up to 230 pounds of force will be applied to the internal retractor arm cable. This force places the cable in tension, and the links in compression. It is under this preload that the arm must be able to withstand 20 pounds of radial force (force at a right angle to the modular arm); this force number comes from the required 20 pounds of force necessary for most abdominal retractions required for abdominal surgeries. This force is applied at the full length of the arm (36 inches), meaning that the arm must support a moment of 720 in-lbf at the lowermost joint.

2.2.3 Allowable Deflection

As mentioned in section 2.2.2, the retractor arm must be able to withstand a radial load of 20 pounds applied at its 36-inch length, or equivalently, a 720 in-lbf moment at the proximal ball/socket joint. Under these conditions, the arm must deflect no more than about 0.4 inches in any direction. The deflection could be due to bending or joint compression/slippage.

The twenty-pound load is applied radially at the distal end, which is considered to be a worst-case scenario. The result of such a loading condition while the arm is fixed at its base can be idealized as a cantilever beam subject to a tip load. The result is that the arm is placed in a state of bending. Deflection of a cantilever beam is predicted by Equation (2-1), where *P* is the tip load, *L* is the length of the arm, *E* is Young's modulus, and *I* is the effective area moment of inertia, which varies along the length of the link and thus arm (*z*-axis).:

$$\delta = \frac{PL^3}{3EI} \tag{2-1}$$

Figure 6 shows the cross section of the current link design. The area moment of inertia for a retractor link can be approximated as [35]:

$$I(z) = \iint_{r_1}^{r_2} r^2 dA(z) \tag{2-2}$$

where r_1(z) and r_2(z) are respectively the inner and outer radii of the links, at a particular location of the link, *z*, *r* is a variable of integration, and d*A*(*z*) is a differential area element. Since *I*(*z*) varies along the length of the link, Equation (2-1) would not apply, and instead deflection would be obtained from the principle of virtual work as

$$\delta = \int_0^L \frac{M(z)m(z)}{EI(z)} dz \tag{2-3}$$

where *M(z)* is the real moment distribution, *m(z)* is the virtual moment distribution, and *I(z)* is given in Equation (2-2) [35]. Rather than deal with the complexity calculations of *M*(*z*), *m*(*z*), and *I*(*z*) for the variable axial cross section of the current link design, an average value for *I* in Equation (2-1), $\bar{I}$, was determined experimentally. This value was also determined numerically in ANSYS. This value would theoretically be calculated as

$$\bar{I} = \frac{1}{l}\int_0^l I(z)dz \tag{2-4}$$

where *l* is the length of a link or the entire arm [35]. The experimentally and numerically determined values for $\bar{I}$, agreed well with an approximate *I* obtained from assuming average values for r_1=0.22 in and r_2=0.61 in in Equation (2-1). For this case,
Equation (2-2) simplifies to [35]:

$$I = \frac{\pi}{4}(r_2^4 - r_1^4) \tag{2-5}$$

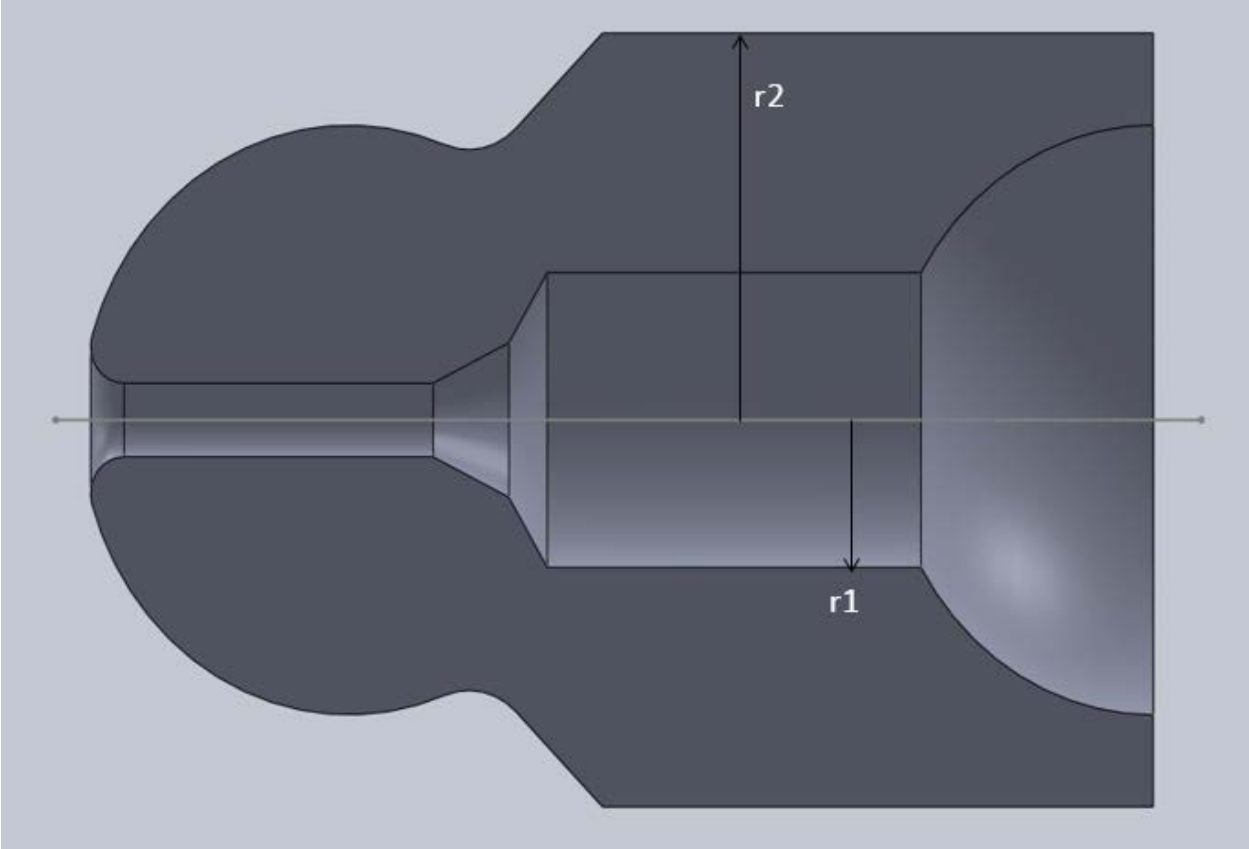

Figure 6. Axial cross section of current link design showing variable radial cross section

2.2.4 System Factor of Safety

The standard minimum factor of safety of three is assumed for this work. Some items will obviously exceed this value, but the overall system factor of safety is determined by the individual component with the lowest factor of safety. There are many components within the retractor system, and the individual factor of safety of any component based on yield stress must not fall below a value of three in order to maximize patient safety by preventing any possibility of failure during use. Factors of safety in all components are based on stress.

3.0 MATERIAL PROPERTY TESTING AND MODELING

Many different materials and manufacturing techniques were considered for the retractor system. Consideration was given to mechanical properties, including coefficient of static friction, elastic modulus, and flexural modulus. The arm of the retractor system represents a cantilevered beam subject to a bending load. Cantilevered beams have a well-defined deflection behavior when subject to a bending load. The deflection is inversely proportional to the flexural stiffness, *EI*, where *E* is the material's modulus of elasticity, a material property, and *I* is the area moment of inertia, a geometric property that is proportional to the radius to the fourth power (see Equation (2-5)). Most isotropic materials have published values for modulus of elasticity. These values are well documented for common metals. For polymers, moduli of elasticity are not always tabulated. Instead, a flexural modulus is provided. For isotropic materials, the flexural and elastic moduli are usually identical. For polymers, the flexural modulus can be up to 30% higher than the material's modulus of elasticity [20] due to anisotropy. Due to the lack of knowledge of elastic moduli for the polymers that were tested, material testing was performed.

3.1 ELASTIC MODULUS TESTING

In order to meet deflection criteria, a flexural stiffness, *EI*, of 777 kip-in^2 is required for the retractor arm. Since the moduli of some of the tested plastics were not published, specimens were tested in a universal testing machine. These specimens were manufactured from PEI, PMMA, and glass fiber reinforced polycarbonate according to the ASTM E8 standard, with circular cross section of diameter 0.25 inches [31]. Two specimens of each material were tested on an MTS 880 machine. One was at 50 μstrain/minute (5%/min) and the other was measured at 2,000 μstrain/min (200%/min), in order to consider the effects of the rate of loading. To ensure uniaxial loading, circular wedge grips were used to grip the specimen in the MTS machine. Strain was measured using an extensometer, while load was measured by the MTS system's load cell. Data files containing load and strain data were created and imported into Microsoft Excel for analysis. Engineering stress was calculated from load and cross-sectional area. Next, engineering stress versus strain plots were created (Figure 7, Figure 8, and Figure 9) for both strain rates of each material. The shapes of the curves at 5%/min (orange markers in Figures 7-9)) strain rate are generally consistent with ductile materials. PMMA (Figure 7) and PEI (Figure 8) seem to exhibit drawing phenomena at strains above 100 μstrain, while the FR-PC (Figure 9) is more consistent with a tough polymer. The test results at higher strain rate (blue markers in Figure 7, Figure 8, and Figure 9) rates were generally consistent, except that the PMMA exhibited a higher modulus and brittle fracture at 200%/min strain rate, which is expected for acrylic [40]. It is important to note that the links are loaded in compression rather than tension when cable preload is applied. Brittle materials, such as PMMA, have higher elastic modulus in compression than in tension. This is

because crack propagation is less severe in compression than in tension; therefore, more pressure can be tolerated in compression before failure. Due to this, the tensile tests represent a worst case elastic modulus estimate [35].

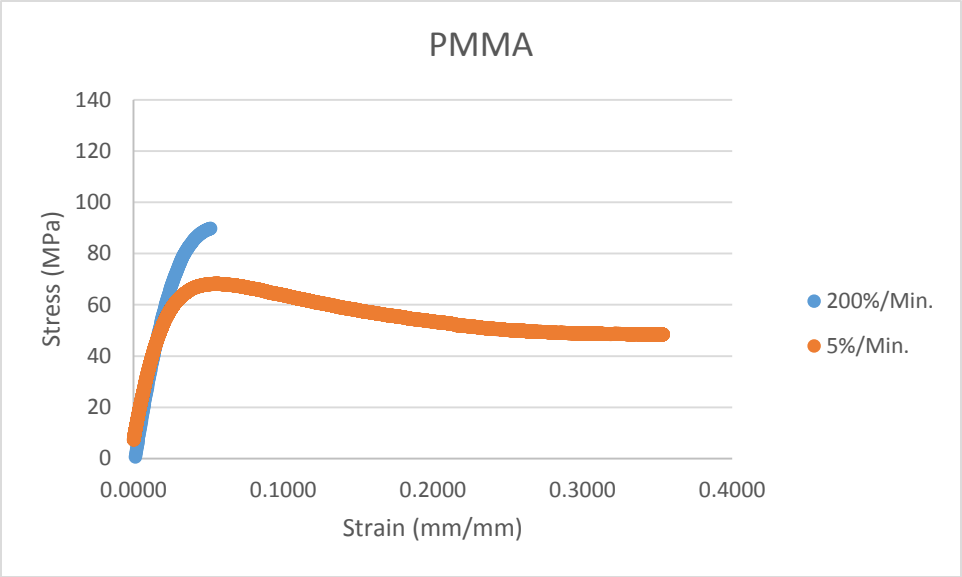

Figure 7. Tensile Testing Results for PMMA at 5%/min and 200%/min

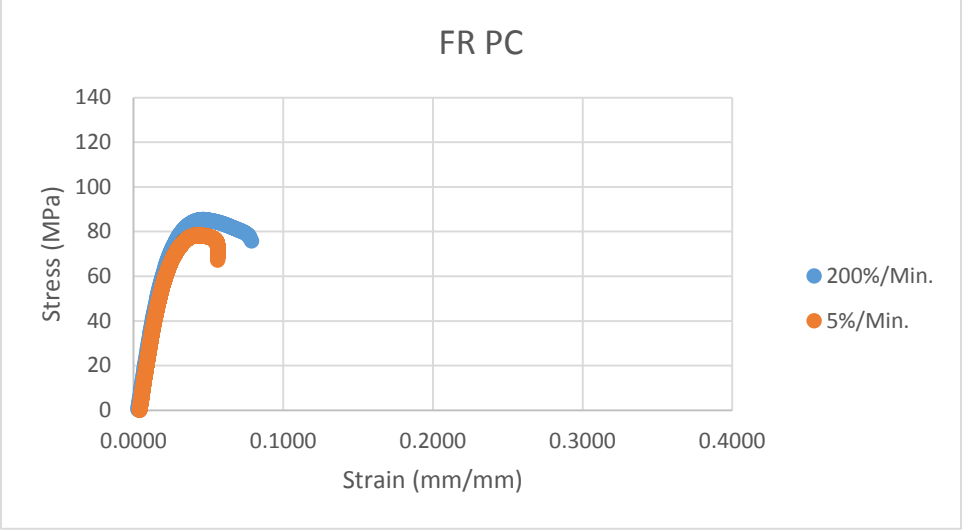

Figure 8. Tensile Testing Results for FR PC at 5%/min and 200%/min

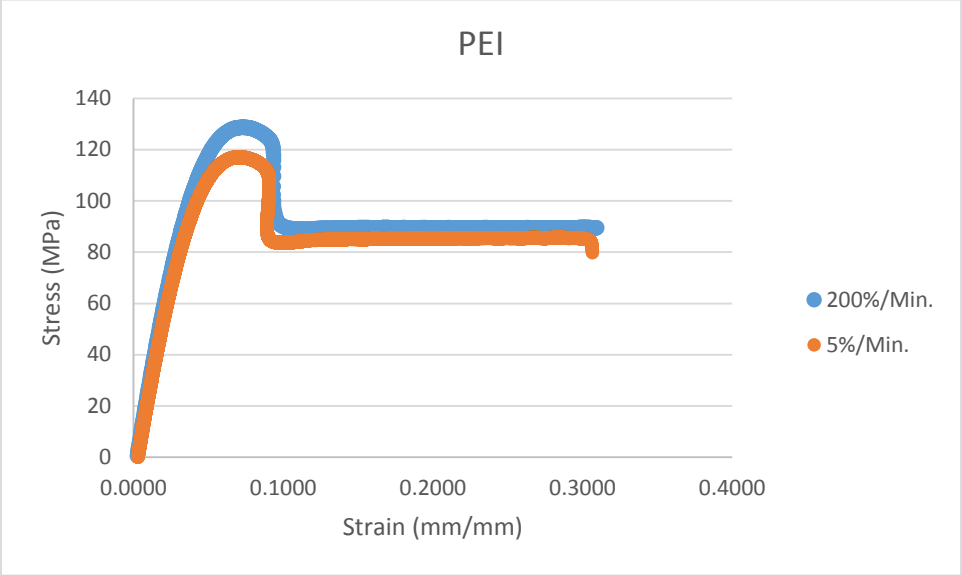

Figure 9. Tensile Testing Results for PEI at 5%/min and 200%/min

To estimate the materials' elastic moduli, data points were selected in the near linear range of the stress-strain plot. These approximately linearly elastic regions of the plots were fitted with a trendline, the slope of which represents the elastic modulus of the material by Hooke's Law. These modified plots are shown in Figure 10, Figure 11, and Figure 12. Similar plots for 200% strain are included in Appendix A. The experimentally determined moduli were similar for both strain rates. A summary of the measured elastic moduli, which range between 3.20-4.36 GPa, is given in Table 2. In the interest of minimizing machining time and cost, one sample per strain rate of each polymer was tested. In total, six specimens were tested. Two samples of each polymer were machined and tested; one at 5%/min strain rate and the other at 200%/min strain rate. PMMA exhibited somewhat (18%) higher modulus when pulled at the higher strain rate, while the other two were relatively insensitive to rate. This result is not surprising, considering the brittle fracture

noted at the higher strain rate for PMMA. Although the FR PC was stronger, even higher moduli were expected.

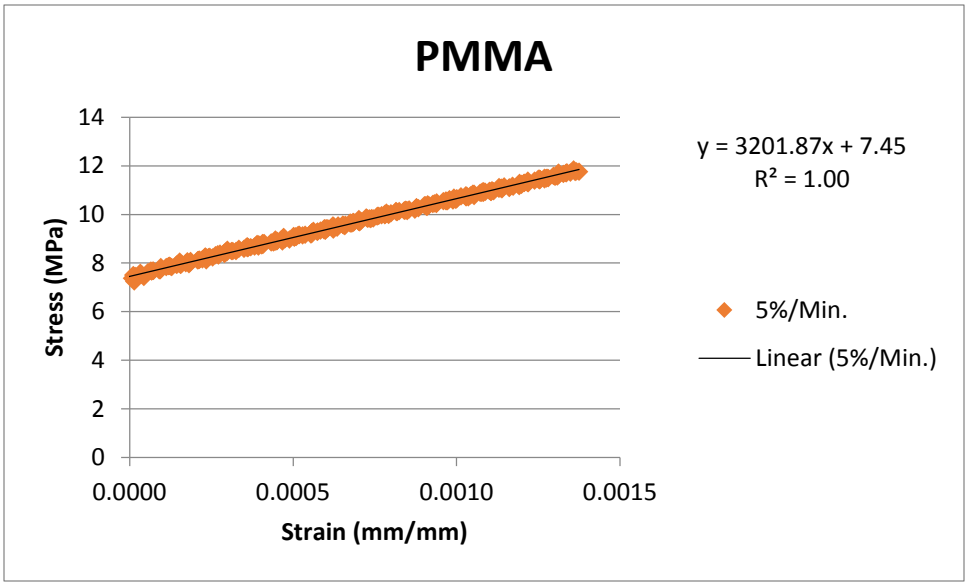

Figure 10. PMMA Linear Region at 5%/min

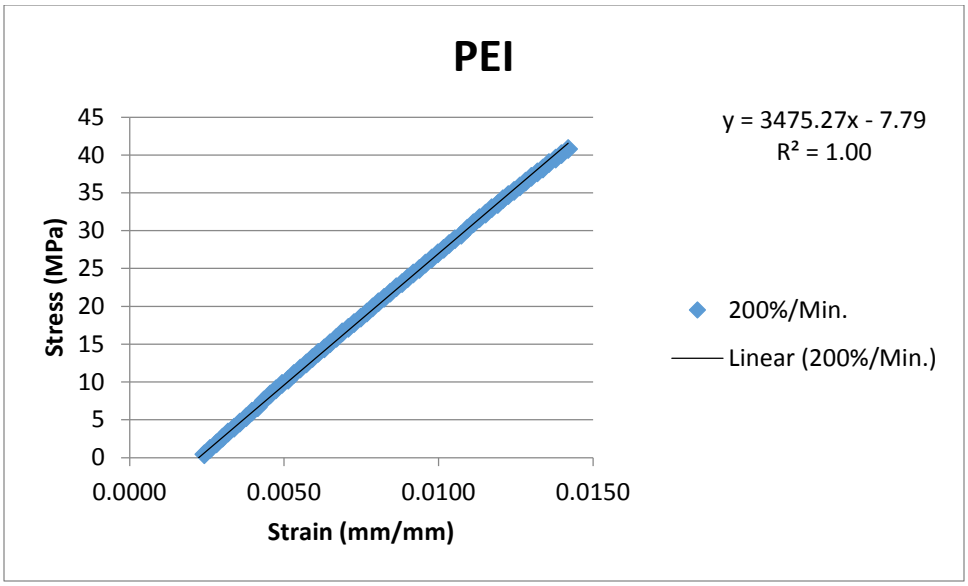

Figure 11. PEI Linear Region at 200%/min

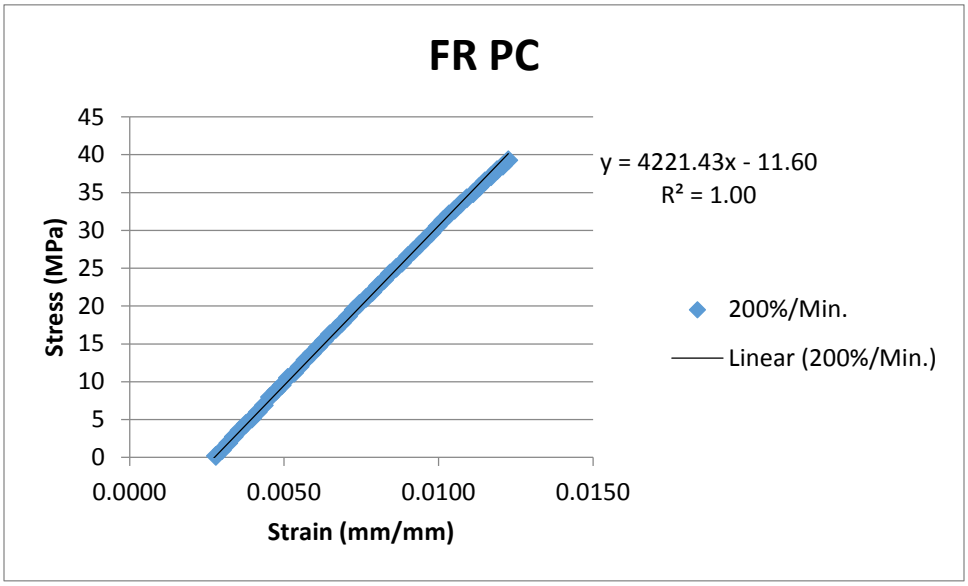

Figure 12. FR PC Linear Region at 200%/min

Table 2. Tested Elastic Modulus Values

Material	E (GPa) 200%/min Strain Rate	E (GPa) 5%/min Strain Rate
PMMA	3.78	3.20
PEI	3.47	3.43
FR PC	4.22	4.37

Since only one sample was tested at two different strain rates for each material, an aluminum specimen was machined and tested as a control. The results are shown in Figure 13. The computed modulus was 71 GPa, which is almost identical to the well-established value of 70 GPa.

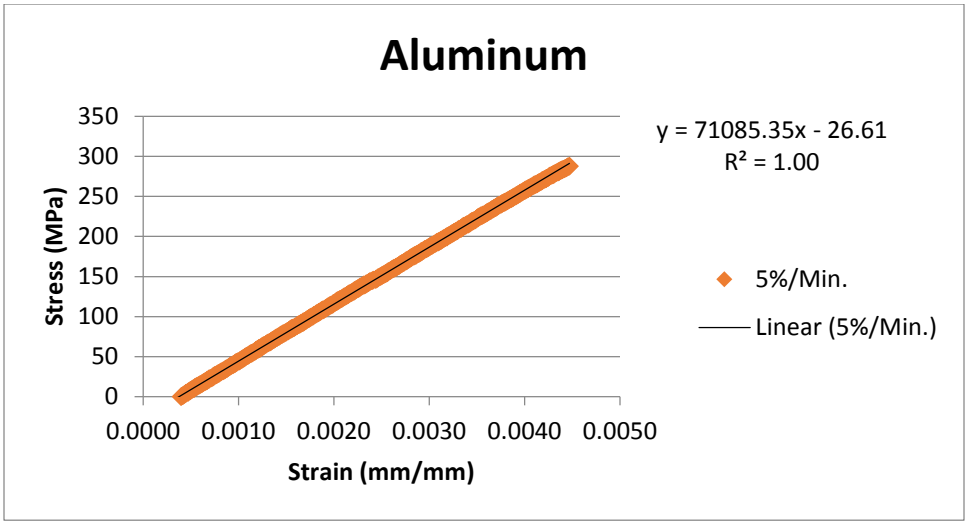

Figure 13. Aluminum at 5%/min

3.2 SIMPLE MECHANICAL MODEL OF ARTICULATING COLUMN

A simple model was developed in MATLAB to predict the beam deflection for the retractor system arm using Equations (2-1) and (2-4). Recall the arm is 36 in in length and has a 20 lbf tip load, and the material moduli were measured and given in Table 2. If tip-force/deflection measurements are made on the arm, then the average moment of inertia can be determined for the complex link geometry.

In Section 5.2, a deflection measurement test rig will be described that was used to measure deflection from tip loading on a shorter-scale arm with the actual, complex link geometry that was developed. The deflection test results will be presented in Section 5.2 and Appendix A.3. The test results are summarized in Table 3. Two trials were conducted for each material, where the force was increased in one-pound increments and the deflection recorded until the friction limit was exceeded. The average across all forces levels are given in columns 2 and 3 of Table 3 for each material. These values were then averaged in column 4 and the overall average of the averages and standard deviation are given in the last two rows of Table 3. Due to the complex geometry of the links, the area moments of inertia presented below were determined from Equation (2-1) using experimental data for E, P, L, and δ, where E was determined from material testing, P was the applied load by the test rig with values ranging from 0-20 lbf, L=7.48 in (19 cm), and δ was the deflection resulting from P as measured by the dial indicator in the test rig in Section 5.2.

Table 3. Effective Area Moment of Inertia

	Effective Area Moment of Inertia		
Material	**Trial 1 (m^4)**	**Trial 2 (m^4)**	**Average**
PEI	2.62E-08	2.55E-08	2.59E-08
PMMA	2.66E-08	2.89E-08	2.77E-08
FRPC	1.98E-08	2.02E-08	2.00E-08
		Overall Average	**2.45E-08**
		Overall Standard Deviation	**3.70E-09**

The MATLAB code, which predicts deflection versus modulus, is given in Appendix A.2. To simulate the required elastic modulus for a full-length arm, Equation (2-1) was solved in closed form. The result was that a full-length arm must be manufactured from a material with an elastic modulus of at least 13 Msi (90 GPa) if the current link design in Figure 6 is to be used. This is verified by the output of the model in Figure 14, considering a maximum deflection of 0.4 in for a 36 in long arm loaded with a force of twenty pounds. The horizontal line in the figure marks indicates 0.4 in of deflection.

As can be seen from Figure 14, the deflection curve has approached the horizontal asymptote at high modulus. In other words, further increasing the modulus will provide little decrease in deflection. A better approach would be to increase the area moment, which would shift the curve downward, such that the 0.4 in deflection would occur closer to the higher slope

region observed in the 1450-5800 ksi (10-40 GPa) range. In this case, increasing the modulus would have much more impact on reducing the deflection.

It is clear that for the current link geometry depicted in Figure 6 which had the experimentally determined area moment given in Table 3, the moduli of the plastic materials tested in the previous section (as PMMA, PEI, and fiber reinforced polycarbonate–Table 2) fall very short. These results were confirmed later when links were machined and tested from these materials. This shortcoming can be ameliorated with a stronger material, stronger geometry, or both. Despite the low modulus, plastics are used extensively throughout this work for development, given their low cost and ease of fabrication, and ability to conduct friction studies, despite their lower strength.

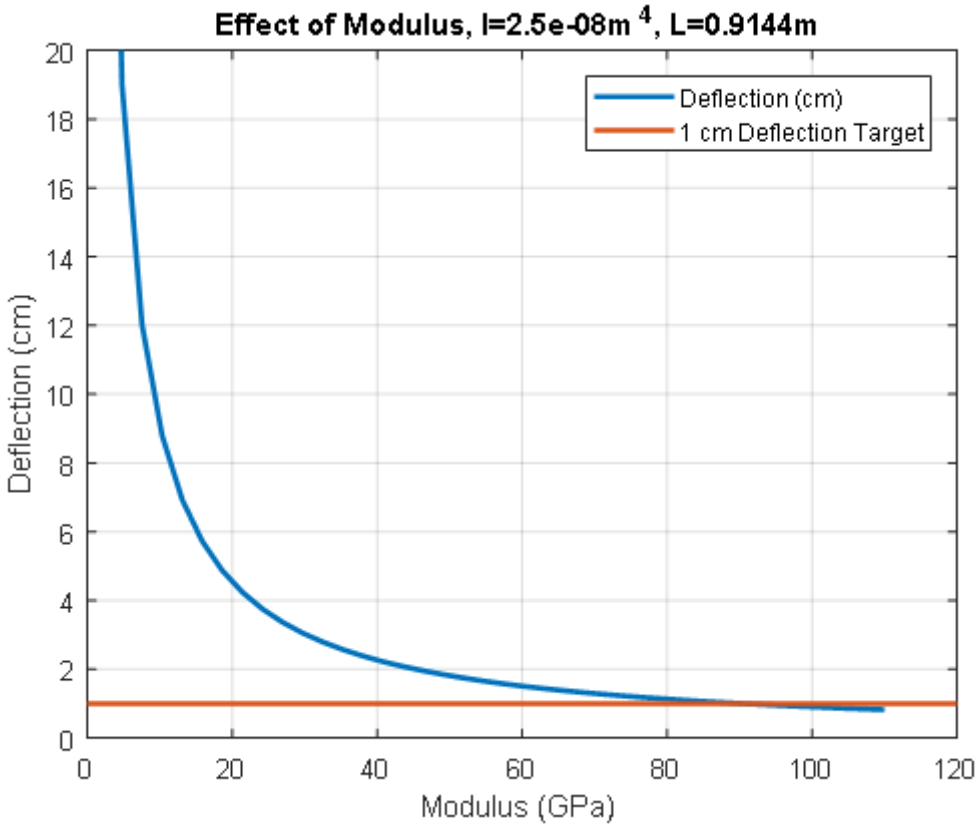

Figure 14. MATLAB Model of Deflection vs. Elastic Modulus

3.3 CABLE FRICTION MODEL

Recall that the integral cable passes through all links in a retractor arm assembly of a given length. Unless the retractor arm is perfectly straight, i.e. the relative angle between all retractor links is zero, the cable will rub against the inside walls of the sockets. This behavior results in parasitic loss of cable tension due to dry friction at each contact point of the cable. The highest cable tension is present at the base of the arm, in the region closest to the linear actuator, while the lowest tension is present at the distal end of the retractor arm. Since the largest bending moment

occurs at the base of the arm, where the cable force is highest, the parasitic losses may not impact slippage of the joints significantly. The frictional losses will increase with the angle of cable bend, such as a situation in which the retractor arm is placed at a severe angle to achieve a certain surgical exposure. A model of this frictional loss behavior for a single link can be found in Figure 15. In the top pane, the axial cross section of the link is shown, along with the cable (thicker, curved line), and the forces acting on the cable. The bottom pane shows just the free body diagram of the cable.

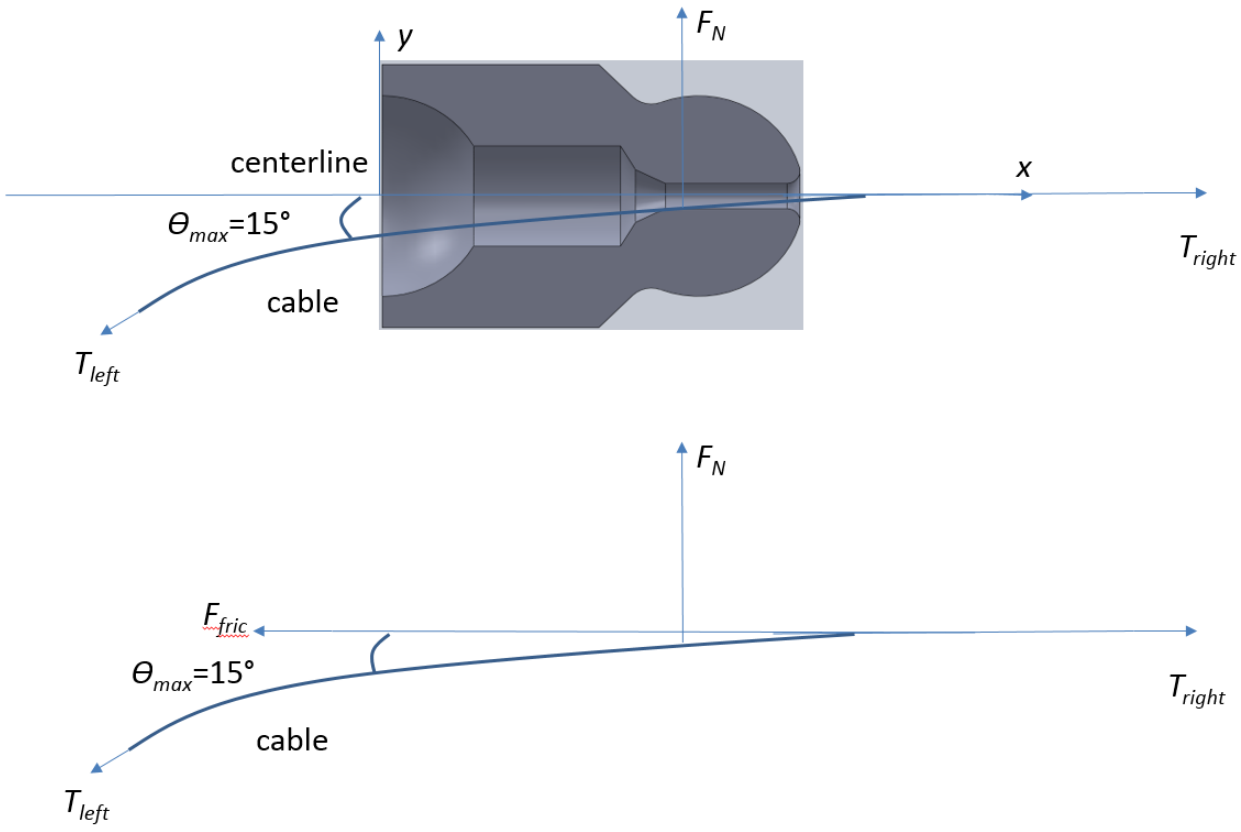

Figure 15. Frictional Losses within a Tensioned Cable

In Figure 15, the base of the arm would be towards the left and the tip is towards the right, such that cable tensions, $T_{left} > T_{right}$. If the interaction between the cable and the plastic is frictionless, then the assembly would act much like a pulley and T_{left} would be equal to T_{right}. However, there is a frictional force, F_{fric}, that is tangent to the cable at the point of contact. Therefore, T_{right} is smaller than T_{left} by an amount F_{fric} as:

$$T_{right} = T_{left} - F_{fric}. \tag{3-1}$$

The normal force, F_N is exerted in the *y*-direction onto the link for the case of the arm curved downward as shown. The geometry of the standard link design constrains the maximum angle between two links to 15 degrees. Therefore, the maximum normal force is:

$$F_N = T_{left} \sin(15^o) = 0.259\ T_{left}. \tag{3-2}$$

Then the maximum friction force (right at the edge of breakaway) would be:

$$F_{fric} = \mu F_N \tag{3-3}$$

where μ is the static coefficient of friction, which is typically around 0.4 for steel on a polymer [10]. Table 4 below gives common coefficients of friction between the materials considered in this work [10]. Note that the value for FR PC/steel was assumed to be equal to polycarbonate/steel, as there are many varieties of FR PC with varying percentages of glass fill. Considering Equations (3-2) and (3-3), maximum possible percentage loss in cable force is

$$\frac{F_{\text{fric}}}{T_{left}} = \frac{0.4\sin(15°)T_{left}}{T_{left}} = 10.4\% \quad \text{(per link)}. \tag{3-4}$$

Table 4. Material Coefficients of Friction [10]

Material Interface	Coef. Of Static Fric.
PMMA/PMMA	0.8
PMMA/Steel	0.68
FR PC/Steel	0.6
PEI/Steel	0.43
ABS/Steel	0.3
Al/Steel	0.35
Steel/Steel	0.54

While this result seems very significant, the reader is cautioned that this would only occur if the cable rubbed with a force that was equivalent to the frictional breakaway force. Nevertheless, it is clear that these frictional forces could be high enough to affect the operation of the arm.

A test was devised to measure the losses across the full 36-inch length of an arm, consisting of 18 links. A load cell was placed in between the actuator and cable, while an additional, "donut" style load cell was placed at the distal end of the column. The column was positioned at 0-degree (i.e. straight) (Figure 16), 90-degree (total, between base and tip) (Figure 18), and 180-degree (total, between base and tip) (Figure 20) angles and data from the load cells was recorded and plotted below. The blue bars represent tension at the column root while the orange bars represent tension at the end of the column.

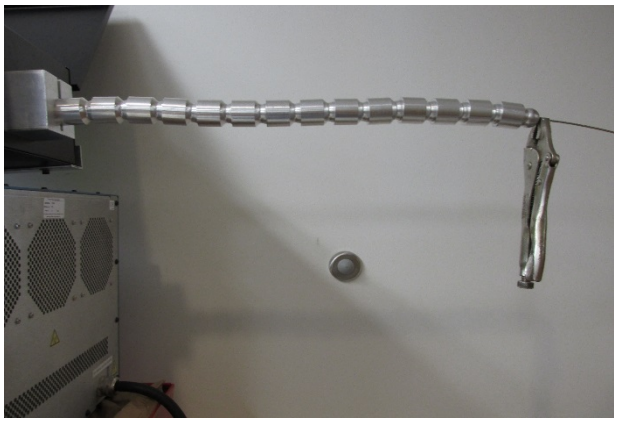

Figure 16. 0° Bend Test Setup

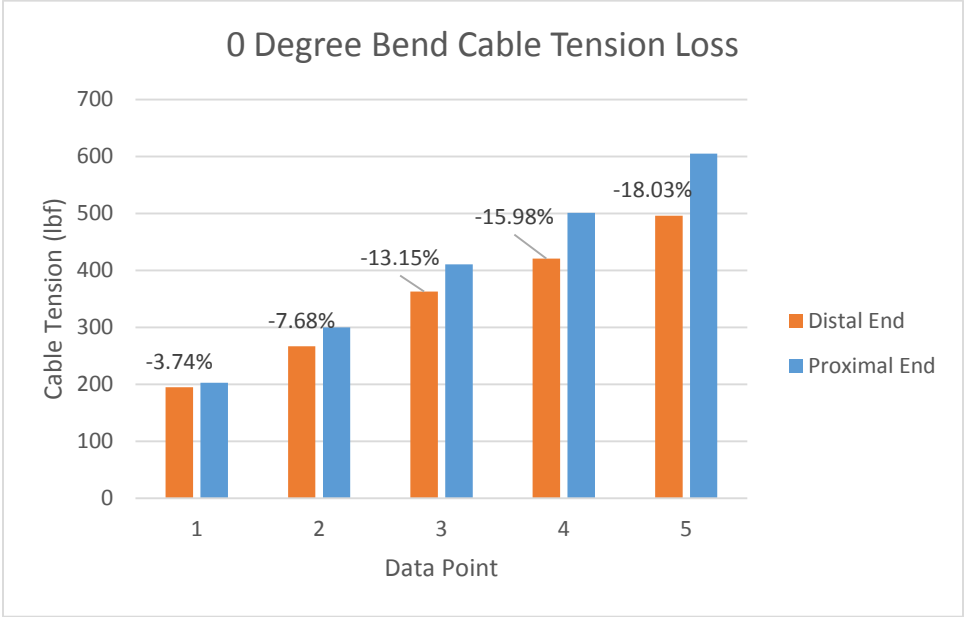

Figure 17. Plot of Frictional Loss for 0° Bend

Figure 18. 90° Bend Test Setup

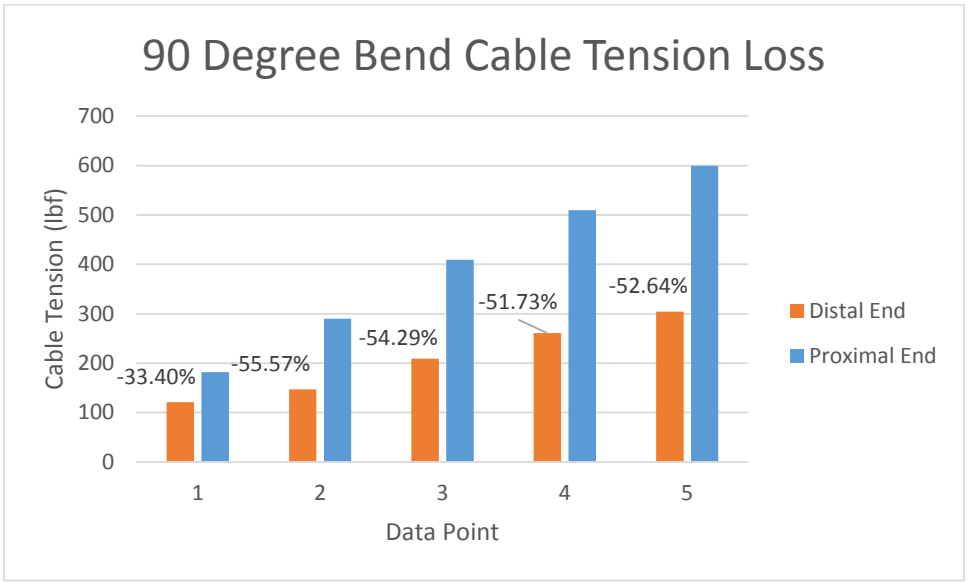

Figure 19. Plot of Frictional Loss for 90° Bend

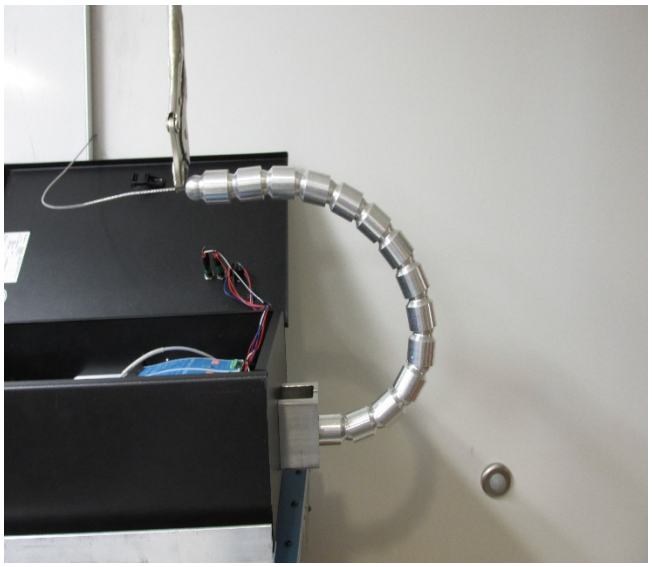

Figure 20. 180° Bend Test Setup

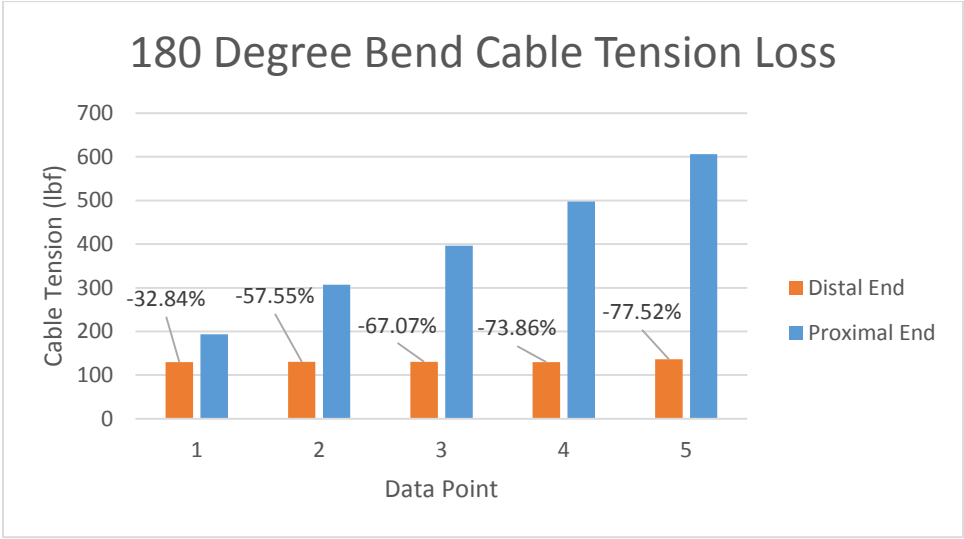

Figure 21. Plot of Frictional Loss for 180° Bend

It is observed from Figure 17 that frictional losses of up to 18% can occur in the arm, even if the arm features no bend. The cable clearance hole of the links is only slightly larger than the

cable diameter; therefore, some contact must occur even when the column is straight. Figure 19 and Figure 21 illustrate that the frictional losses are far greater as bend radius increases. In fact, over 50% of the root cable tension is lost at the tip when the column smoothly bends a total of 90°. Finally, nearly 80% of the root cable tension is lost when the arm is bent at a 180° angle. This is likely due to the fact that such a large amount of tension is lost at these angles that a small force change at the proximal end is not entirely reflected at the distal end.

4.0 ACTUATION MECHANISMS

Linear actuation was chosen to apply and release cable tension to the arm. The Generation I or "Gen-I" device featured an electrical linear actuator. The current, Generation II ("Gen-II") prototype features a pneumatic linear actuator. The author helped design and fabricate the Gen-I prototype as an undergraduate student and the Gen-II prototype development is the focus of this thesis. For completeness, some details of the Gen-I prototype will be given in places.

4.1 COMPONENTS OF GEN-I ACTUATOR

4.1.1 Mechanical System

The Gen-I retractor system prototype uses an electric linear actuator in order to supply mechanical preload to the articulating column. Supporting electronics are housed in the "motor box," which is shown in Figure 22. In the picture, the linear actuator can be seen along the horizontal centerline of the box. A structural steel "L" bracket supports the motor within the box. At the far right of the actuator, a white wire is seen attached to an in-line force gauge. Along the bottom, toward the left, the black motor housing can be seen with a silver tag on it. The rotary motor drives a worm gear that moves the actuator shaft left and right. Figure 23 shows the top of the motor box (attached to a hospital bed rail) with the arm (purple) mounted to the top. One of the limitations of Gen-I is the bulky size, as observed in the picture.

Figure 22. Internal View of Gen-I Design

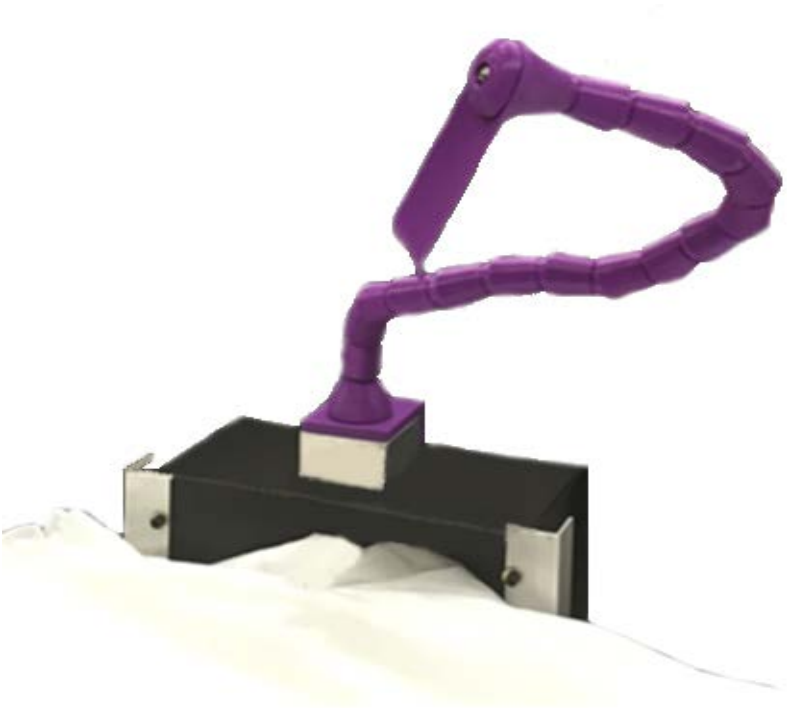

Figure 23. Gen-I Design

4.1.2 Electrical System

The components of the electrical system allow the column to achieve a specified preload within its joints to lock the retractor where it is placed during surgery. When the unit is energized, the arm is still flexible and can be placed by the surgeon. By pressing a footswitch, the motor is activated to apply cable tension, locking the arm in place. Pressing the footswitch again, toggles the force state in the cable, allowing the arm to be repositioned as many times as necessary.

The components of the electrical system can also be seen in Figure 22, a small, custom circuit that conditions the force gauge signal can be seen at the bottom, far-left corner. Toward

the middle bottom is a red microcontroller board with a custom developed transistor board below. Moving further along to the right are two relays and two powers supplies that are used to drive the motor. The force gauge was described above. These components are described in greater detail below.

At the core of the control system is the red, SparkFun RedBoard™ (Arduino) microcontroller [29]. Code was developed for the RedBoard to operate the linear actuator, as per the logic shown in Figure 24. This code implemented the state toggling between a tensioned and un-tensioned state. After installing an arm and energizing the unit, the user starts in the top left corner of the diagram. The blade at the end of the un-tensioned arm is used to retract tissue into place by the surgeon, and then the footswitch is pressed. When that occurs, power is supplied to the motor until a prespecified cable tension is achieved, and then the motor shuts off, representing the rigid arm state. The system again waits for a foot switch to be pressed (e.g. if the surgeon needs to reposition the arm), reversing the process by moving the motor outward for a specified time, and then the cycle repeats.

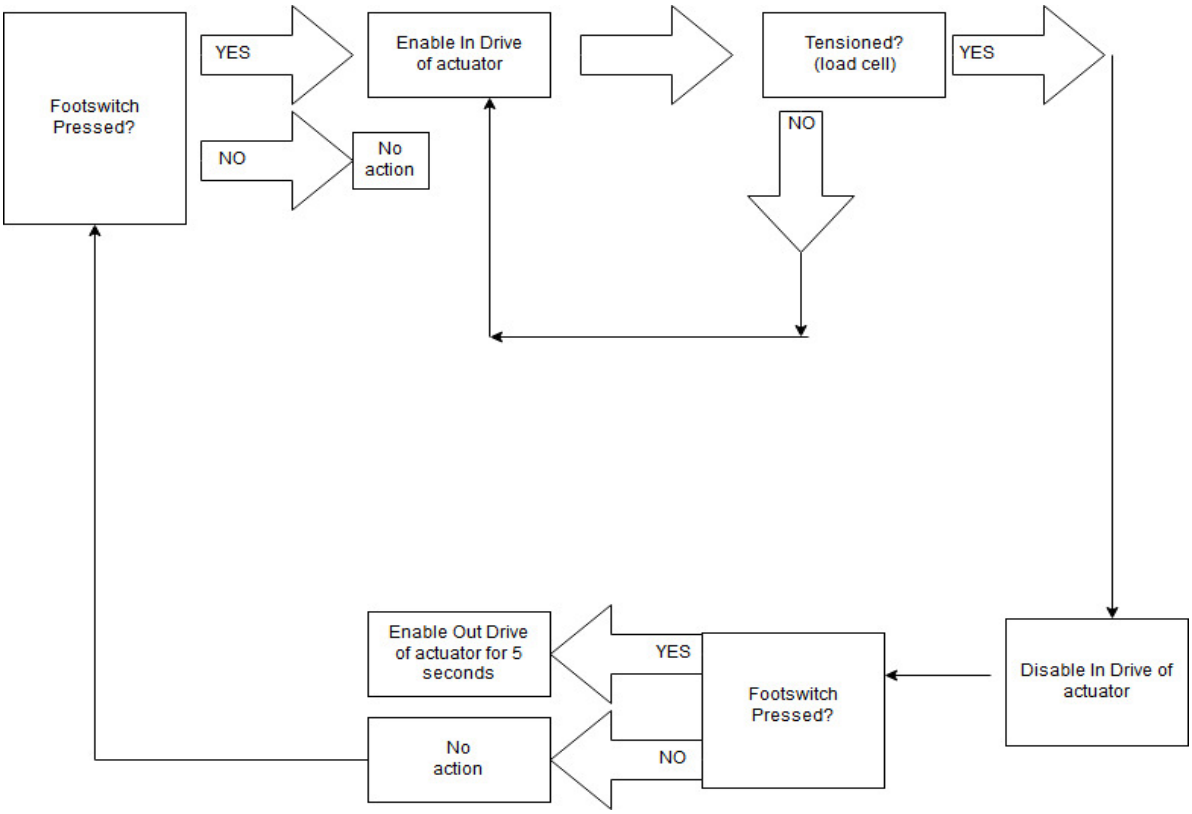

Figure 24. Arduino Microcontroller Logic Diagram

During the tensioning phase, the RedBoard™ supplied power to the drive electronics while simultaneously taking readings from the load cell on the in-drive channel. When the prescribed preset tension was achieved, the RedBoard™ disabled power to the drive electronics. The RedBoard™ performed the out-drive task for five seconds, and this allowed the retractor to be fully extended, until there is zero applied cable tension.

Two channels were needed, one for moving the actuator in each direction: an “in-drive” and an “out-drive.” The actuator’s power demands were 12 VDC at 10 A, which was far greater than could be supplied by the microcontroller. Therefore, a relay circuit with single pole, double throw relays (SPDT) was designed. Two Meanwell® model NDR-120-12 power supplies were

used to power the RedBoard™, actuator, and load cell. Both relays were actuated by the microcontroller; one relay served to change the direction of the actuator for tensioning and relieving tension in the column, while the other served as a power switch for the actuator. The RedBoard™ output 5 VDC; however, 12 VDC relays were used. To allow the Arduino to switch the higher voltage relays, two transistor drive circuits were designed using NPN transistors and 1 kΩ resistors; each outputting 12 VDC.

Finally, the Arduino's analog to digital converter was only able to accept voltages between 0-5 VDC (0-1024 bits). At full tension of the column, the load cell output was only 2.1 mV; therefore, a multi-stage, differential amplifier was developed to amplify the signal. It consisted of an input differential amplifier stage, followed by two inverting op-amp stages, and one non-inverting final stage, as shown schematically in Figure 25. Its effective gain was approximately 1,100; however, a potentiometer was used in the final stage to adjust the gain to the desired level. A TL084 quad op-amp was used to create this circuit. This amplifier produced a signal that was around 2.5 VDC at full column tension, thus more fully utilizing the input range of the RedBoard. The final prototype performed as expected, and the electronics proved to be fully functional and reliable.

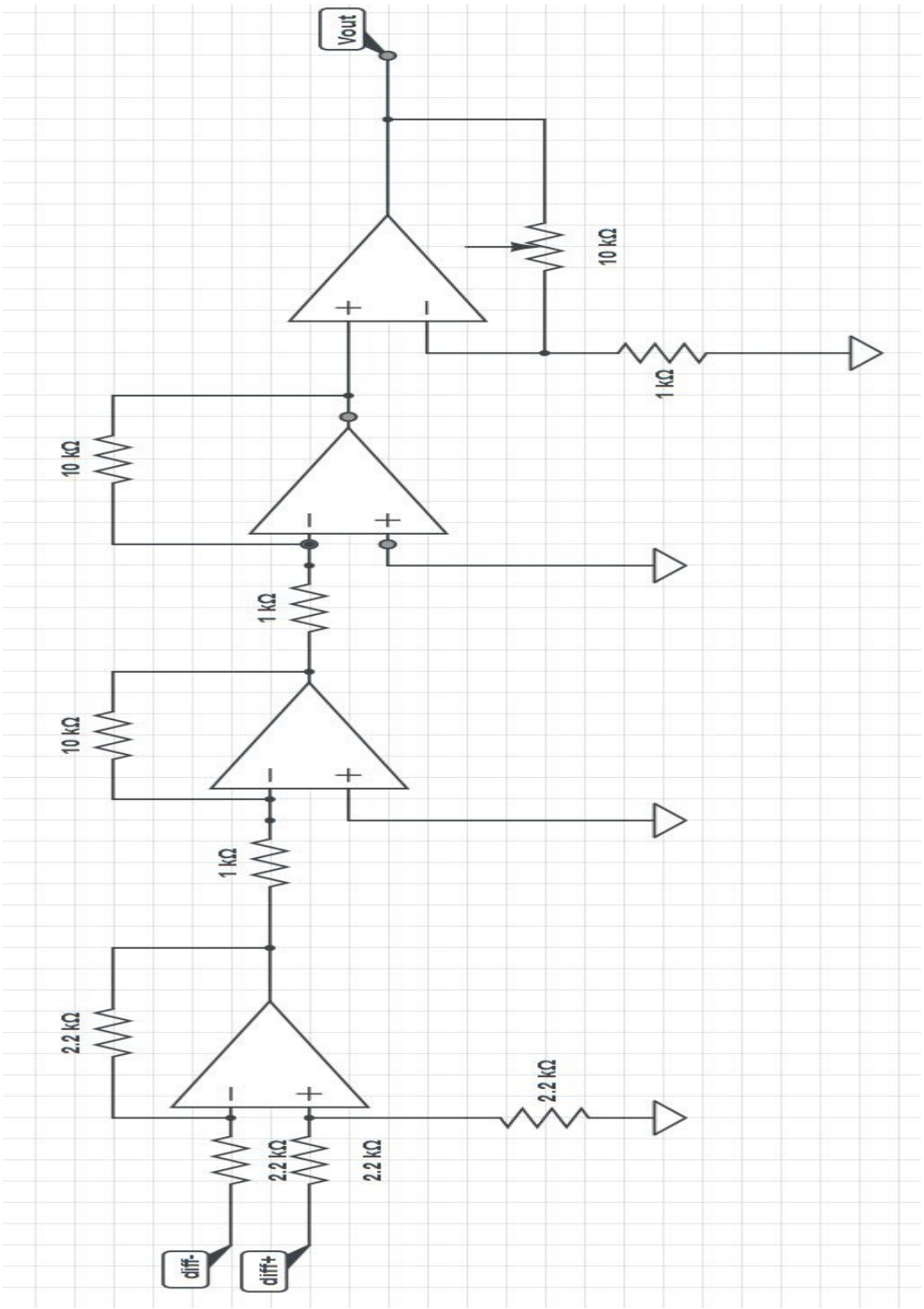

Figure 25. Load Cell Amplifier Schematic

4.2 GEN-II ACTUATOR

The Gen-I prototype was a successful representation of the new retractor technology. It was demonstrated before a group of surgeons and engineers in an operating room at Mercy Hospital. Although the device demonstrated that it could potentially perform the work of a Bookwalter or Thompson retractor kit, it suffered from some shortcomings. For example, the motor box containing all structural components, electronics, and mounting hardware was heavy and bulky. Another shortcoming was that actuation speed of the device was quite slow. The partner physicians requested that the time required to go from one tensioned state to the other should not exceed one second, since the retractor position is typically adjusted many times during a normal surgery. The Gen-I device fell well short of this criterion, with an actuation time of seven seconds. Although seven seconds is still much faster than adjustments to the Bookwalter and Thompson retractors, which often require that the whole system be taken apart and setup to gain a new exposure, speed is a virtue when appealing to surgeons. A final shortcoming of the Gen-I device was that the footswitch controlling the retractor was exposed to body fluids and could easily be bumped or lost track of during a surgery, resulting in unintended movement of the retractor during a surgical procedure, which could be life-threatening or inconvenient in the least. In addition, controlling multiple arms, each with their own floor switch, could become confusing. With this feedback, design commenced on the Gen-II prototype.

4.3 COMPONENTS OF GEN-II ACTUATOR

In order to simplify development and speed up the operation of the device, a pneumatic actuator was chosen for Gen-II. Pneumatic actuators contain only a piston and cylinder, eliminating the motor and gearing. All hospital operating rooms contain connections for oxygen, nitrous oxide, vacuum, and Nitrogen (well over 100 psi), which is already used to drive numerous pneumatic surgical instruments. A pneumatic actuator with a 3.25-inch bore was chosen for this next generation prototype. Preliminary testing of the actuator indicated that actuation time of less than one second could be achieved; satisfying the requirements of surgeons while dramatically simplifying the control system for the actuator. Cable/arm preload can be controlled entirely by regulating the supply pressure to the actuator. This eliminates most of the electrical components that were used in the Gen-I prototype to achieve force feedback control. Instead of a footswitch, a button was developed that mounts to the end of the retractor arm.

The pneumatic actuation system consists of the pneumatic actuator, a solenoid valve, a pressure regulator, and a relay circuit, as shown by the schematic in Figure 26. The pressure regulator controls the force applied to the cable, when considering the active area of the pneumatic cylinder.

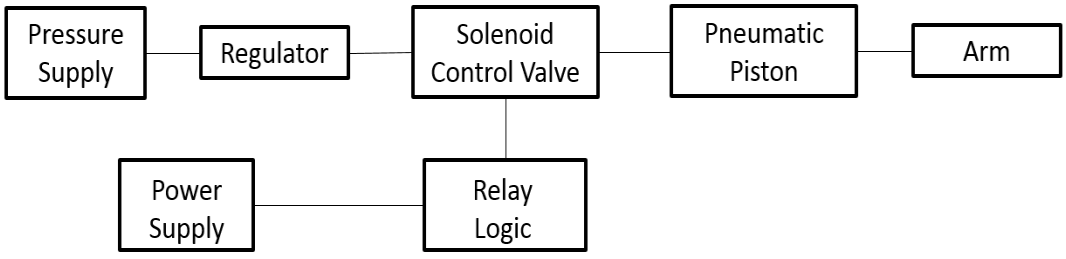

Figure 26. Basic Schematic of Pneumatic System

The cylinder is supplied air through the bi-directional, solenoid control valve, as shown in Figure 27. The truth table for the solenoid valve is given in Table 5. From Table 5, Case 1 ("Off") is if the unit is not powered, Cases 2 ("Load") and 4 ("Button Press") are for attaching the arm or making it flexible, and Case 3 ("Run") is for when the arm is rigid. The solenoid valve has a center exhaust position, meaning that all pressure is exhausted when electrical power is removed from the device.

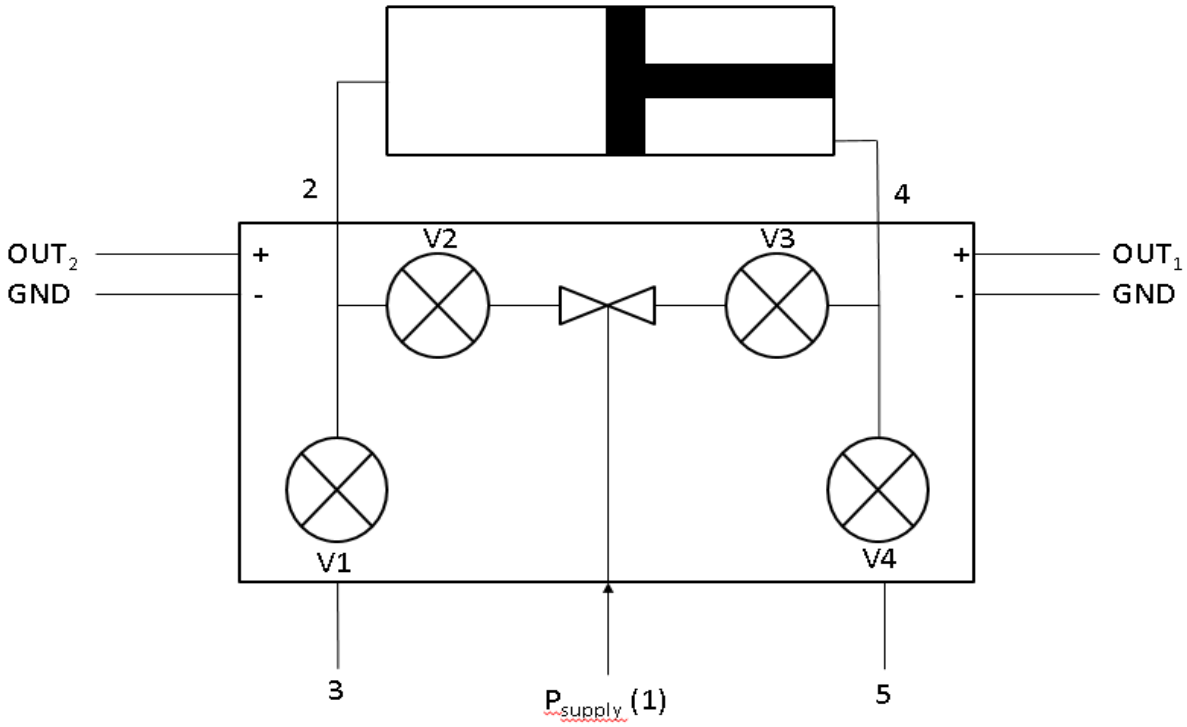

Figure 27. Pneumatic Schematic for Solenoid Valve and Pneumatic Actuator

Table 5. Solenoid Valve/Actuator Truth Table

Valve Truth Table					
Case	**Mode**	**V1**	**V2**	**V3**	**V4**
Case 1	Off	Open	Closed	Closed	Open
Case 2	Load	Open	Closed	Open	Closed
Case 3	Run	Closed	Open	Closed	Open
Case 4	Button Press, Load	Open	Closed	Open	Closed

4.4 PACKAGING AND SIZING OF COMPONENTS

Size and weight were also reduced in the Gen-II design. The Gen-I prototype enclosure was quite heavy and bulky, making it difficult to mount to an operating table rail. Due to its large size, it was also quite difficult for surgeons to work around the enclosure when it was mounted into position. After considering mechanical loading of the components in the enclosure, the steel "L" bracket in Gen-I was replaced with an aluminum bracket to save weight. An ANSYS simulation was conducted on the new design, which determined that a load of up to 230 lbf could be applied to the center of the end plate, and still result in a factor of safety of 9.33 when considering material yield stress, which exceeds the desired overall FOS of 3.0. The four actuator mounting holes were modeled as fixed supports.

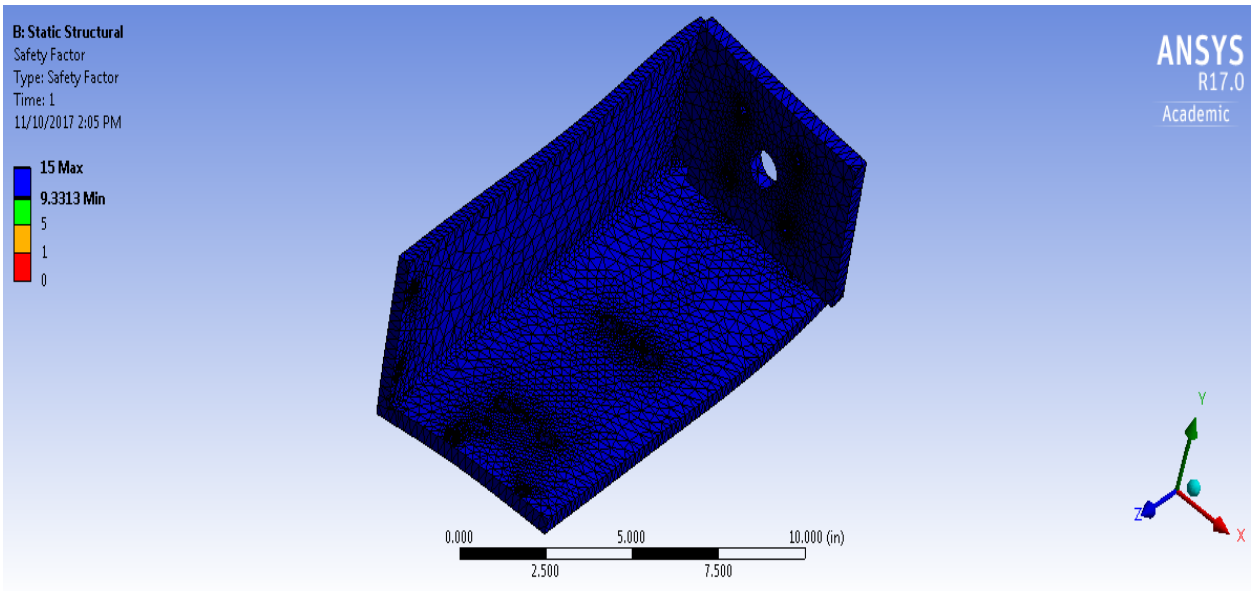

Figure 28. ANSYS Simulation of Aluminum "L" Bracket

Also, the removal and replacement of electrical components with pneumatic components further reduced size and weight. In fact, the Gen-II assembly was 33% lighter than the Gen-I prototype. The electrically operated linear actuator used in Gen-I contained a large motor mounted on its side. It was determined that since the Gen-II device can be powered by nitrogen that is well over 100 psi pressure, the pneumatic actuator could be reduced in size to achieve the desired preload of approximately 230 lbf as detailed in Chapter 2.0. This slimmer actuator would be smaller and lighter weight, allowing the enclosure to be more compact. This would make the entire system, including the enclosure, more compact, allowing surgeons and other medical staff to freely work around the operating table.

5.0 EVOLUTION OF ARTICULABLE COLUMN DESIGN

The mating surfaces between individual links in the articulable arm form ball and socket joints, as shown in Figure 29.

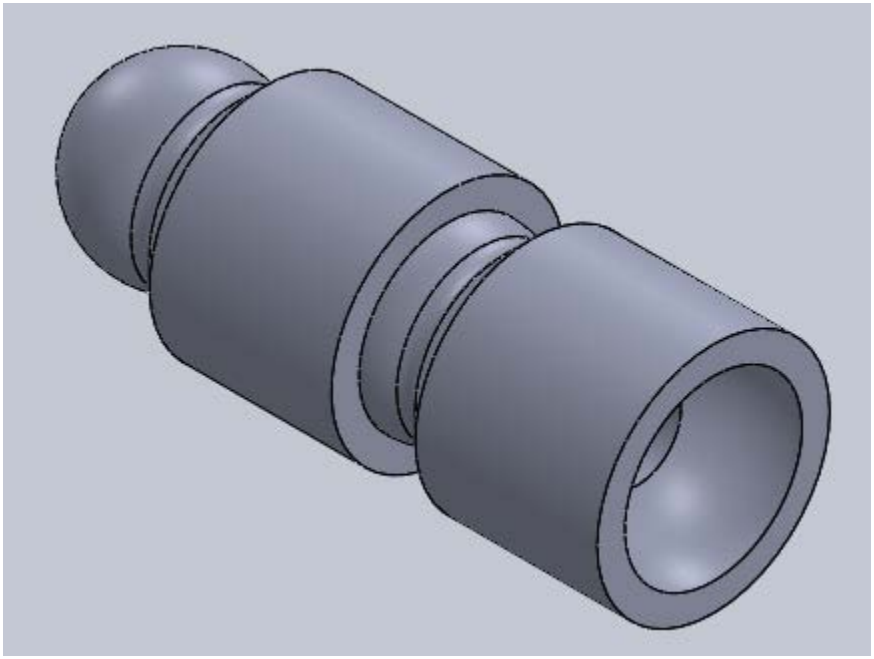

Figure 29. Assembly of Two Links

As with other articulable columns, the retractor device requires a series of these joints to rigidly lock into place when the central cable is tensioned. Likewise, the assembly must move freely when the cable is de-tensioned. Ball and socket joints are widely used in numerous applications and can be found anywhere from the human body to machine tools. These joints are intended to allow spherical motion between multiple mechanically loaded members. In most

systems, it is desired to reduce friction in joints. However, here the joint must supply adequate friction to sufficiently lock the arm, yet break free when the arm is un-tensioned. As such, an important design consideration for this device is the choice of material and design of the mating surfaces of the links.

Numerous options have been considered to improve joint friction, including interfacial solutions, such as rubber inserts and coatings, which may enhance friction. Also, mechanical texturing processes, such as sandblasting and application of a tungsten carbide coating to metal links, have been explored. Materials include printed and machined polymers and machined metals. The mechanical strength of the arm material is also important, and was considered in detail in Chapter 3.0 of this thesis.

5.1 MATERIAL SELECTION

5.1.1 Strength

The links that comprise the articulating arms must provide adequate stiffness to maintain the 0.4 in deflection and also must not slip in order to sustain the specified tip load of 20 lbf. When the arm is locked, no rotation should occur between joints. The arm is primarily loaded in bending. Since the maximum load, P, is fixed at 20 lbf, the arm deflection can be controlled through selecting the appropriate stiffness of the material, E, and the geometry of the links (L, I), as given in Equations (2-1) and (2-5). Because the required length is fixed and there are limitations in the maximum diameter of the arm, a minimum modulus for the link material is required. The

maximum arm diameter will be determined in future work as part of a human factors study, but for now it is assumed to be about 1.5 inches. Deflection can also occur from using compliant friction enhancers at the joint interfaces. Slippage is an obvious failure mode. The highest bending moment is at the root of the arm, which is consistent with experimental observations where slippage failures usually occur in the first joint of the arm.

In total, arms from seven different materials have been fabricated and tested. These include printed links of ABS, PLA, and machined links made of PMMA, PEI, fiber reinforced polycarbonate, aluminum, and stainless steel. Although the polymers do not meet the strength requirements determined in Chapter 3.0, they were still tested for their interfacial friction properties. Friction properties for selected materials were presented above [10] in Table 4. These values were determined by using steel as the moving specimen and the material in the table as the fixed specimen [10].

The MATLAB simulation performed earlier reflected links of two-inch length and one-inch ball and socket diameter. With assistance from an undergraduate student, a simple, iterative optimization was performed to determine a suitable link geometry that when used for an arm would meet the deflection specification when made of a 4 Msi (27 GPa) material. This value represents a very strong, fiber reinforced polymer material. It was determined that three-inch length links of 1.75” diameter having ball and socket joints that are 1.32 inches in diameter, a 36” arm with a 20 lbf tip load would have a deflection of 0.267 inches (0.6774 centimeters), which meets the deflection design specification. Figure 30 shows this result from the numerical simulation.

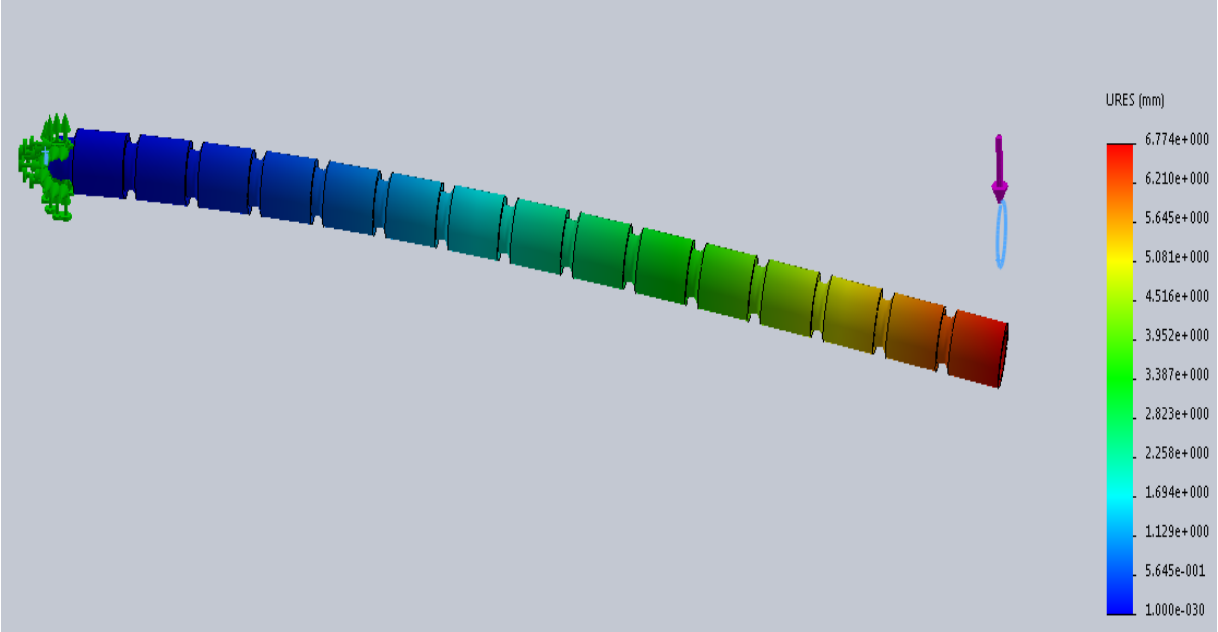

Figure 30. Deflection Simulation to find Suitable Geometry for 27 GPa Modulus Material.

Some reinforced polymers have elastic moduli that are within this range. Pultruded glass fiber/epoxy composites have a flexural modulus as high as 3 Msi (20 GPa) [1], and some injection moldable polymers with glass fibers and beads have bending moduli as high as 4 Msi (27 GPa) [23]. Alternately, by using Equation (2-1), it was determined that if a 4 Msi (27 GPa) modulus material were used with the current link geometry, the arm would need to be shortened to 25.7 inches, which is not acceptable. Alternately, from Figure 30, the arm can be made larger to meet the specification. Future human factors studies will determine if an arm of this diameter is acceptable to surgeons.

5.1.2 Interfacial Friction

Another important focus of this chapter is creating a ball and socket interface that provides adequate friction when preload is applied to the articulating column, but is also freely movable when preload is released. A delicate balance exists between the materials and the methods that are used to promote friction at the ball/socket interface. The materials must have sufficient elastic modulus to provide adequate flexural stiffness, but must also provide sufficient joint friction to hold the arm in place when locked. Many friction enhancing techniques have been tested. First, using a conformal rubber ring within the socket region of the links was explored. Next, conformal coatings were applied to the ball portions of the links. Finally, links were machined from various polymer stock.

5.1.3 Deflection Testing Rig

A rig was developed that can accurately apply a static tip load and measure the deflection. The rig was used for two purposes: to experimentally determine the area moment of inertia, as reported in Table 3 above and to determine at what applied force (moment) the joints will slip. Shorter scale (7.48 in length) arms made of links from each of the seven materials were deflection tested on the test rig pictured below in Figure 31. The Gen-II prototype assembly was used to provide tension to test arms. A stiff “L bracket” was mounted to the side of the actuator assembly at the top and bottom. The bracket extended above the motor box, parallel to the arm. As can be seen from Figure 31, on the right side of the arm is a ¼”-20 fastener that is threaded through the “L” bracket to provide a normal force to the arm. The larger, metal cylindrical device between the end of the bolt and the test arm is a load cell to measure force. A dial indicator was placed on the

opposite side of the arm from the load cell to quantify column deflection, as the force was increased in steps, from 0-20 lbf, by turning the bolt. Raw deflection data for each material is given in Appendix A. All tests were conducted at 60 psi, which corresponds to a cable tension of 500 lbf.

The data can be extrapolated to represent a full length (36 in) column. To extrapolate the tip load for friction failure at 19 cm (7.48 in) to 36 in arm, the moments ($P \times L$), when considering Equation (2-1) must be the same. Thus, when the friction failure load of the 7.48 ($P_{7.48}$) in arm is extrapolated to 36" using the ratio of the short to long arm lengths as

$$P_{36} = \frac{19}{2.54} \times \frac{1}{36} P_{7.48} = 0.2078\, P_{7.48} \tag{5-1}$$

Similarly, the deflection for the 7.48 in arm ($\delta_{7.48}$) can be extrapolated using the cube of the length ratio, when considering Equation (2-1) as

$$\delta_{36} = \left[\frac{36}{7.48}\right]^3 \times P_{7.48} = 111.5 \times \delta_{7.48} \tag{5-2}$$

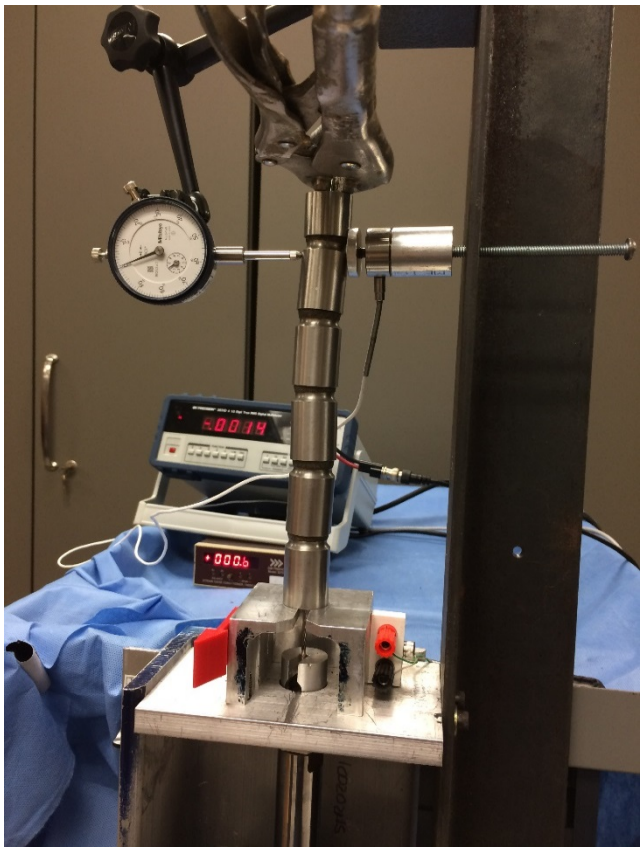

Figure 31. Force versus Deflection Test Rig

5.2 POLYMER LINKS

This section outlines the development and testing of various polymer links for the articulating arm.

5.2.1 Gen-I Printed Links

The Gen-I prototype retractor arm was manufactured from PLA plastic that was 3D printed on a MakerBot® 3D printer. This type of 3D printer extrudes PLA filament from a roll and builds parts by adding thin, extruded lines of molten material. The first printed link design featured smooth balls and sockets. Due to the nature of the printing, the part retains a concentric circular pattern reminiscent of tool marks left from conventional machining. Upon loading the 24-inch-long column, the links would compress together and grip, possibly with assistance from the concentric printing pattern. However, the arm that featured printed links lacked sufficient friction and slipped under minimal torque. In fact, slippage of the proximal ball and socket joint took place at a 3 lbf tip load on a 24-inch arm, supporting a moment of only 72 in-lbf. Due to this unacceptable performance, other ideas were explored. The next printed link concept featured printed ridges on the surfaces of the balls. Eleven ridges were printed on each link. The functional concept of the ridges is that the sockets would deform around these ridges, enhancing gripping power. This idea was quite successful; however, the links showed visible wear after one or two loading cycles. It is important to note that these printers manufacture parts with a hexagonal infill pattern at specified density (50% in this case), meaning that the part was not solid, but rather only half as dense as an equivalent geometry part made by conventional manufacturing methods. This also means that the area moment of inertia, *I*, was approximately half of what it would be for a solid, machined part, when considering Equation (2-2). Since the retractor arm represents a cantilevered beam subject to a bending load during use, the area moment of inertia is a critical geometric property affecting the bending deflection of the arm. For these reasons, the Gen-I retractor arm lacked sufficient rigidity and durability.

An ANSYS model of a single link was created to predict the average value of *I*, using the geometry shown in Figure 6. The geometry was imported from SolidWorks into ANSYS as a Parasolid file. The well-documented elastic modulus for PLA of 507,632 psi (3.5 GPa) was used in the simulation. ANSYS SOLID187 elements were used, which feature ten node second order tetrahedral elements. An automatically generated mesh was used and refined until the resulting deflection value did not change with further mesh refinement. The socket was modeled as a fixed support while the 20 lbf tip load was placed on the ball surface.

It is important to note that this simulation did not consider the fact that the previous links were 3D printed and were not "solid" parts. This means that the actual deflection would be twice as substantial since the area moment of inertia value for printed links containing the hexagonal infill printing pattern would be approximately half of the value for a solid link (100% fill).

Note that traditional beam theory (Equation (2-1)) cannot be used to predict *I*. The ANSYS model represents a short cantilever beam with small aspect ratio. The effects of transverse shear stress dominate in short beams and this will impact the results. For traditional Euler-Bernoulli beam theory to apply, the beam must have an aspect ratio of at least 20:1, which is to say that the beam should be at least 20 times longer than it is thick [35]. The aspect ratio of the link simulated in ANSYS was 1.5:1; far less than recommended for application Euler-Bernoulli beam theory. Therefore, Timoshenko beam theory must be used to determine *I* values [42].

$$w = \frac{PL}{kAG} + \frac{PL^3}{3EI} \tag{5-3}$$

In Equation (5-3), *w* represents the simulated deflection of the PLA link of 713 microinches, *P* represents the applied tip load of 20 lbf, *L* represents the length of the beam (2 inches), *k* represents a shear stress form factor, which is 9/10 for circular sections, A=1.158 in^2 is the cross-sectional area of the beam, G=246,564 psi (1.7 GPa) is the material shear modulus,

E=507,632 psi (3.5 GPa) is the material elastic modulus, and I is the area moment of inertia of the beam, to be determined. The results for ANSYS and MATLAB I values are summarized in Table 6 below.

The ANSYS model (Figure 32) predicted a deflection of approximately 1.4 thousandths of an inch after correcting for 50% infill, resulting from a 20 lbf tip load applied to one PLA link. Using the deflection simulated in ANSYS for one two-inch length link subject to a 20 lbf bending load, Equation (5-3) was used to determine effective area moment of inertia, I for a retractor link manufactured with 50% infill. The resulting value, correcting for 50% infill, was I=0.094 in^4 (3.9e-8 m^4). Now, these results can be extrapolated for a 36-inch-long articulating column. Substituting I=0.094 in^4 (3.9e-8 m^4) (calculated from ANSYS), E=507,632 psi (3.5GPa) (PLA), P=20 lbf, and L=36 in (design requirements), the calculated deflection was δ=6.52 inches. This far exceeds the specification from Chapter 2.0. The MATLAB model had predicted elastic modulus based on solid cross sections (100% infill). The equivalent I value from the model above for a solid link is I=0.188 in^4 with a resulting deflection, δ, of 713 microinches for one link. Note that this effective I value is 2.44 times larger than the experimentally determined area moment of inertia given in Table 3. Using this result, from Equation (2-1), it can be shown that a material with elastic modulus of at least 4.1 Msi (28.4 GPa) must be selected for this link geometry in order to meet design specifications for a full-length arm, which differs from the estimate from the MATLAB model of 13 Msi (90 GPa).

These differences are likely due to errors in measurement during the deflection tests that were used to determine effective I for the MATLAB model, since I values were determined experimentally from force and deflection data. Unobserved slippage in the links may have contributed to this difference, since measured force and deflection values were used in the

MATLAB model. If slippage occurred, deflection would be exaggerated, artificially decreasing *I*. With a smaller effective *I,* the MATLAB model predicted larger *E* in order to make up for this difference. In fact, the MATLAB predicted *E* is also a factor of 2.44 times greater than the ANSYS predicted *E,* just as the effective *I* value from ANSYS was 2.44 times greater than the MATLAB model. Because ANSYS was based on simulation only, these errors were not present in the model; therefore, a larger *I* was predicted, minimizing required *E.*

The area moment of inertia could also be estimated by integrating along the length of a link using Equation 2-2; however, the link geometry is complicated, and this would require an iterative process.

Table 6. Comparing Effective Area Moment of Inertia/Elastic Modulus by Modeling Strategy

	MATLAB	**ANSYS**
Estimated Area Moment of Inertia, *I* (m^4)	2.50E-08	7.83E-08
Required Elastic Modulus, *E* (GPa)	90	28.4

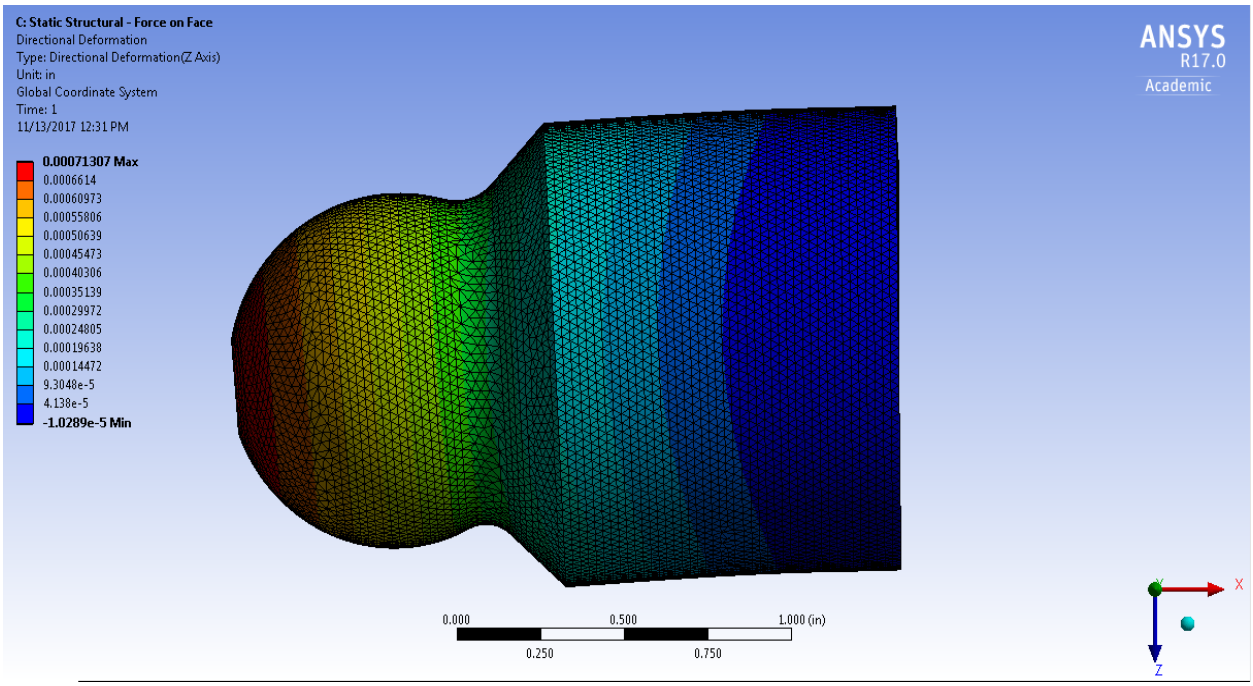

Figure 32. ANSYS Deflection Simulation of One PLA Link

The Gen-I link design provided an adequate demonstration and proof of concept for the idea of a surgical retractor that operates on the principle of an articulating column; however, the PLA printed arm in Gen-I lacked sufficient rigidity, and the gripping ridges on the links were subject to rapid wear. In some cases, the arm wore quickly enough that it would not last for an entire surgical procedure and would need to be replaced mid-procedure.

5.2.2 Rubber Conformal Ring

For the Gen-II prototype arm, other friction enhancing and wear reducing ideas were explored. The idea of using a rubber insert between the ball and socket interface was pursued. In theory, a thin rubber insert would compress under column preload and allow the plastic links to

grip more securely, all while greatly reducing wear of the ball and socket joints. This would allow a single retractor arm to easily survive a lengthy surgical procedure. Design modifications were made, and smooth links were printed. The socket feature of these links featured added clearance to accommodate the thin rubber insert. The rubber inserts were printed on a Lulzbot TAZ® 3D printer using NinjaFlex® rubber filament to a thickness of 0.030 inches. NinjaFlex® features a 12 MPa elastic modulus and an 85 Shore A durometer [18]. An arm was assembled using these new links. Upon application of preload to the column, significant deformation occurred due to compression of the rubber inserts, severely reducing flexural stiffness. This was because the rubber inserts did not compress fully, producing solid on solid contact, thus becoming part of the arm assembly's structural geometry. The resolution of the LulzBot® printer was not high enough to allow for smaller links to be printed. Due to the poor performance of these links, only the qualitative results were observed.

5.2.3 Conformal Coatings

Next, focus was placed on coating the ball and socket joints with an approximately 0.070-inch-thick conformal coating. This would allow the links to benefit from increased friction at the joints. Samples of Dow Corning 1-2577, 1-2620, and 3-1953 were acquired. The durometer values as rated on a Shore A scale were 80, 80, and 34 respectively and were rated at 3 MPa, 3 MPa, and 0.5 MPa tensile strength respectively [26]. These conformal coatings were applied directly to the untreated PLA ball and socket surfaces and allowed to cure for a full 72 hours, as directed. Upon testing, it was determined that adhesion was poor, resulting in the coatings quickly and easily shearing from the surfaces. Next, PLASTI-DIP®, a common rubber tool handle coating, was tested. The Shore A durometer was 70 while tensile strength was 3740 psi (26 MPa), significantly

higher than the Dow Corning coatings [22]. Also, this material formed a substantially stronger bond with the PLA plastic. The PLASTI-DIP® survived many more tensioning cycles than the other conformal coatings; however, the added thickness of the coating increased the column's compliance, and the column lacked sufficient rigidity while under load. While the balls and sockets coated with PLASTI-DIP® improved frictional performance, they allowed for too much deflection of the arm under load. In fact, the arm deflected under its own weight as it did with the conformal rubber rings. Also, they stuck together after relieving arm preload, making it difficult to readjust and reposition the arm during use. Since the approach obviously failed, only qualitative observations were made.

5.2.4 Bulk Machining of Plastic Links

Gen-II demonstrated improvements to link design that featured methods to increase friction at the ball and socket interfaces with limited success (Sections 5.2.2 and 5.2.3). The tool handle coatings were significantly stronger than the Dow coatings; however, they were still subject to significant wear over time and were not a viable solution.

To speed up development, bulk machining was employed to manufacture the links. By machining links rather than printing them, full infill density (100%) is achieved. This would increase the area moment of inertia of the retractor links, resulting in approximately a two-fold increase in flexural stiffness and thus less deflection under load. Additional polymers were researched for biocompatibility and desirable mechanical properties since PLA and ABS printed links lacked sufficient area moment of inertia and elastic modulus. In addition to elastic modulus, the material coefficient of static friction was considered for these new stock materials. To continue the evolution of the Gen-II design, bar stock of PEI, PMMA, and glass fiber reinforced

polycarbonate was purchased in 1.5-inch diameter sections. Most of the above listed polymers were chosen due to their moderately high coefficients of friction, which were given in Table 4. As established in Chapter 3.0, none of these materials is strong enough for this application. However, conducting surface friction studies was still valuable, particularly considering the cost and ease of machining. All links were machined to a turned finish of approximately 30 μin R_a, where R_a is the arithmetic mean of surface roughness, given by Equation (5-4),

$$R_a = \frac{1}{N}\sum_{n=1}^{N} |y_i| \tag{5-4}$$

where $y_i$is a measured point with respect to the mean line. All surface roughness measurements were made with a stylus profilometer.

Five links were manufactured from PEI, PMMA, and glass fiber reinforced polycarbonate. Due to their smooth turned finish, the links exhibited poor frictional performance. In fact, a 19 cm (7.48 in) length PMMA arm only supported 5 lbf before failure in the form of slippage at the ball and socket joint occurred. PMMA was tested due to its very high coefficient of static friction (0.8). Since performance was poor with the highest coefficient of friction material, no further testing was performed on the as-machined links.

5.2.5 Sandblasting of Plastic Links

5.2.5.1 Friction Testing Results

To increase friction at the ball and socket interfaces, the link balls and sockets were sandblasted to achieve a random, rougher surface finish of approximately 120 μin *Ra*. This modification allowed the glass fiber reinforced polycarbonate links, PEI links, and PMMA links to support loads of 20 lbf, 11 lbf, and 19 lbf respectively; however, these loads were applied to

arms with a length of only 19 centimeters, resulting in moments of 150, 82.5, and 142.5 in-lbf respectively. These were extrapolated to at 36" arm using Equation (5-1) and the results are given in Table 10 through Table 15 of the Appendix.

5.2.5.2 Deflection Results

The data was also extrapolated to predict the deflection for a 36" arm, using Equation (5-2) and are presented in Figures 33-35. Some unexpected, minor nonlinearity is observed in these plots, possibly due to micro-slipping at the joint or elastic relaxation of the polymer chains after application of the tip loads [41]. It can be seen that the experimental deflections were much higher than the theoretical deflection. This is likely a combination of unobserved slippage resulting in excess deflection. Also, some deflection of the test rig may have occurred, exaggerating these values further, especially since the raw data for Runs 1 and 2 were extrapolated (scaled) to a full-length arm from the original data. As shown in Figure 33, a full-length PEI arm would deflect about 6.5 inches, while PMMA and FR PC arms would deflect about 11.5 inches (Figure 34 and Figure 35). Theoretical deflection due to beam theory is also plotted for each material using elastic modulus values from Chapter 3.0. This raw test data is tabulated in Table 10 through Table 15 in Appendix A. Also, it was observed that due to the soft nature of these polymers, the rough finish from sandblasting was polished by the compressive preload as well as the slippage at the ball/socket interfaces, resulting in diminishing performance.

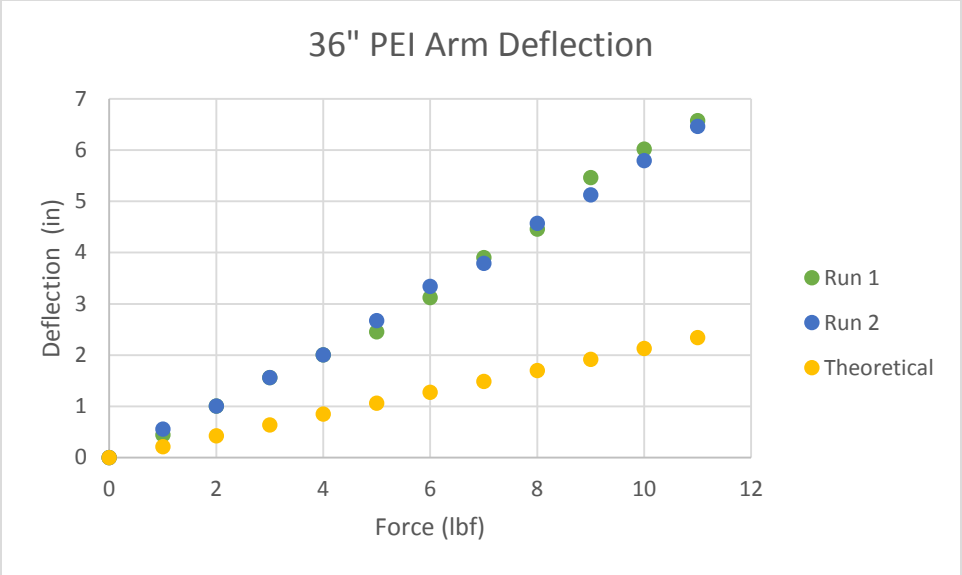

Figure 33. Extrapolated Deflection vs. Force Plot for a Full Length (36”) PEI Arm

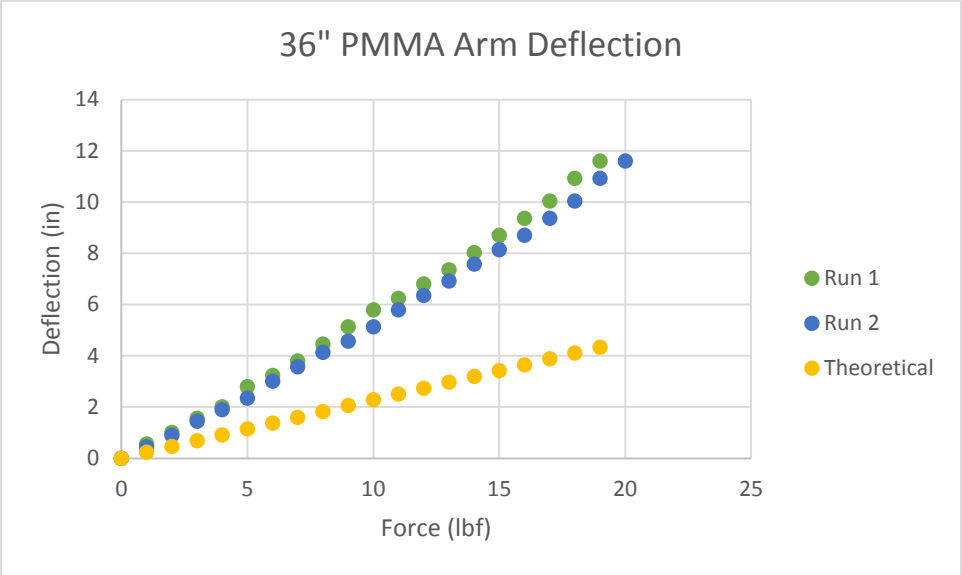

Figure 34. Extrapolated Deflection vs. Force Plot for a Full Length (36”) PMMA Arm

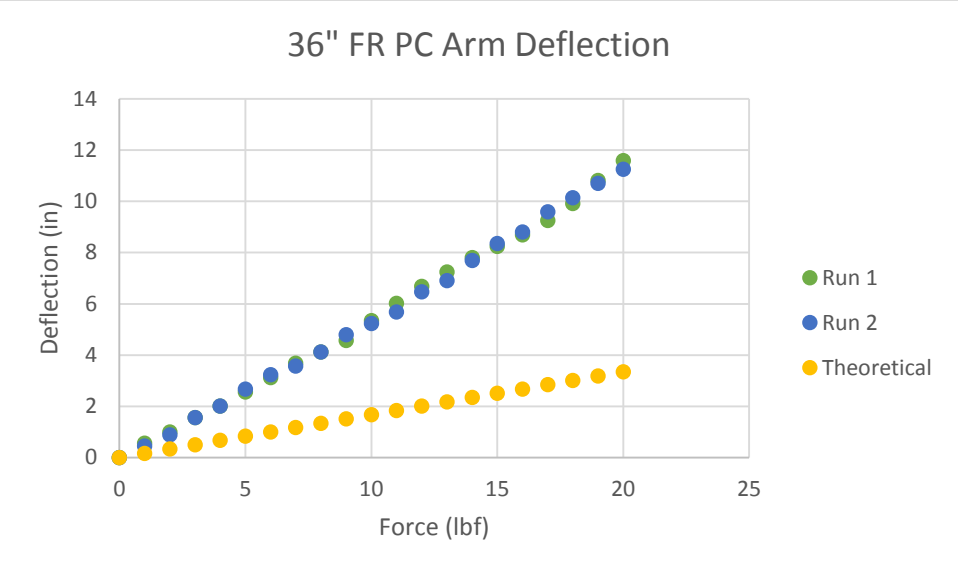

Figure 35. Extrapolated Deflection vs. Force Plot for a Full Length (36") FR PC Arm

5.3 METAL LINKS

Next, manufacturing links from aluminum and stainless steel was explored, particularly considering that the current link geometry would require a modulus of at least 85 GPa. Aluminum is a less typical medical device material, but is lighter, cheaper, and easier to machine. The limiting consideration for these materials is the interfacial friction.

5.3.1 Stainless Links

In an effort to manufacture links with adequate flexural stiffness, 16 links were machined from 303 stainless steel. With an elastic modulus of 30.5 Msi (210 GPa), this value far exceeds the

recommended value of 12.3 Msi (85 GPa) from the simulation in Chapter 3.0. Although stainless steel is quite heavy and more expensive, it is often used in the medical field. A static/structural analysis was performed in ANSYS for one stainless steel link for comparison to the previous PLA links. An automatically generated mesh was used and refined until the resulting deflection value did not change with further mesh refinement. ANSYS SOLID187 elements were used, which feature ten node second order tetrahedral elements. The socket was modeled as a fixed support while the tip load was placed on the ball surface.

Recall from Figure 32 that finite element analysis predicted a deflection of approximately 713 microinches resulting from a 20 lbf bending load applied to one solid PLA link. If stainless steel was chosen, deflection decreases to a value of 12.3 microinches (Figure 36), a factor of 58 less than the PLA links. Recall that the elastic modulus of PLA is approximately 508 ksi (3.5 GPa), and the elastic modulus of stainless steel is 30.5 Msi (210 GPa). Thus, the factor of 58 difference in the deflections is reasonable, since the deflection would scale by the ratio of the moduli when considering Equation (2-1). Using the deflection value simulated by ANSYS in Figure 36, the deflection of a 36-inch stainless steel articulating column can be extrapolated as before. The resulting value is approximately 0.1 inches of deflection (0.25 cm) when stainless steel is used, assuming a 20 lbf bending load applied to a 36-inch articulating column.

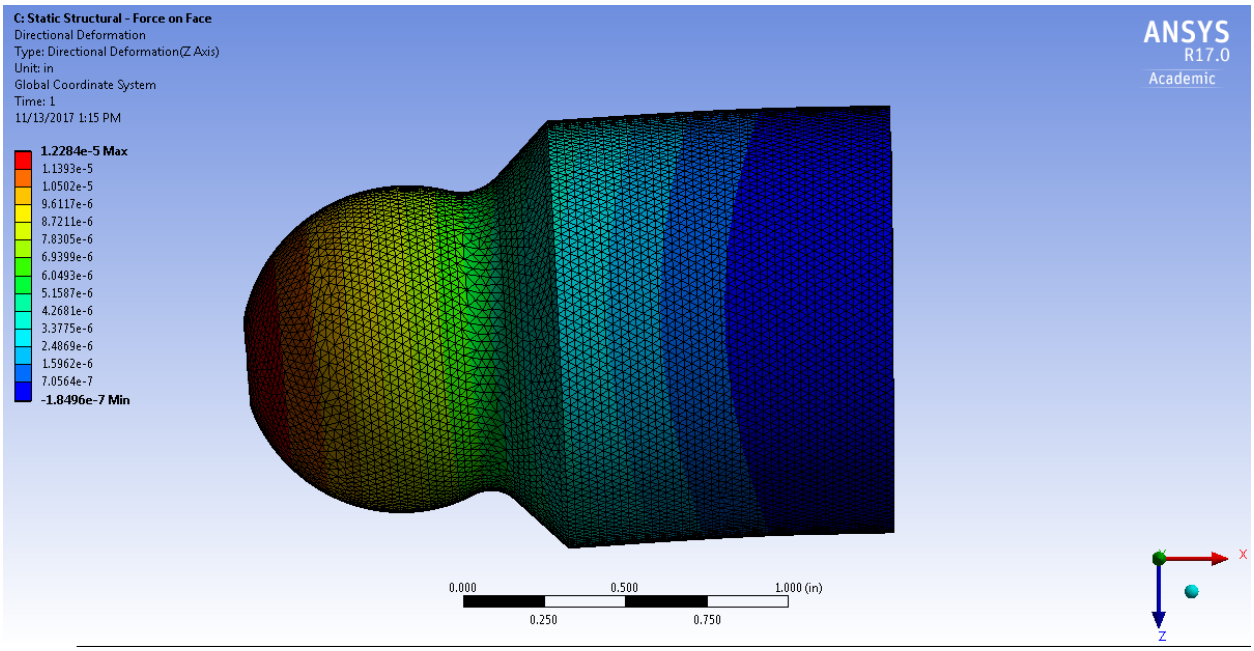

Figure 36. ANSYS Simulation of One Stainless Steel Link

5.3.2 Aluminum Links

Links were also manufactured from aluminum because it has an elastic modulus of 10.1 Msi (70 GPa), which is close to 12.3 Msi (85 GPa), the minimum value required for retractor links according to the model in Chapter 3.0. As with the stainless-steel links, stock surface finish was measured to be approximately 30 μin *Ra*. This was far too smooth to achieve adequate friction, and performance was just as poor as it was with the smooth PMMA links.

An additional attempt to increase ball/socket interface friction was made. O-ring grooves were turned within the socket regions of the retractor links (Figure 37). It was thought that the O-ring would crush to a solid length when the arm was preloaded and allow the aluminum ball to touch the aluminum socket. In this way, the O-rings would not create any additional compliance,

but rather, they would apply an additional normal force to the ball/socket interface. Since their Neoprene rubber is soft and compliant, it was thought that these O-rings would improve interface friction and prevent slippage. Unfortunately, the O-rings provided minimal additional friction and performance was substandard and behaved similarly to the conformal coatings, resulting in the column deflecting under its own weight as it did with the conformal coatings and the conformal ring.

Figure 37. Aluminum Link with O-Ring

5.3.3 Sandblasted Metal Links

As with the polymer links, the aluminum links were sandblasted to increase surface roughness. As with the polymer links, slip at the lower-most link occurred at approximately 20 lbf on a 7.48-inch length arm. The equivalent deflection of a full-length arm was 11.59 in (Table 7). This provided confirmation that the failure mode of the links was slippage at the ball and socket interface rather than deflection due to insufficient flexural stiffness. From Figure 38, a full-length aluminum arm would deflect about 2-3 inches. The non-linearities in the plot are likely due to unobserved slippage during testing. It can be seen that the experimental deflections were much higher than the theoretical deflection. This is likely a combination of unobserved slippage resulting in excess deflection. Also, some deflection of the test rig may have occurred, exaggerating these values further, especially since the raw data for Runs 1 and 2 was extrapolated (scaled) to a full-length arm from the original data. Subsequent design iterations were performed with aluminum and 303 stainless steel links, since the flexural stiffness, *EI*, of these materials is adequate. From Section 5.2.3, it was learned that silicone based conformal coatings do not possess adequate shearing strength for this application. Also, slight improvement was observed in the sandblasted links over the smooth links, confirming that surface finish is directly related to performance of the ball and socket interface.

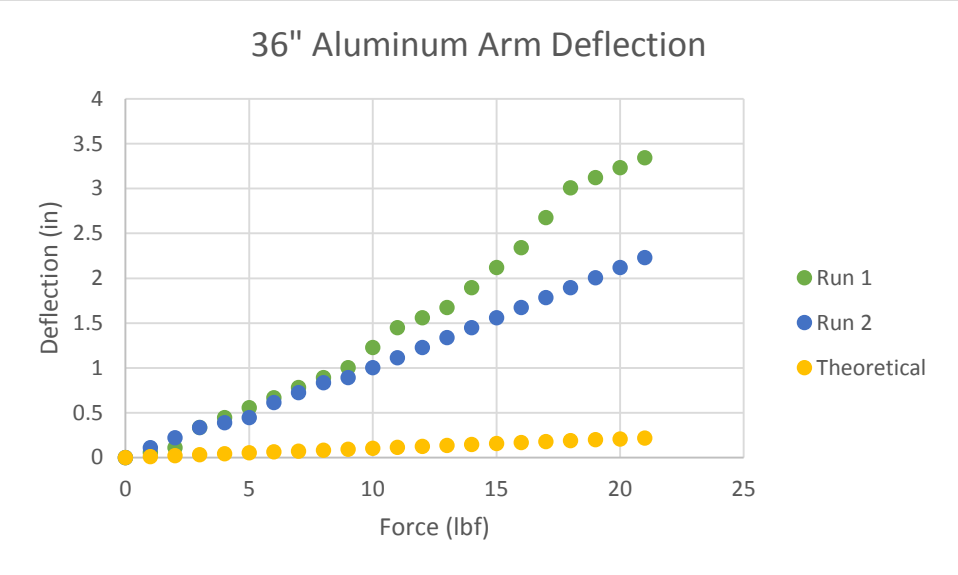

Figure 38. Extrapolated Deflection vs. Force Plot for a Full Length (36") Aluminum Arm

5.3.4 Carbinite Stainless Links

It was desired to obtain a random rough and durable surface finish, such as that of sandpaper grit. A tungsten carbide surface finish was electrically fused to the metal balls using a process developed by Carbinite Metal Coatings [38]. The tungsten carbide leaves a very rough and durable surface finish that is fused to the substrate material itself, resulting in excellent wear resistance. Thirteen links were machined from 303 stainless steel and sent to this company for trial coatings of tungsten carbide. Coating only the balls of the links with tungsten carbide, an arm was assembled with the thirteen links. The retractor arm featured five stainless steel lengths at a length of 19 cm (7.48 in) and supported 26 lbf before failure resulting from slippage at the base link (a moment of 194 in-lbf). This was an improvement from the 20 lbf applied to the 19 cm (7.48 in) polymer arms, which supported a moment of 149 in-lbf. Changing from links manufactured from

various polymers to links manufactured from stainless steel, and coating them with a 266 µin *Ra* tungsten carbide coating, allowed a 7.48 in length arm to withstand a 26-pound tip load before failure, which was 6 pounds more than any sandblasted link. This corresponds to a deflection of 6.24 in on a full-length arm (Table 7). A full-length arm manufactured from tungsten carbide coated stainless steel links would deflect between 4-6.25 in under the 26 lbf tip load (Figure 39). This value range is larger than the deflection predicted in Figure 36, and this may be due to the base link lifting onto its edge during testing, exaggerating the deflection values. In Figure 31, the bottom stainless steel link would occasionally tilt on edge during deflection testing and form corresponding indentations in the square aluminum retractor arm mount at the base of the test rig. The performance observed in the tungsten carbide coated stainless steel links was the most significant advancement achieved and it allowed the retractor arm to progress further toward the design specifications in Chapter 2.0. Despite this improved behavior, the arm still does not meet design specifications. The full-length arm must deflect no more than 0.4 inches when subject to a 20 lbf tip load.

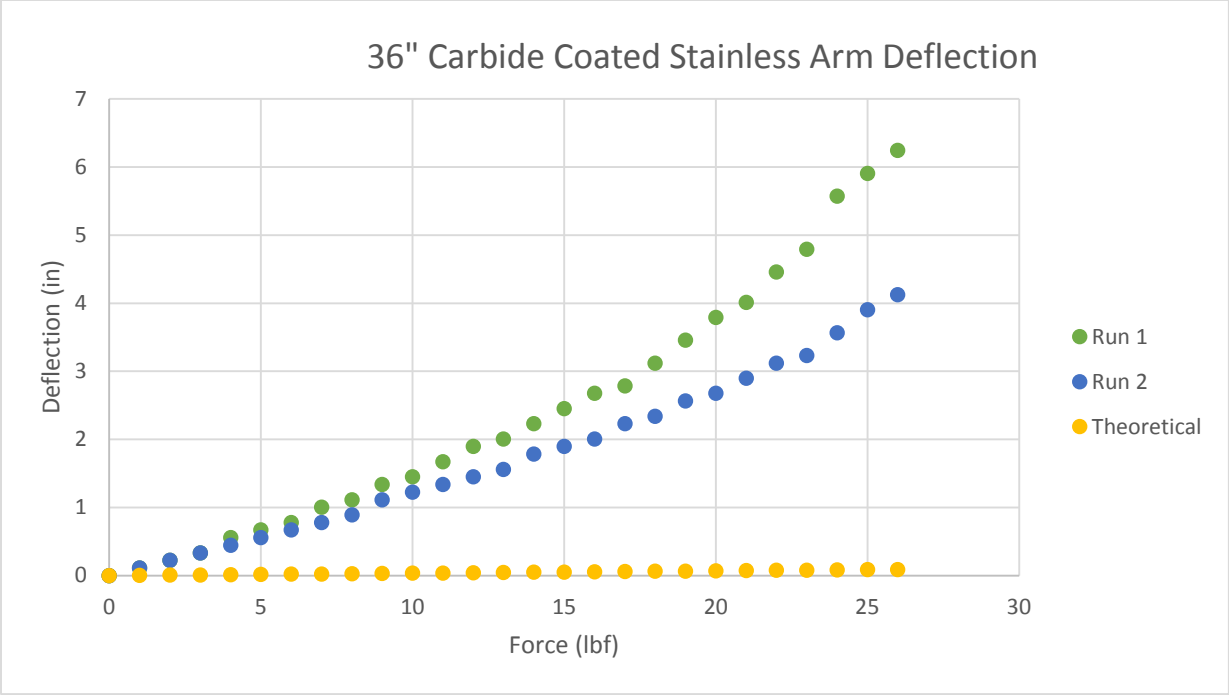

Figure 39. Extrapolated Deflection vs. Force Plot for Full Length Stainless Arm w/ Carbinite

5.4 SUMMARY OF TESTING RESULTS

At this point, many materials and manufacturing methods were attempted in order to manufacture links that meet design specifications. Links manufactured from 3D printed PLA, and links machined from PEI, PMMA, FR PC, aluminum, and stainless steel were tested. The deflection testing results are summarized in Table 7 below. The table represents that maximum tip load that each column could withstand before failure in the form of slippage at the ball/socket interface. The results were extrapolated to a 36” arm and presented in Table 8. All values presented represent links where methods of mechanical texturing were employed. No data is presented for

links where the conformal ring, O-rings, or conformal coatings were used, since these links exhibited severe deflection under their own weight. The force values in Table 7 and Table 8 represent the maximum force that could be applied before breakaway. Many links clearly did not provide the adequate joint stiffness or friction and were only qualitatively observed. For the better performing interfaces, numeric data is given.

Table 7. Summary of Friction Break Away Forces for 7.48" Arms

Material	Ra (μin)	Force (lbf) (7.48" Length)	Deflection (in) (7.48" Length)
PEI	77.6	11	0.059
PMMA	74.9	19	0.104
FR PC	138.7	20	0.104
Aluminum	103.8	21	0.02
Stainless Steel	266	26	0.056

Table 8. Summary of Predicted Friction Breakaway Forces for 36" Arms

Material	Ra (μin)	Force (lbf) (36" Length)	Deflection (in) (36" Length)
PEI	77.6	2.28	6.57
PMMA	74.9	3.95	11.59
FR PC	138.7	4.16	11.59
Aluminum	103.8	4.36	2.23
Stainless Steel	266	5.40	6.24

5.5 SUMMARY

The evolution of link design stage is the longest stage of the engineering process for the retractor system. This process has progressed through the course of one year and evolution of the retractor arm will continue even beyond the entry of the device into the medical device market after receiving feedback from partner physicians. The retractor arm has progressed from smooth, two-part links with steel balls and sockets to links with combined balls and sockets that were 3D printed from PLA plastic. Next, coatings and rubber inserts at the ball and socket interface were explored in an unsuccessful effort to increase the rigidity of the arm. This has progressed to the idea of manufacturing links from bulk polymer materials and sandblasting their ball and socket surfaces to increase friction. Ironically, when these ideas proved unsuccessful, metal links were explored one again, with the aid of an aggressive tungsten carbide coating that fused to the metal surfaces of the links. This process dramatically increased load capacity over the polymer link designs; however, the retractor arm still does not perform in accordance with the design specifications in Chapter 2.0. Sufficient flexural stiffness was obtained with stainless steel links; however, adequate friction could not be achieved with the ball and socket geometry and the coating that was used. The tungsten carbide coating exhibits superior wear resistance when compared to any other coating method that was attempted.

The full evolution of the link design is represented in Figure 40, although the first six links shown were not included in this document. Deflection data for the tungsten carbide coated stainless steel links can be found in the appendix in Table 18 and Table 19.

.

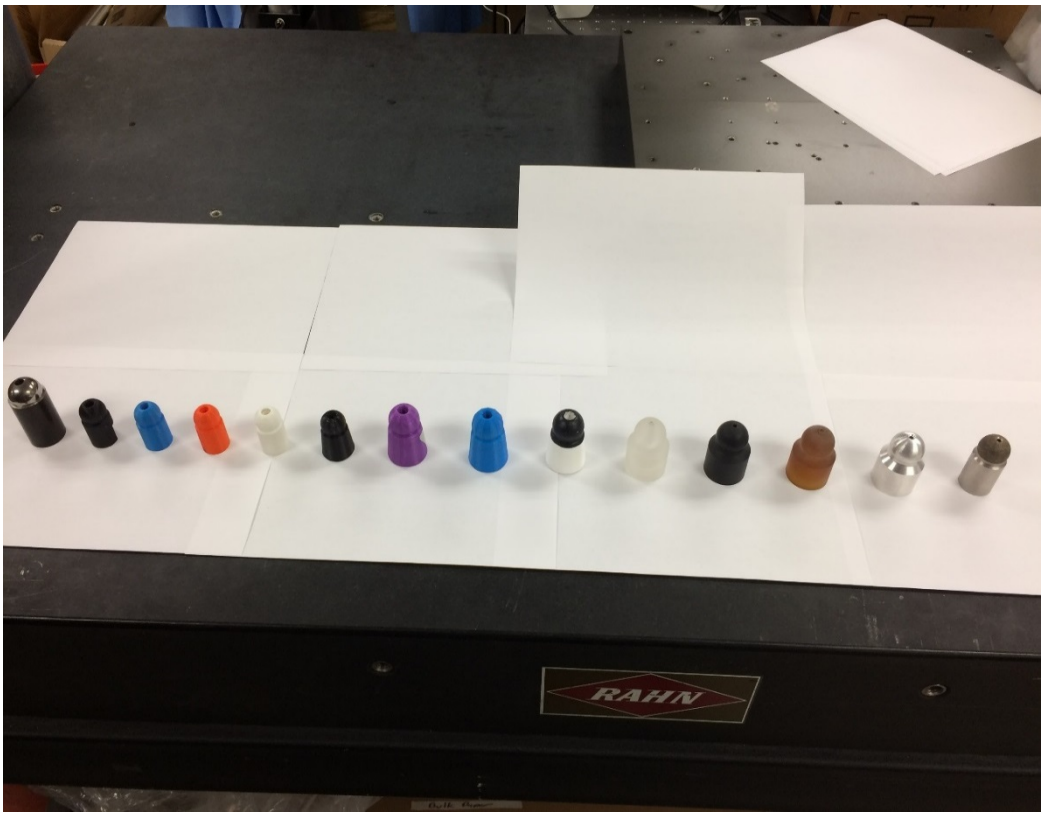

Figure 40. Evolution of Link Design

6.0 ARM END CONNECTIONS

There are two interfaces for the arm – one at the base that attaches between the motor box and the arm and one at the other end, which is the adapter that connects Bookwalter blades to the arm.

6.1 BOOKWALTER BLADE ACCEPTOR

To make this surgical aide more appealing to practicing surgeons, an adapter was developed to accommodate blades from a Bookwalter Retractor kit. After interviewing surgeons, it was determined that they prefer to use retractors with which they are familiar. For example, most surgeons that were interviewed use malleable retractors in most surgeries. This adapter allows surgeons to use malleable retractors, as well as any other type of retractor from a Bookwalter kit. This allows them to use the tools that they are already quite experienced with, without having to perform the lengthy setup of a Bookwalter kit itself.

6.1.1 Design

The Bookwalter blade adapter was designed with two halves that bolt together, as shown in Figure 41. A square hole accommodates all retractors from the Bookwalter system. The core of the device contains a spring-loaded component with teeth that interlock with Bookwalter retractor blades. The teeth permit ratcheting to permit the blades to be inserted into the holder. The ratchet mechanism also would permit tightening of the retractor. A button can be pushed to disengage the

teeth in order to remove or extend the blade. This behavior is consistent with the operation of the Bookwalter system; however, the retractor system can also be easily adjusted by releasing the arm tension, repositioning, and re-tensioning it in its intended manner of use.

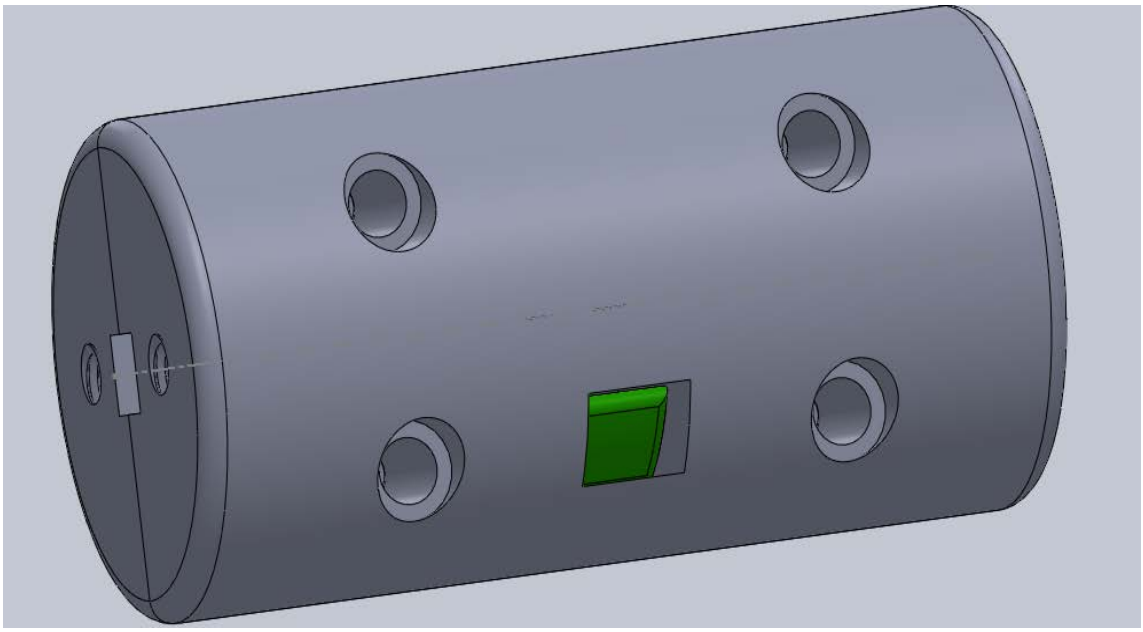

Figure 41. Bookwalter Blade Acceptor

With assistance from an undergraduate student, an adaptor was designed that couples the Bookwalter blade acceptor shown in Figure 41 to the articulating column of the retractor system. The modification is shown in Figure 42. The final link of the arm can be seen at the top and the Bookwalter retractor is seen extending from the blade acceptor. The device is functional, but additional refinements are planned to improve ergonomics.

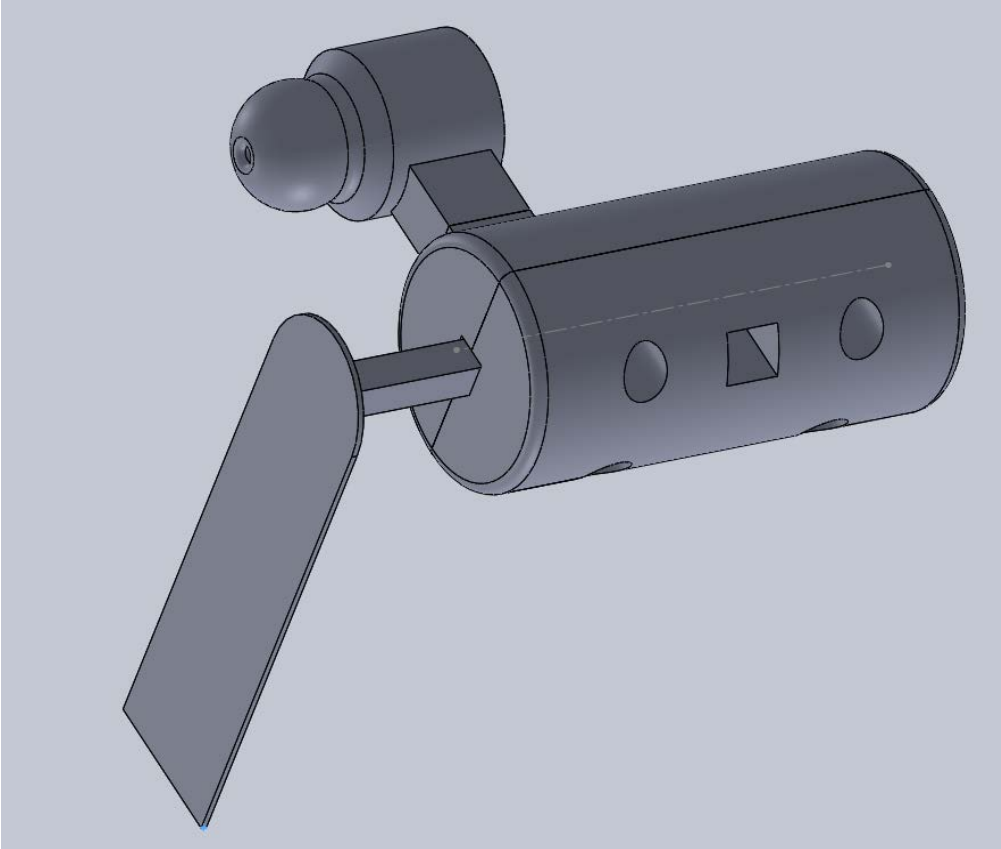

Figure 42. Bookwalter Blade Acceptor Isometric View

6.1.2 Failure Testing

All components of the current prototype of the Bookwalter blade acceptor were printed from PLA plastic on a MakerBot® Replicator® 3D printer. Although the Bookwalter blade acceptor (Figure 41) was mostly designed by the author, the teeth in Figure 44 were designed by an undergraduate student assistant. Strength testing was performed on the device to ensure safety. The testing apparatus shown in Figure 43 was designed and used to test the strength of the teeth in Figure 44 on an Instron Model 4240 tensile tester. These teeth interlock with the teeth on a retractor

blade from a Bookwalter kit, allowing the adapter to grip and hold the blade. To engage the teeth of the Bookwalter blade acceptor for tensile testing purposes, a modified Bookwalter retractor was used. The blade was removed from the retractor and two flats were machined on the portion of the blade containing teeth to aide in gripping the device in the Instron machine.

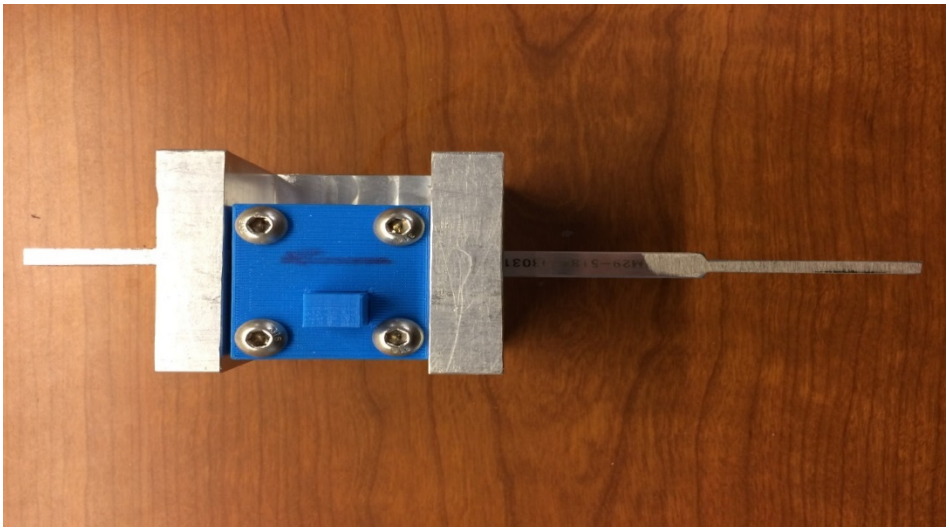

Figure 43. Testing Apparatus for Teeth Strength Tests

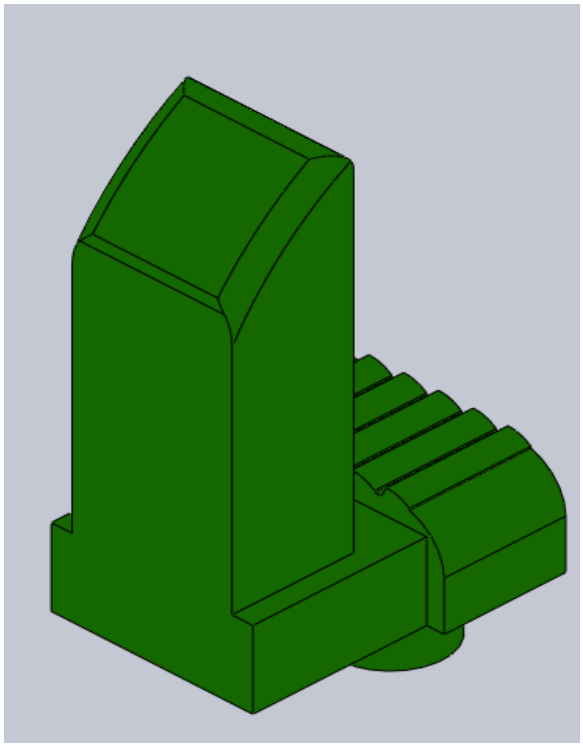

Figure 44. Teeth for Bookwalter Blade Acceptor

Seven samples of the teeth were tested until failure. For safety, a displacement limit of one quarter of an inch was used. Load was increased until failure occurred and plots of load versus displacement were obtained. An extension rate of 0.05 in/min was used to apply load to the teeth until failure was observed. The test concluded after failure of the teeth after the quarter inch displacement was reached. The test regimen was implemented in Instron's Bluehill testing software. A total of seven trials were conducted with the results given in Table 9.

Table 9. Teeth Strength Test Results

Trial	Load at Failure (lbf)
1	180
2	195
3	200
4	170
5	178
6	187
7	200
MEAN	187
STD. ERROR	4.42
95% BOUNDS	187+/-10.81

Recall that from interviews with surgeons, it was determined that the retractor system must be able to withstand a 20 lbf load without failure. Referencing Table 9, it is observed that the PLA printed teeth of the Bookwalter blade acceptor exceed these strength criteria with an approximate factor of safety of 9 when considering yield stress. Plots of load versus deflection during testing can be found in Figures 45-51 below. Figure 47 is unique in appearance. Failure clearly took place at 200 lbf; however, the data after failure was lost, resulting in the atypical appearance. The remaining plots of the samples appear as expected. Load rises sharply until failure of the teeth. After failure, the load drops suddenly.

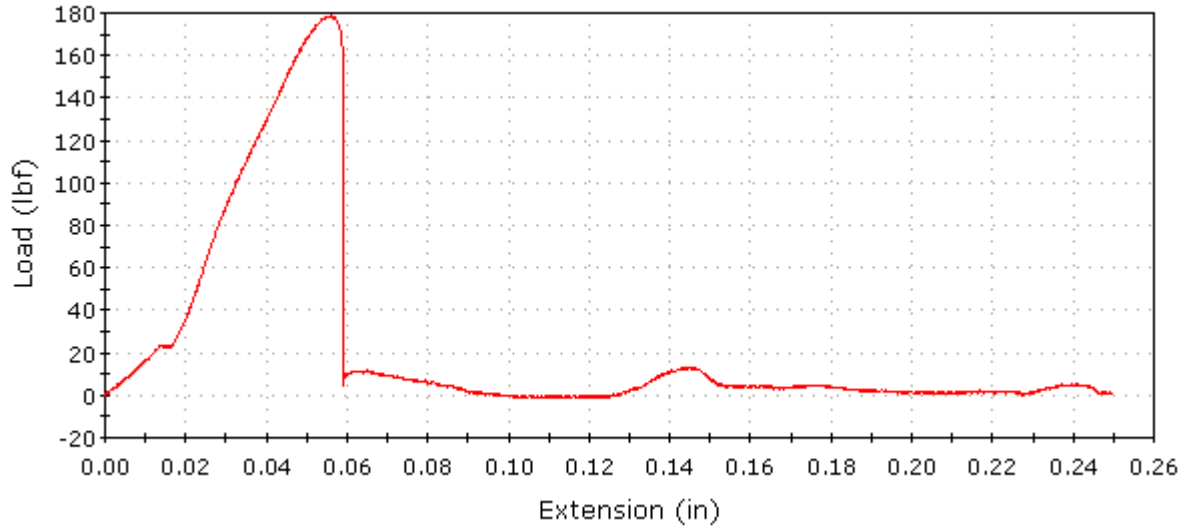

Figure 45. Teeth Strength Testing Trial 1

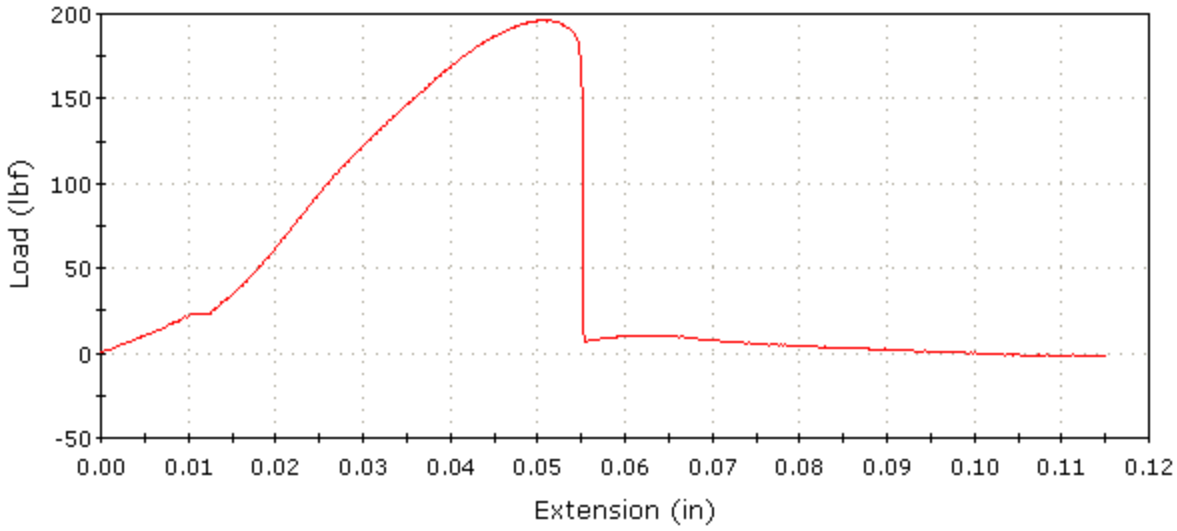

Figure 46. Teeth Strength Testing Trial 2

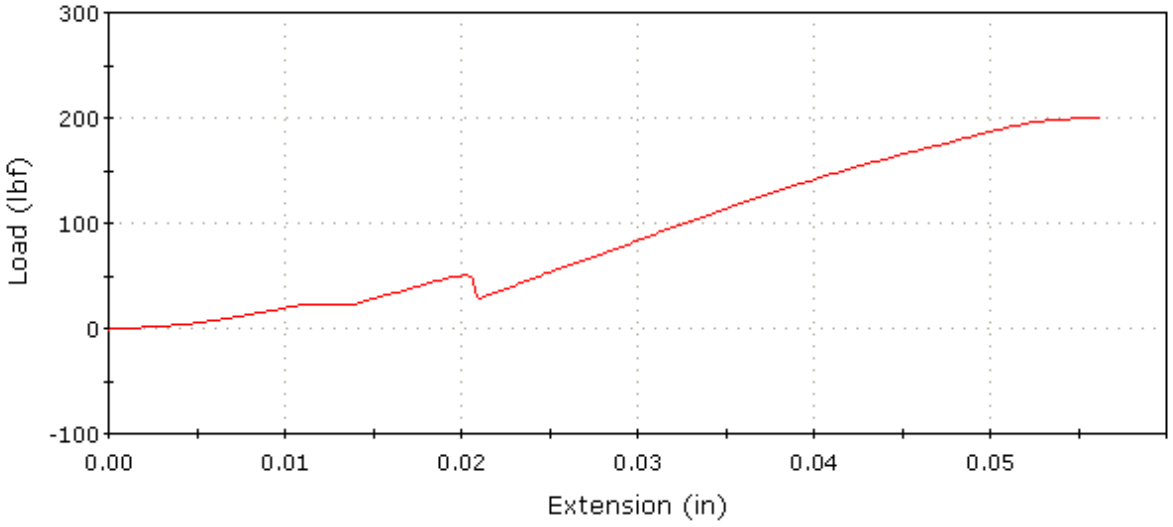

Figure 47. Teeth Strength Testing Trial 3

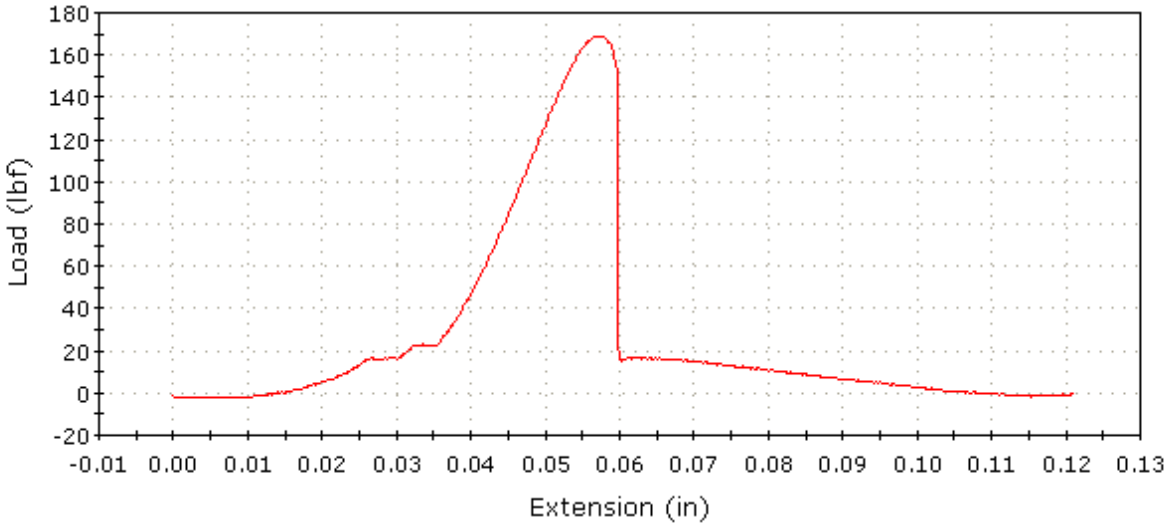

Figure 48. Teeth Strength Testing Trial 4

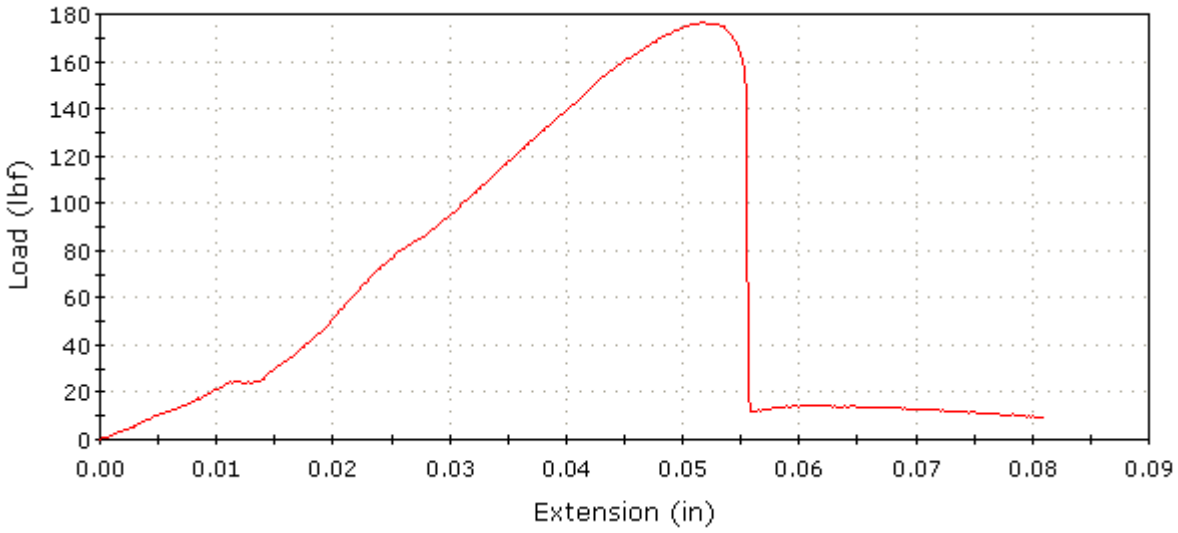

Figure 49. Teeth Strength Testing Trial 5

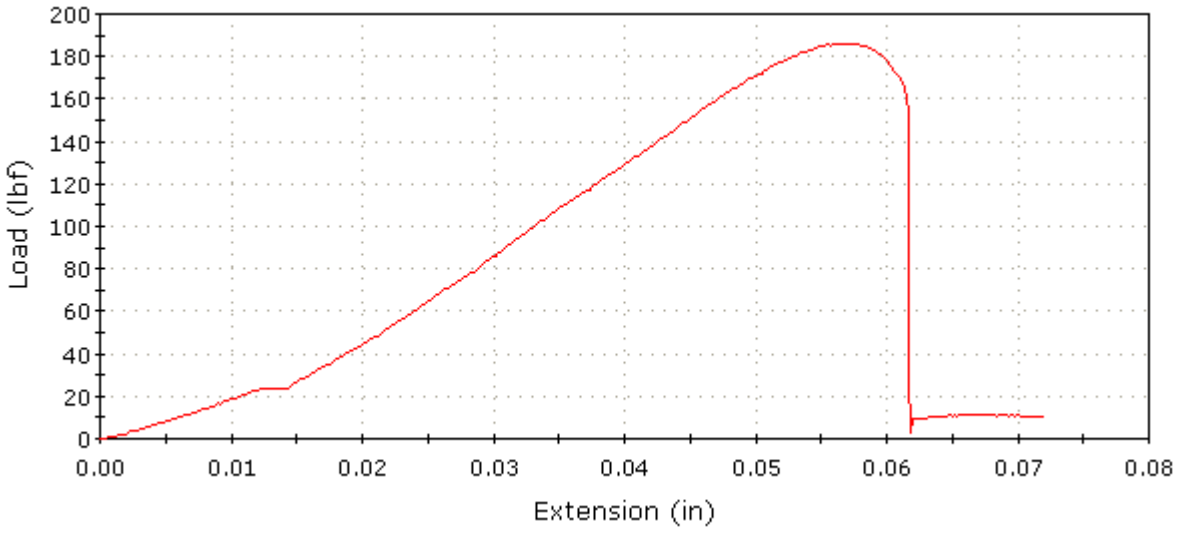

Figure 50. Teeth Strength Testing Trial 6

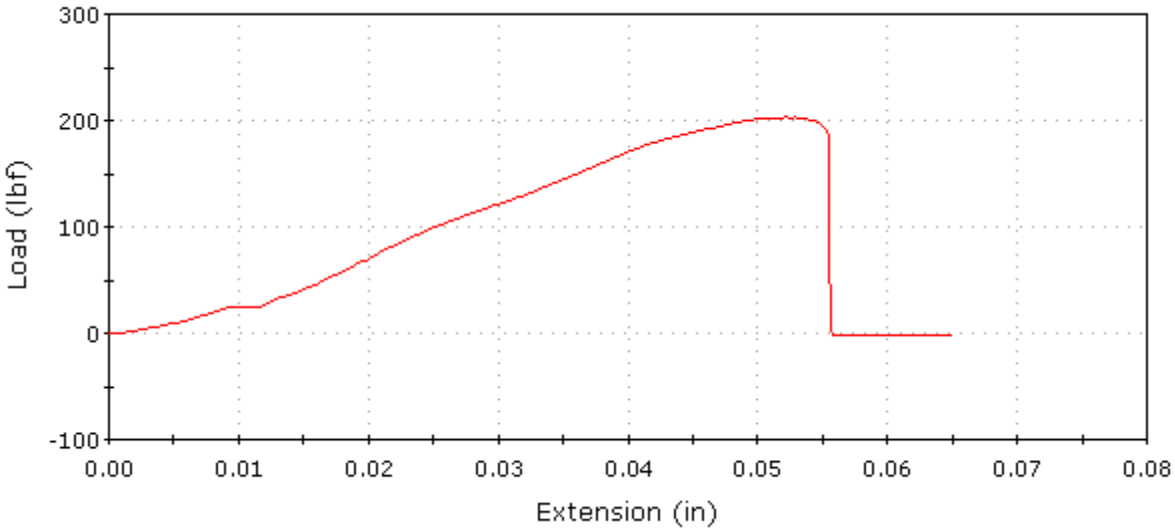

Figure 51. Teeth Strength Testing Trial 7

6.2 BASE ATTACHMENT ADAPTER

After a few iterations, a base adaptor was realized that minimized rotation at the base link when testing at angles that apply torque about the axis of the base link. The presence of rotation severely affected the system's load capacity. In an effort to maintain rigidity at all angles of retraction, a new and improved base link (Figure 52) was developed by the author.

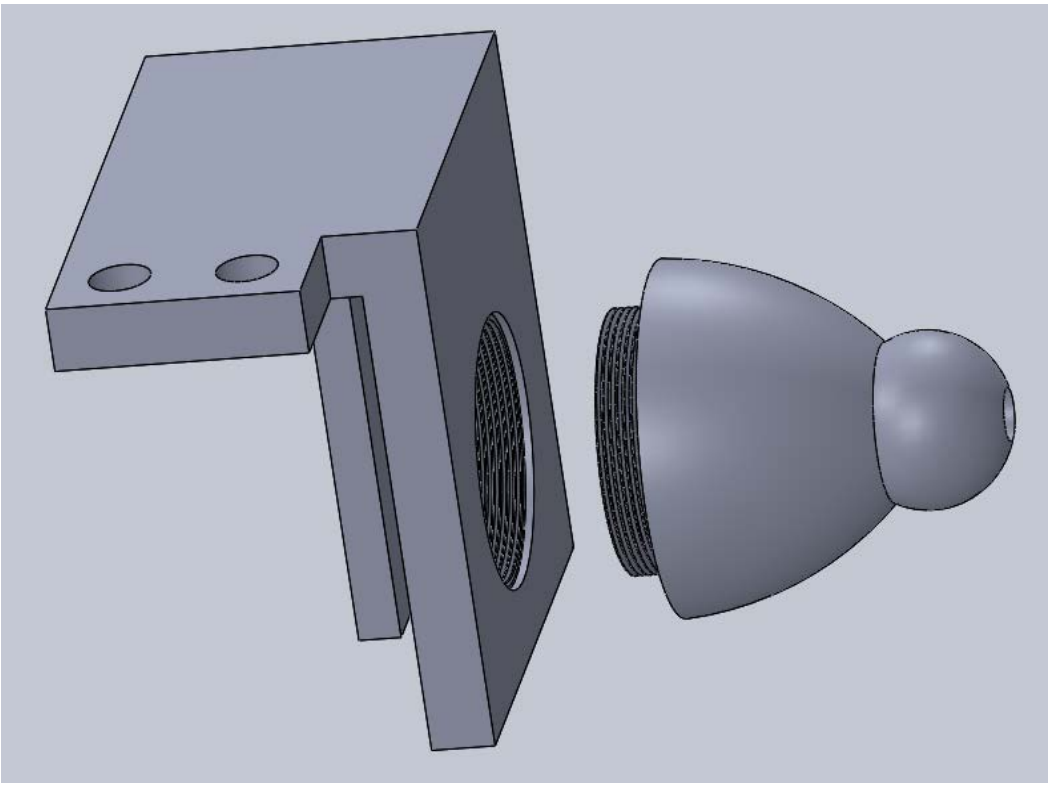

Figure 52. Anti-Rotation Base Link Assembly

The assembly in Figure 52 features 1.5”-24 TPI threads. When the retractor arm is subject to torsional loading, the threads can be tightened to the point of locking, preventing rotation. This maximizes load capacity of the retractor arm.

7.0 CONCLUSIONS

The contributions of this thesis include:

- Development of an improved motor box that uses pneumatic actuation
- Establishment of strength requirements for link geometry
- Friction testing results for various materials
- Testing methods and results from potential friction enhancements (sandblasting, conformal coatings, rubber inserts, and Carbinite.
- Design of Proximal and distal column interfaces

The new motor box features pneumatic actuation. Improvements in speed and weight were realized. Development was simplified as well, replacing an electronic force control system with switching logic and solenoid valve designed for bidirectional pneumatic cylinders. The device would operate off the house nitrogen supplies found in every hospital.

Throughout the course of this work, the two most important design considerations when selecting a material have been mechanical strength and coefficient of friction. Many materials were considered for the design of retractor system links. In order to select a material with appropriate elastic modulus, simulations were performed.

It was established that to meet the deflection specification with the link geometry, a modulus of 13 Msi (90 GPa) would be required. For typical medical devices, this would require exotic composites, such as carbon fiber or stainless steel. The arm could also be made slightly larger to increase the area moment and use aluminum. The polymer materials (PMMA, PEI, FR PC, PLA, and ABS) that were tested had moduli up to just over 580 ksi (4 GPa), eliminating their

use for any reasonable geometry. It was determined that if we use an intermediate strength material, e.g. a 4 Msi (27 GPa) modulus material, the arm would need to be 1.75 inches in diameter to meet deflection specifications.

In short, the required friction specification was not met with any solution that was attempted. This included printed, machined, Carbinite, and sandblasted surface finishes, as well as conformal coatings and rubber inserts. The best performer was a Carbinite finish, which could withstand the equivalent tip load of 5.4 lbf, which is 3.7 times lower than the required 20 lbs. Sandblasting of the PEI, PMMA, and glass fiber reinforced polycarbonate was found to increase the load capacity of the columns. Continued joint interface design will need to be the source of future work.

Finally, end interfaces were designed for the column. At the proximal end, a threaded link assembly was designed to prevent rotation of the column. The base link threads into an adapter that securely mounts the arm to the motor box. Also, a blade holder was designed for the distal end of the column. This adapter accepts retractor blades from Bookwalter kits, allowing surgeons to use retractors with which they are familiar.

APPENDIX A

A.1 ELASTIC MODULUS RESULTS

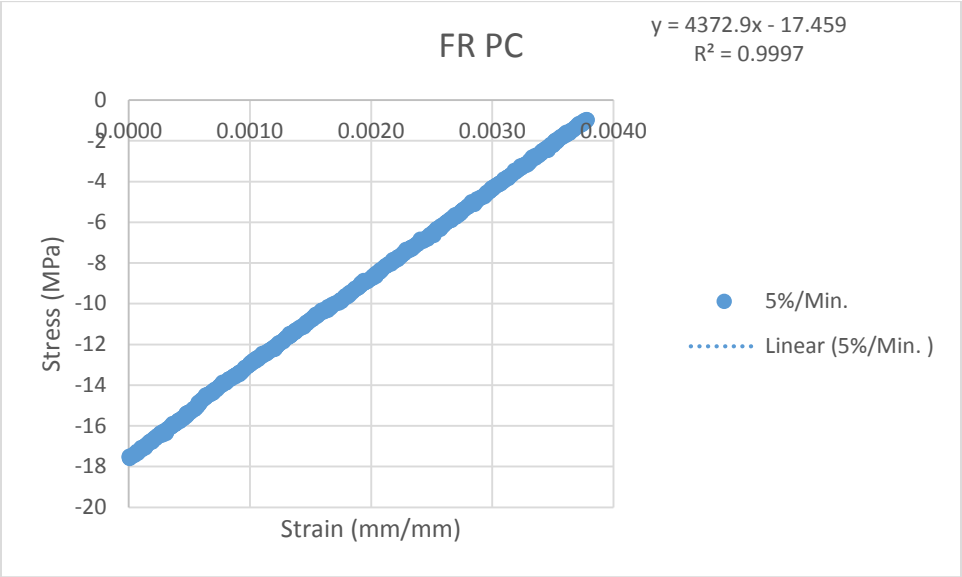

Figure 53. Glass Fiber Reinforced Polycarbonate at 5%/min Strain Rate

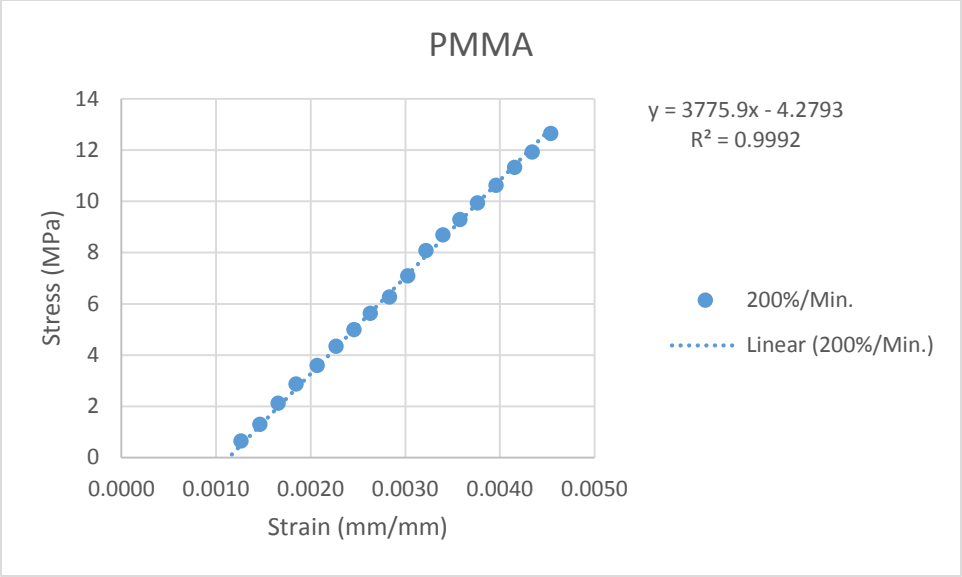

Figure 54. PMMA at 200%/min Strain Rate

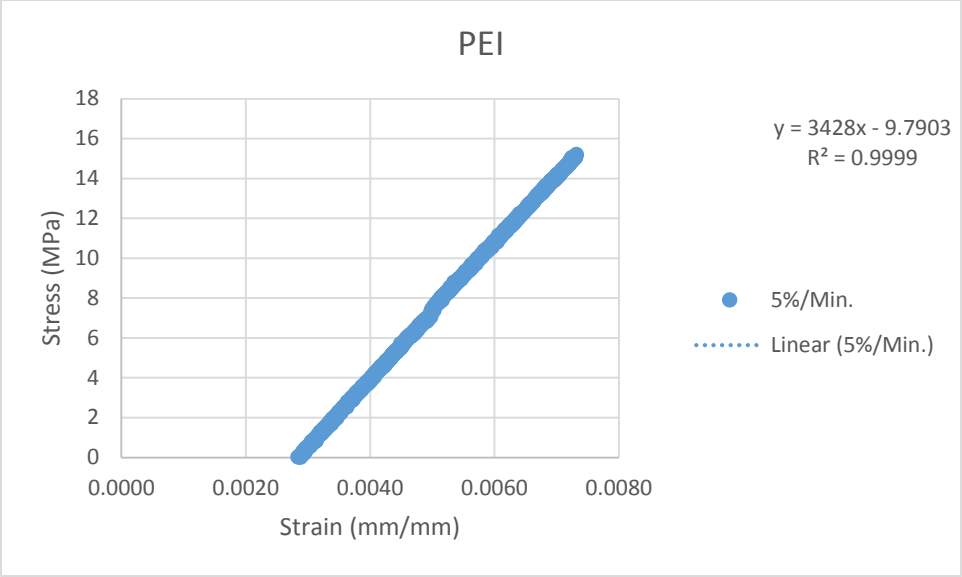

Figure 55. PEI at 5%/min Strain Rate

A.2 MATLAB MODEL CODE

```
% Ratio of rough cross section meters

%% Average Inner and outer radii in meters (could validate by comparing
actual geometry to pipe in ANSYS).

% R1 = 0.22  * 0.0254;
% R2 = 0.615  * 0.0254;
%% Arm length, m

L = 36 * 0.0254;
% Lv = linspace(0,L,100);

%%Area moment of Inertia
% I = pi/64 * ((2*R2)^4 - (2*R1)^4)
I=2.5e-8;

%% Moduli, Pa, vector

E = linspace(2e9, 80e9, 40);

%% Tip force, N (20 lbs)

F = 20   * 4.448222;

%% Deflection like PL^3/(3EI), cm

d = F .* L.^3 ./ 3 ./ E ./ I * 100;

%% Rotation (FL^2) / (2EI), in degrees

rotdeg = F .* L.^2 ./ 2 ./ E ./ I * 180 / pi;

%disp('Looks like we want at least 25 GPa modulus (3.6ksi)')

plot(E/1e9, d)
ylim([0 50]);
xlim=get(gca,'xlim');
hold on
plot(xlim,[1 1])
set(findall(gca, 'Type', 'Line'),'LineWidth',2);
```

```
      legend('Deflection (cm)')
      xlabel('Modulus (GPa)')
      ylabel('Deflection (cm)')
      %title(['Effect of Modulus, L=',num2str(L),'m, R2=',num2str(100*R2),'cm,
R1=',num2str(100*R1),'cm'])
      title(['Effect of Modulus, I=',num2str(I),'m^4, L=',num2str(L),'m'])
      grid on
      %ax=axis;, axis([ax(1:2) 0 10])
      gcf
```

A.3 DEFLECTION TESTS

Table 10. PEI Trial 1 Force versus Deflection Data

RUN 1	PEI	500 lb Preload	77.6 Ra Finish		E=3.2 GPa	
		L=19cm L=7.48 in	L=19cm L=7.48 in	Full Length (36 in)		
Force (lbf)	Voltage (V)	Deflection (in)	Deflection (mm)	Deflection (in)	Force (N)	I (m^4)
0	0	0	0	0	0	
1	0.0025	0.004	0.1016	0.445869577	4.44822	3.13E-08
2	0.005	0.009	0.2286	1.003206549	8.89644	2.78E-08
3	0.0075	0.014	0.3556	1.560543521	13.34466	2.68E-08
4	0.01	0.018	0.4572	2.006413099	17.79288	2.78E-08
5	0.0125	0.022	0.5588	2.452282676	22.2411	2.84E-08
6	0.015	0.028	0.7112	3.121087042	26.68932	2.68E-08
7	0.0175	0.035	0.889	3.901358803	31.13754	2.50E-08
8	0.02	0.04	1.016	4.458695775	35.58576	2.50E-08
9	0.0225	0.049	1.2446	5.461902324	40.03398	2.30E-08
10	0.025	0.054	1.3716	6.019239296	44.4822	2.32E-08
11	0.0275	0.059	1.4986	6.576576268	48.93042	2.33E-08
						AVERAGE
						2.62E-08

Table 11. PEI Trial 2 Force versus Deflection Data

RUN 2	PEI	500 lb Preload	77.6 Ra Finish		E=3.2 GPa	
		L=19cm L=7.48 in	L=19cm L=7.48 in	Full Length (36 in)		
Force (lbf)	Voltage (V)	Deflection (in)	Deflection (mm)	Deflection (in)	Force (N)	I (m^4)
0	0	0	0	0	0	
1	0.0025	0.005	0.127	0.557336972	4.44822	2.50E-08
2	0.005	0.009	0.2286	1.003206549	8.89644	2.78E-08
3	0.0075	0.014	0.3556	1.560543521	13.34466	2.68E-08
4	0.01	0.018	0.4572	2.006413099	17.79288	2.78E-08
5	0.0125	0.024	0.6096	2.675217465	22.2411	2.61E-08
6	0.015	0.03	0.762	3.344021831	26.68932	2.50E-08
7	0.0175	0.034	0.8636	3.789891409	31.13754	2.58E-08
8	0.02	0.041	1.0414	4.570163169	35.58576	2.44E-08
9	0.0225	0.046	1.1684	5.127500141	40.03398	2.45E-08
10	0.025	0.052	1.3208	5.796304507	44.4822	2.41E-08
11	0.0275	0.058	1.4732	6.465108873	48.93042	2.37E-08
						AVERAGE
						2.55E-08

Table 12. PMMA Trial 1 Force versus Deflection Data

RUN 1	PMMA	500 lb Preload	74.9 Ra Finish		E=3 GPa	
		L=19cm L=7.48 in	L=19cm L=7.48 in	Full Length (36 in)		
Force (lbf)	Voltage (V)	Deflection (in)	Deflection (mm)	Deflection (in)	Force (N)	I (m^4)
0	0	0	0	0	0	
1	0.0025	0.005	0.127	0.557336972	4.44822	2.67E-08
2	0.005	0.009	0.2286	1.003206549	8.89644	2.97E-08
3	0.0075	0.014	0.3556	1.560543521	13.34466	2.86E-08
4	0.01	0.018	0.4572	2.006413099	17.79288	2.97E-08
5	0.0125	0.025	0.635	2.786684859	22.2411	2.67E-08
6	0.015	0.029	0.7366	3.232554437	26.68932	2.76E-08
7	0.0175	0.034	0.8636	3.789891409	31.13754	2.75E-08
8	0.02	0.04	1.016	4.458695775	35.58576	2.67E-08
9	0.0225	0.046	1.1684	5.127500141	40.03398	2.61E-08
10	0.025	0.052	1.3208	5.796304507	44.4822	2.57E-08
11	0.0275	0.056	1.4224	6.242174085	48.93042	2.62E-08
12	0.03	0.061	1.5494	6.799511057	53.37864	2.63E-08
13	0.0325	0.066	1.6764	7.356848028	57.82686	2.63E-08
14	0.035	0.072	1.8288	8.025652395	62.27508	2.60E-08
15	0.0375	0.078	1.9812	8.694456761	66.7233	2.57E-08
16	0.04	0.084	2.1336	9.363261127	71.17152	2.54E-08
17	0.0425	0.09	2.286	10.03206549	75.61974	2.52E-08
18	0.045	0.098	2.4892	10.92380465	80.06796	2.45E-08
19	0.0475	0.104	2.6416	11.59260901	84.51618	2.44E-08
						AVERAGE
						2.66E-08

Table 13. PMMA Trial 2 Force versus Deflection Data

RUN 2	PMMA	500 lb Preload	74.9 Ra Finish		E=3 GPa	
		L=19cm L=7.48 in	L=19cm L=7.48 in	Full Length (36 in)		
Force (lbf)	Voltage (V)	Deflection (in)	Deflection (mm)	Deflection (in)	Force (N)	I (m^4)
0	0	0	0	0	0	
1	0.0025	0.004	0.1016	0.445869577	4.44822	3.34E-08
2	0.005	0.008	0.2032	0.891739155	8.89644	3.34E-08
3	0.0075	0.013	0.3302	1.449076127	13.34466	3.08E-08
4	0.01	0.017	0.4318	1.894945704	17.79288	3.14E-08
5	0.0125	0.021	0.5334	2.340815282	22.2411	3.18E-08
6	0.015	0.027	0.6858	3.009619648	26.68932	2.97E-08
7	0.0175	0.032	0.8128	3.56695662	31.13754	2.92E-08
8	0.02	0.037	0.9398	4.124293592	35.58576	2.89E-08
9	0.0225	0.041	1.0414	4.570163169	40.03398	2.93E-08
10	0.025	0.046	1.1684	5.127500141	44.4822	2.90E-08
11	0.0275	0.052	1.3208	5.796304507	48.93042	2.82E-08
12	0.03	0.057	1.4478	6.353641479	53.37864	2.81E-08
13	0.0325	0.062	1.5748	6.910978451	57.82686	2.80E-08
14	0.035	0.068	1.7272	7.579782817	62.27508	2.75E-08
15	0.0375	0.073	1.8542	8.137119789	66.7233	2.74E-08
16	0.04	0.078	1.9812	8.694456761	71.17152	2.74E-08
17	0.0425	0.084	2.1336	9.363261127	75.61974	2.70E-08
18	0.045	0.09	2.286	10.03206549	80.06796	2.67E-08
19	0.0475	0.098	2.4892	10.92380465	84.51618	2.59E-08
20	0.05	0.104	2.6416	11.59260901	88.9644	2.57E-08
						AVERAGE
						2.89E-08

Table 14. Glass Fiber Reinforced Polycarbonate Trial 1 Force versus Deflection Data

RUN 1	FR PC	500 lb Preload	138.7 Ra Finish		E=4.2 GPa	
		L=19cm L=7.48 in	L=19cm L=7.48 in	Full Length (36 in)		
Force (lbf)	Voltage (V)	Deflection (in)	Deflection (mm)	Deflection (in)	Force (N)	I (m^4)
0	0	0	0	0	0	
1	0.0025	0.005	0.127	0.557336972	4.44822	1.91E-08
2	0.005	0.009	0.2286	1.003206549	8.89644	2.12E-08
3	0.0075	0.014	0.3556	1.560543521	13.34466	2.04E-08
4	0.01	0.018	0.4572	2.006413099	17.79288	2.12E-08
5	0.0125	0.023	0.5842	2.563750071	22.2411	2.07E-08
6	0.015	0.028	0.7112	3.121087042	26.68932	2.04E-08
7	0.0175	0.033	0.8382	3.678424014	31.13754	2.02E-08
8	0.02	0.037	0.9398	4.124293592	35.58576	2.06E-08
9	0.0225	0.041	1.0414	4.570163169	40.03398	2.09E-08
10	0.025	0.048	1.2192	5.35043493	44.4822	1.99E-08
11	0.0275	0.054	1.3716	6.019239296	48.93042	1.94E-08
12	0.03	0.06	1.524	6.688043662	53.37864	1.91E-08
13	0.0325	0.065	1.651	7.245380634	57.82686	1.91E-08
14	0.035	0.07	1.778	7.802717606	62.27508	1.91E-08
15	0.0375	0.074	1.8796	8.248587183	66.7233	1.93E-08
16	0.04	0.078	1.9812	8.694456761	71.17152	1.96E-08
17	0.0425	0.083	2.1082	9.251793733	75.61974	1.95E-08
18	0.045	0.089	2.2606	9.920598099	80.06796	1.93E-08
19	0.0475	0.097	2.4638	10.81233725	84.51618	1.87E-08
20	0.05	0.104	2.6416	11.59260901	88.9644	1.83E-08
						AVERAGE
						1.98E-08

Table 15. Glass Fiber Reinforced Polycarbonate Trial 2 Force versus Deflection Data

RUN 2	FR PC	500 lb Preload	138.7 Ra Finish		E=4.2 GPa	
		L=19cm L=7.48 in	L=19cm L=7.48 in	Full Length (36 in)		
Force (lbf)	Voltage (V)	Deflection (in)	Deflection (mm)	Deflection (in)	Force (N)	I (m^4)
0	0	0	0	0	0	
1	0.0025	0.004	0.1016	0.445869577	4.44822	2.38E-08
2	0.005	0.008	0.2032	0.891739155	8.89644	2.38E-08
3	0.0075	0.014	0.3556	1.560543521	13.34466	2.04E-08
4	0.01	0.018	0.4572	2.006413099	17.79288	2.12E-08
5	0.0125	0.024	0.6096	2.675217465	22.2411	1.99E-08
6	0.015	0.029	0.7366	3.232554437	26.68932	1.97E-08
7	0.0175	0.032	0.8128	3.56695662	31.13754	2.09E-08
8	0.02	0.037	0.9398	4.124293592	35.58576	2.06E-08
9	0.0225	0.043	1.0922	4.793097958	40.03398	2.00E-08
10	0.025	0.047	1.1938	5.238967535	44.4822	2.03E-08
11	0.0275	0.051	1.2954	5.684837113	48.93042	2.06E-08
12	0.03	0.058	1.4732	6.465108873	53.37864	1.97E-08
13	0.0325	0.062	1.5748	6.910978451	57.82686	2.00E-08
14	0.035	0.069	1.7526	7.691250212	62.27508	1.93E-08
15	0.0375	0.075	1.905	8.360054578	66.7233	1.91E-08
16	0.04	0.079	2.0066	8.805924155	71.17152	1.93E-08
17	0.0425	0.086	2.1844	9.586195916	75.61974	1.88E-08
18	0.045	0.091	2.3114	10.14353289	80.06796	1.89E-08
19	0.0475	0.096	2.4384	10.70086986	84.51618	1.89E-08
20	0.05	0.101	2.5654	11.25820683	88.9644	1.89E-08
						AVERAGE
						2.02E-08

Table 16. Aluminum Trial 1 Force versus Deflection Data

RUN 1	Al	500 lb Preload	103.8 Ra Finish		E=70 GPa
		L=19cm L=7.48 in	L=19cm L=7.48 in	Full Length (36 in)	
Force (lbf)	Voltage (V)	Deflection (in)	Deflection (mm)	Deflection (in)	Force (N)
0	0	0	0	0	0
1	0.0025	0.0005	0.0127	0.055733697	4.44822
2	0.005	0.001	0.0254	0.111467394	8.89644
3	0.0075	0.003	0.0762	0.334402183	13.34466
4	0.01	0.004	0.1016	0.445869577	17.79288
5	0.0125	0.005	0.127	0.557336972	22.2411
6	0.015	0.006	0.1524	0.668804366	26.68932
7	0.0175	0.007	0.1778	0.780271761	31.13754
8	0.02	0.008	0.2032	0.891739155	35.58576
9	0.0225	0.009	0.2286	1.003206549	40.03398
10	0.025	0.011	0.2794	1.226141338	44.4822
11	0.0275	0.013	0.3302	1.449076127	48.93042
12	0.03	0.014	0.3556	1.560543521	53.37864
13	0.0325	0.015	0.381	1.672010916	57.82686
14	0.035	0.017	0.4318	1.894945704	62.27508
15	0.0375	0.019	0.4826	2.117880493	66.7233
16	0.04	0.021	0.5334	2.340815282	71.17152
17	0.0425	0.024	0.6096	2.675217465	75.61974
18	0.045	0.027	0.6858	3.009619648	80.06796
19	0.0475	0.028	0.7112	3.121087042	84.51618
20	0.05	0.029	0.7366	3.232554437	88.9644
21	0.0525	0.03	0.762	3.344021831	93.41262

Table 17. Aluminum Trial 2 Force versus Deflection Data

RUN 2	Al	500 lb Preload	103.8 Ra Finish		E=70 GPa
		L=19cm L=7.48 in	L=19cm L=7.48 in	Full Length (36 in)	
Force (lbf)	Voltage (V)	Deflection (in)	Deflection (mm)	Deflection (in)	Force (N)
0	0	0	0	0	0
1	0.0025	0.001	0.0254	0.111467394	4.44822
2	0.005	0.002	0.0508	0.222934789	8.89644
3	0.0075	0.003	0.0762	0.334402183	13.34466
4	0.01	0.0035	0.0889	0.39013588	17.79288
5	0.0125	0.004	0.1016	0.445869577	22.2411
6	0.015	0.0055	0.1397	0.613070669	26.68932
7	0.0175	0.0065	0.1651	0.724538063	31.13754
8	0.02	0.0075	0.1905	0.836005458	35.58576
9	0.0225	0.008	0.2032	0.891739155	40.03398
10	0.025	0.009	0.2286	1.003206549	44.4822
11	0.0275	0.01	0.254	1.114673944	48.93042
12	0.03	0.011	0.2794	1.226141338	53.37864
13	0.0325	0.012	0.3048	1.337608732	57.82686
14	0.035	0.013	0.3302	1.449076127	62.27508
15	0.0375	0.014	0.3556	1.560543521	66.7233
16	0.04	0.015	0.381	1.672010916	71.17152
17	0.0425	0.016	0.4064	1.78347831	75.61974
18	0.045	0.017	0.4318	1.894945704	80.06796
19	0.0475	0.018	0.4572	2.006413099	84.51618
20	0.05	0.019	0.4826	2.117880493	88.9644
21	0.0525	0.02	0.508	2.229347887	93.41262

Table 18. Trial 1 Deflection of Stainless Steel Links featuring Tungsten Carbide Coating

RUN 1	303 SS Coated	500 lb Preload	266 Ra Finish		E=210 GPa
		L=19cm L=7.48 in	L=19cm L=7.48 in	Full Length (36 in)	
Force (lbf)	Voltage (V)	Deflection (in)	Deflection (mm)	Deflection (in)	Force (N)
0	0	0	0	0	0
1	0.0025	0.001	0.0254	0.111467394	4.44822
2	0.005	0.002	0.0508	0.222934789	8.89644
3	0.0075	0.003	0.0762	0.334402183	13.34466
4	0.01	0.005	0.127	0.557336972	17.79288
5	0.0125	0.006	0.1524	0.668804366	22.2411
6	0.015	0.007	0.1778	0.780271761	26.68932
7	0.0175	0.009	0.2286	1.003206549	31.13754
8	0.02	0.01	0.254	1.114673944	35.58576
9	0.0225	0.012	0.3048	1.337608732	40.03398
10	0.025	0.013	0.3302	1.449076127	44.4822
11	0.0275	0.015	0.381	1.672010916	48.93042
12	0.03	0.017	0.4318	1.894945704	53.37864
13	0.0325	0.018	0.4572	2.006413099	57.82686
14	0.035	0.02	0.508	2.229347887	62.27508
15	0.0375	0.022	0.5588	2.452282676	66.7233
16	0.04	0.024	0.6096	2.675217465	71.17152
17	0.0425	0.025	0.635	2.786684859	75.61974
18	0.045	0.028	0.7112	3.121087042	80.06796
19	0.0475	0.031	0.7874	3.455489225	84.51618
20	0.05	0.034	0.8636	3.789891409	88.9644
21	0.0525	0.036	0.9144	4.012826197	93.41262
22	0.055	0.04	1.016	4.458695775	97.86084
23	0.0575	0.043	1.0922	4.793097958	102.3091
24	0.06	0.05	1.27	5.573369719	106.7573
25	0.0625	0.053	1.3462	5.907771902	111.2055
26	0.065	0.056	1.4224	6.242174085	115.6537

Table 19. Trial 2 Deflection of Stainless Steel Links featuring Tungsten Carbide Coating

RUN 2	303 SS Coated	500 lb Preload	266 Ra		E=210 GPa
		L=19cm L=7.48 in	L=19cm L=7.48 in	Full Length (36 in)	
Force (lbf)	Voltage (V)	Deflection (in)	Deflection (mm)	Deflection (in)	Force (N)
0	0	0	0	0	0
1	0.0025	0.001	0.0254	0.111467394	4.44822
2	0.005	0.002	0.0508	0.222934789	8.89644
3	0.0075	0.003	0.0762	0.334402183	13.34466
4	0.01	0.004	0.1016	0.445869577	17.79288
5	0.0125	0.005	0.127	0.557336972	22.2411
6	0.015	0.006	0.1524	0.668804366	26.68932
7	0.0175	0.007	0.1778	0.780271761	31.13754
8	0.02	0.008	0.2032	0.891739155	35.58576
9	0.0225	0.01	0.254	1.114673944	40.03398
10	0.025	0.011	0.2794	1.226141338	44.4822
11	0.0275	0.012	0.3048	1.337608732	48.93042
12	0.03	0.013	0.3302	1.449076127	53.37864
13	0.0325	0.014	0.3556	1.560543521	57.82686
14	0.035	0.016	0.4064	1.78347831	62.27508
15	0.0375	0.017	0.4318	1.894945704	66.7233
16	0.04	0.018	0.4572	2.006413099	71.17152
17	0.0425	0.02	0.508	2.229347887	75.61974
18	0.045	0.021	0.5334	2.340815282	80.06796
19	0.0475	0.023	0.5842	2.563750071	84.51618
20	0.05	0.024	0.6096	2.675217465	88.9644
21	0.0525	0.026	0.6604	2.898152254	93.41262
22	0.055	0.028	0.7112	3.121087042	97.86084
23	0.0575	0.029	0.7366	3.232554437	102.3091
24	0.06	0.032	0.8128	3.56695662	106.7573
25	0.0625	0.035	0.889	3.901358803	111.2055
26	0.065	0.037	0.9398	4.124293592	115.6537

A.4 FRICTION TABLES

Table 20. Frictional Loss with No Bend

TRIAL 1									
0-degree bend									
Futek (distal)	Arm End			Omega (proximal)	Arm Root		Total		
Voltage (V)	Load (lbf)			Voltage (V)	Load (lbf)				
0.003725	195			0.001288	203		3.74%	-3.74%	1
0.00509	267			0.001835	300		7.68%	-7.68%	2
0.006933	363			0.00261	410.719		13.15%	-13.15%	3
0.00804	421			0.003185	501.203		15.98%	-15.98%	4
0.00947	496			0.003845	605.063		18.03%	-18.03%	5

Table 21. Frictional Loss with 90° Bend

TRIAL 2									
90-degree bend									
Futek (distal)	Arm End			Omega (proximal)	Arm Root		Total		
Voltage (V)	Load (lbf)			Voltage (V)	Load (lbf)				
0.002313	121			0.001156	182		33.40%	-33.40%	1
0.002801	147			0.00184	290		55.57%	-55.57%	2
0.003992	209			0.0026	409		54.29%	-54.29%	3
0.00499	261			0.0033	510		51.73%	-51.73%	4
0.0058	304			0.0038	600		52.64%	-52.64%	5

Table 22. Frictional Loss with 180° Bend

TRIAL 3									
180-degree bend									
Futek (distal)	Arm End			Omega (proximal)	Arm Root		Total		
Voltage (V)	Load (lbf)			Voltage (V)	Load (lbf)				
0.002481	130			0.00123	193.56		32.84%	-32.84%	1
0.002487	130.26			0.00195	306.86		57.55%	-57.55%	2
0.002493	130.57			0.00252	396.56		67.07%	-67.07%	3
0.002483	130			0.00316	497.27		73.86%	-73.86%	4
0.0026	136.18			0.00385	605.85		77.52%	-77.52%	5

BIBLIOGRAPHY

[1] Adams, Kay. (2017, November 9). Personal Interview.

[2] Allen, Peter, M.D. (2016, December 6). Personal Interview.

[3] Allen, Peter, M.D. (2017, November 2). Personal Interview.

[4] "Balfour Retractor - Abdominal Retractors - Retractors." *Sklar Surgical Instruments*. N.p., n.d. Web.

[5] Barr, Justin, MD, PhD, and Kenneth L. Brayman, MD, PhD, FACS. "Development and Evolution of Self-Retaining Retractors in Surgery: The Example of the Bookwalter Retractor." *Journalacs.org*. N.p., n.d. Web.

[6] "Bookwalter Abdominal Retractor Set BR18-77000." *Bookwalter Retractor Set BR18-77000 Single*. N.p., n.d. Web. <https://www.global-medical-solutions.com/Bookwalter-Abdominal-Retractor-Set-BR18-77000_p_8658.html>.

[7] Bookwalter, John R., M.D. "A New Table-Fixed Retractor." *Surgical Clinics of North America*. Elsevier, 01 Aug. 2016. Web. 01 Nov. 2017. <https://www.sciencedirect.com/science/article/pii/S0039610916420888>.

[8] Bookwalter, John R., M.D. Surgical Retractor Assembly. Codman & Shurtleff, Inc., assignee. Patent 4254763. 10 Mar. 1981. Print.

[9] Clunie, Aurelia. "History of Surgery." *Hartford Stage*. N.p., n.d. Web.

[10] Davis, Joseph R. "Coefficients of Friction." *Concise Metals Engineering Data Book*. Materials Park, OH: ASM International, 1997. N. pag. Print.

[11] Haubrich, William S. "Balfour of the Balfour Retractor." *Gastroenterology* 135.3 (2008): 723. Web.

[12] "History of the Thompson Retractor." *The Leader in Surgical Retraction*. N.p., n.d. Web. 17 Oct. 2017. <http://thompsonsurgical.com/history/>.

[13] I-Corps Teams: Surgical Retractor System Is the Title of the Study. Period of Performance 7/1/17-7/2/18. Jeffrey S. Vipperman, PI.

[14] Irving, Jenni. "Trephination." *Ancient History Encyclopedia*. N.p., 01 May 2013. Web. 01 Nov. 2017. <https://www.ancient.eu/Trephination>.

[15] Kim, Peter, MD. "Surgical Entrepreneurism An Interview With the Inventor of the Bookwalter Retractor." *General Surgery News*. N.p., n.d. Web.

[16] McMahon, Mary, and O. Wallace. "What Is a Balfour Retractor?" *WiseGEEK*. Conjecture Corporation, 02 Sept. 2017. Web.

[17] "Medical Tools." *Surgical Retractor Types and Usage*. Medical/Surgical Instruments and Technolofy Blog, n.d. Web. 03 Nov. 2017. <http://www.medical-tools.com/blog/medical-tools-instruments/surgical-retractors-types-usage-kinds-listing/>.

[18] "NinjaFlex 85A TPU Flexible 3D Printing Filament." *NinjaTek*. N.p., n.d. Web. 06 Nov. 2017.

[19] "Omni-Tract System." *Integra LifeSciences | Medical Device Company - Medical Technologies*. N.p., n.d. Web.

[20] Paloheimo, Markus, M.S. Sc. "Tensile or Flexural Strength: Is There Really a Difference?" *Plastiprop.com*. N.p., n.d. Web. 05 Nov. 2017.

[21] Pelta, Samuel. Surgical Retractor Support. Pilling Co., assignee. Patent 4971037. 20 Nov. 1990. Print.

[22] "PLASTI DIP Multi Purpose Rubber Coating" *Performix Brand*. N.p., N.d. Web. 06 Nov. 2017.

[23] Prospector, UL. "Edgetek™ SF-40CF/000 Datasheet." *Edgetek™ SF-40CF/000 PolyOne*. N.p., n.d. Web. 09 Nov. 2017.

[24] "Retractor Frame Components." *The Leader in Surgical Retraction*. N.p., n.d. Web. <http://thompsonsurgical.com/retractor-frame-components/>.

[25] "Science Museum. Brought to Life: Exploring the History of Medicine." *Surgery*. N.p., n.d. Web. 01 Nov. 2017. <http://broughttolife.sciencemuseum.org.uk/broughttolife/themes/surgery>.

[26] "Silicones from Dow Corning." *Dow Corning*. N.p., n.d. Web. 06 Nov. 2017.

[27] Six, Cheryl, D.O. (2017, April 19). Personal Interview.

[28] Smith, David P., Table Supported Abdominal Retractor. David P. Smith, Assignee. Patent 2594086. 22 Apr. 1952. Print.

[29] "SparkFun RedBoard - Programmed with Arduino." *SparkFun Electronics*. N.p., n.d. Web. 06 Nov. 2017.

[30] Stacey-Clear, A., and C. W. Jamieson. "Omnitract Retractor." *BJS*. John Wiley & Sons, Ltd., 06 Dec. 2005. Web. 01 Nov. 2017. <http://onlinelibrary.wiley.com/doi/10.1002/bjs.1800740107/pdf>.

[31] "Standard Test Methods for Tension Testing of Metallic Materials," ASTM International, West Conshohocken, PA, 2014, DOI: 10.1520/E0008_E0008M-13A, www.astm.org."

[32] Steele, P. R., J. F. Curran, and R. E. Mountain. "Current and Future Practices in Surgical Retraction." *The Surgeon*. Elsevier, 06 Aug. 2013. Web. 03 Nov. 2017. <https://www.sciencedirect.com/science/article/pii/S1479666X13000802>.

[33] "Symmetry Surgical." *Bookwalter Retractor*. N.p., n.d. Web. 08 Nov. 2017.

[34] Thompson, Richard C., M.D. System and Apparatus for Positioning and Securing Surgical Implements. Pa Co Inc Du, assignee. Patent US 3221743 A. 7 Dec. 1965. Print.

[35] Ugural, Ansel C., and Saul K. Fenster. "Chapter 5." *Advanced Strength and Applied Elasticity*. Upper Saddle River, NJ: Prentice Hall, 2003. N. pag. Print.

[36] West, Alan I. "A Stress Analysis of Surgical Retractors: Implications in Design." Thesis. Tufts University, 1979. Print.

[37] Wilford, John Noble. "When Humans Became Human." *The New York Times*. The New York Times, 25 Feb. 2002. Web. 01 Nov. 2017. <http://www.nytimes.com/2002/02/26/science/when-humans-became-human.html>.

[38] "Workholding Solutions." *Carbinite Metal Coatings*. N.p., n.d. Web. 06 Nov. 2017.

[39] Zeltzman, Phil, DVM, DACVS, and Myron O. Downs, DVM, PhD, DACVS. "Surgical Sponges in Small Animal Surgery." *VetFolio*. Compendium-Continuing Education for Veterinarians, n.d. Web. 02 Nov. 2017.

[40] Wu, Hengyi, Gang Ma, and Yuanming Xia. "Experimental Study of Tensile Properties of PMMA at Intermediate Strain Rate." *Materials Letters*. North-Holland, 17 Aug. 2004. Web. 10 Nov. 2017.

[41] Polymerdatabase.com, CROW © 2015. "Polymer Properties Database." *Stress Relaxation*. N.p., n.d. Web. 26 Nov. 2017.

[42] Gere, James M., and Stephen Timoshenko. “Deflections of Beams.” *Mechanics of Materials,* PWS-KENT Pub. Co, 1990.